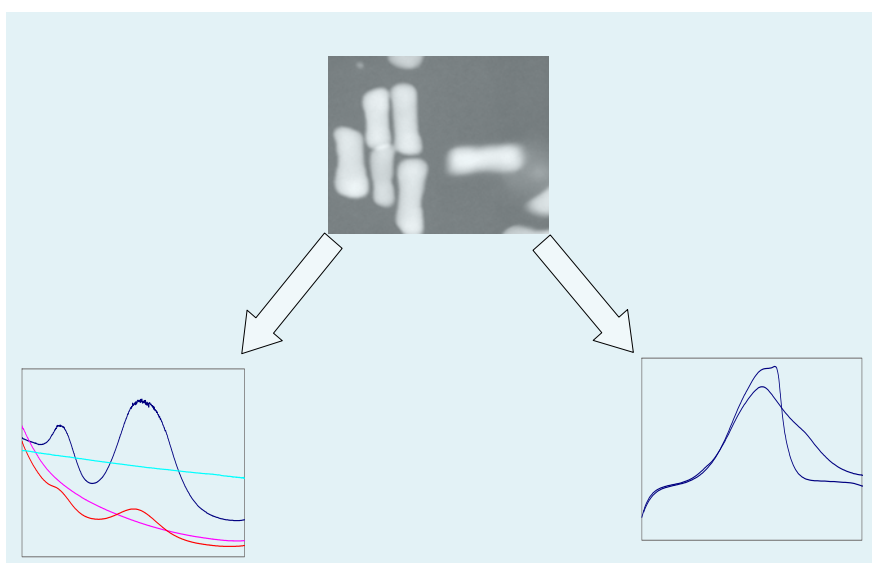




UNIVERSITY OF
BIRMINGHAM

SYNTHESIS, CHARACTERISATION AND APPLICATIONS OF BI-METALLIC NANOPARTICLES



A Thesis Presented To the School of Chemistry,
University Of Birmingham,
In Partial Fulfilment of the Requirements for the Degree
Master of Science

By

Anicetus Muche Tanyi
Dr. Sarah L Horswell, Supervisor
September, 2009

UNIVERSITY OF
BIRMINGHAM

University of Birmingham Research Archive

e-theses repository

This unpublished thesis/dissertation is copyright of the author and/or third parties. The intellectual property rights of the author or third parties in respect of this work are as defined by The Copyright Designs and Patents Act 1988 or as modified by any successor legislation.

Any use made of information contained in this thesis/dissertation must be in accordance with that legislation and must be properly acknowledged. Further distribution or reproduction in any format is prohibited without the permission of the copyright holder.

Acknowledgement

Firstly I must express my gratitude towards the generous funding provided by the Engineering and Physical Sciences Research Council (EPSRC) and the School of Chemistry, University of Birmingham, without which this project would not have been possible for me to undertake. Also I will like to thank Centrala Studiestödsnämnden (CSN) Sverige (The Swedish National Grant Agency) for providing me extra financial support to help me through my studies in Birmingham.

Secondly, I must say I am indebted to all the people who helped me through this journey of postgraduate studies.

Foremost, I am grateful to my research supervisor Dr. Sarah L Horswell for her constant encouragement. She presented me the opportunity to work in an interdisciplinary program that allowed me to interact with researchers from diverse fields such as physics. Many thanks go to Dr. Ziyou Li (Collaborator) in the Nanoscale Physics Research Laboratory in the School of Physics and Astronomy University of Birmingham for providing and helping me with the Electron microscope imaging.

I cannot thank my family and friends enough for their inspiration and support throughout my endeavours to pursue higher studies. I am truly indebted to my parents, brothers and sisters for considering my dreams as theirs and providing me the strength and enthusiasm to reach my goals. My late father's unrelenting support and my mother's confidence in my abilities gave me confidence to look beyond the horizon. The unconditional love of my daughter was instrumental in helping me stay focused on the project.

And, above all, I want to thank the Lord Almighty for making all the above acknowledged happen and for giving me the life and strength to achieve all what I have in life.

Dedication

I dedicate this work to my late father Joseph Patrick Tanyi (May God Almighty take good care of him), my beloved mother Anastasia Dinga and my beloved daughter Anastasia Ngella Yanu M. Alm.

SYNTHESIS, CHARACTERISATION AND APPLICATIONS OF BIMETALLIC NANOPARTICLES

Anicetus Muche Tanyi, Thesis Author

Dr. Sarah L. Horswell, Thesis supervisor

Abstract

The use of nanostructured materials has increased over the past decades and is attracting much attention. This has led to much enthusiasm in their studies across disciplines in chemistry, physics and biomedicine. Gold nanoparticles find applications in catalysis, as biosensors and cancer therapy, based on their optical properties.

Fabricating nanoparticles comes with challenges such as control of size and shape which entails choosing fabrication methods carefully. There are various methods for fabricating and characterising nanoparticles and their alloys.

This project has employed the versatile wet chemical synthesis to fabricate high aspect ratios, high yield gold nanorods and core-shell Au-Metal NRs. Powerful experimental techniques viz. UV-Vis NIR spectroscopy and electron microscopy (STEM) were employed to characterise the monometallic and bimetallic AuNRs.

AuNSs, AuNRs, Au@Pd NRs, Au@Pd NSs, Au@Pt NRs and Au@Rh core-shell nanorods were synthesised and characterised by one or both of the methods mentioned above.

The core-shell structures of gold with other precious metals studied in this work leads to enhanced electro-catalytic activity, which make them applicable to the DFAFCs and DMFCs to generate power for portable electronic devices.

These core-shell nanoparticles have proved to be CO tolerant in the electro-oxidation of methanol and formic acid investigated in this project.

Au@Rh has proved to be a good catalyst for oxygen reduction. This can make Rh a possible substitute for Pt in ORRs.

Keywords: Gold Nanorods, Core-shell, Palladium, Platinum, Rhodium, UV-Vis spectrophotometry, Cyclic voltammetry, Electro-catalysis, FA & Methanol electro-oxidation, CO-stripping.

List of Abbreviations

APTES	Aminopropyltriethoxysilane
AuNPs	Gold Nanoparticles
AuNRs	Gold Nanorods
AuNSs	Gold Nanospheres, core-shell
Au@Pd	Gold Palladium, core-shell
Au@Pt	Gold Platinum, core-shell
Au@Rh	Gold Rhodium, core-shell
Au@Pd/C	NRs Carbon Supported Gold Palladium
Au@Pt/C	NRs Carbon Supported Gold Platinum
Au@Rh/C	NRs Carbon Supported Gold Platinum
BSA	Bovine Serum Albumin
BTUD	Biotinyl-3,6,9-trioxaundecanediamine
CTAB	Cetyltrimethylammonium bromide
DFAFCs	Direct Formic Acid Fuel Cells
DMFCs	Direct Methanol Fuel Cells
EM	Electromagnetic spectrum
EO	Electrooxidation
FA	Formic acid
H _{ads/des}	Hydrogen adsorbed/desorbed
IgG	Immunoglobulin G
j/mA ^ cm ⁻²	Current density (j) in milliampere per square centimetre
LPB	Longitudinal Plasmon Band
MPA	Mercaptopropionic Acid
ORR	Oxygen Reduction Reaction
PGSTAT12	Potentiostat/Galvanostat
PVP	Polyvinylpyrrolidone
RDE	Rotating Disk Experiment
RPM	Revolutions Per Minute
SCE	Standard Calomel Electrode
SEM	Scanning Electron Microscope
SPR	Surface Plasmon Resonance
STEM	Scanning Transmission Electron Microscope

TCAB	Tetradodecylammonium Bromide
TEM	Transmission Electron Microscope
TPB	Transverse Plasmon Band
EXAFS	Extended X-Ray Absorption Fine Structure
XPS	X-ray Photoelectron Spectroscopy

TABLE OF CONTENTS

ACKNOWLEDGEMENT	i
ABSTRACT	iii
LIST OF ABBREVIATIONS	iv
CHAPTER1 INTRODUCTION	1
1.1 Nanoparticles	1
1.2 Gold Nanoparticles and their optical properties	2
1.2.1 AuNPs Size Determination from UV-Vis Spectra	3
1.3 AuNPs in Cancer Imaging and therapy	4
1.4 AuNPs in Biosensors Applications	5
1.5 Catalysis	6
1.6 Nanoparticles as catalysts	8
1.7 Synthetic Methods	8
1.7.1 The Template method	9
1.7.2 The Electrochemical Method	10
1.7.3 The Seeded Mediated Method	12
1.7.4 Thermal Decomposition of Transition-Metal Complexes	13
1.7.5 Synthesis in Molecular Beams	13
1.7.6 Synthesis by Co-Reduction	15
1.7.7 Radiolysis	16
1.7.8 Sonochemical Synthetic Method	17
1.7.9 Ion Implantation	18
1.7.9.1 In-Vivo Biogenesis	18
CHAPTER 2 EXPERIMENTAL TECHNIQUES	20
2.1 Electron microscopy	20
2.1.1 Transmission electron microscopy (TEM)	20
2.1.2 Scanning electron microscopy (SEM)	21
2.2 Ultraviolet-Visible near infrared spectrophotometry (UV-Vis NIR)	22
2.3 Electrochemistry	23
2.3.1 Cyclic Voltammetry	24

CHAPTER 3 EXPERIMENTAL	25
3.0 Materials and methods	25
3.1 Synthesis of Gold nanorods	25
3.1.1 Preparation of Seed solution	25
3.1.2 Preparation of Growth solution	25
3.1.3 Growth of Nanorods	25
3.1.4 Coating Au Rods with Pd (bimetallic rods)	27
3.1.5 Coating Au Rods with Rh (bimetallic rods)	27
3.1.6 Coating Au Rods with Pt (bimetallic rods)	28
3.2 Synthesis of Citrate stabilised Au nanospheres	28
3.2.1 Coating AuNSs with Pd (bimetallic AuNSs) Au-Pd bimetallic	29
3.2.2 Characterization of Particles AFM and TEM Studies	29
3.2.3 Coating Au Rods with Pt electrochemically by Cu UPD	29
3.2.4 Catalysis	31
3.2.4a Electrooxidation of Formic Acid and Methanol on Au@Pd and Au@Pt NRs	31
3.2.4b CO Stripping on Au@Pt Nanorods	33
3.2.4c Oxygen reduction by the RDE on Au@Pt NRs	33
CHAPTER 4 RESULTS AND DISCUSSION	34
4.1 Synthesis and characterization	34
4.1a AuNRs synthesis	34
4.1b Au nanospheres Synthesis and coating	38
4.1c Palladium coated AuNRs	39
4.1d Coating AuNRs and Au@Pd NRs with Rh	41
4.1e Coating Au NRs with Pt in aqueous solution	42
4.1f Coating Au NRs with Pt by the displacement deposition process; UPD of Cu	43
4.2 Electrochemistry	46
4.2.1 Electro-oxidation of Formic acid (HCOOH)	50
4.2.2 Electro-oxidation of Methanol (CH ₃ OH)	60
4.2.3 Oxygen Reduction Reaction (ORR) on Au@Pt NRs	65
4.2.3a ORR on Au@Pt/C NRs	65
4.2.3b ORR on Au@PRh/C NRs	66

4.2.4 Carbon monoxide (CO) Stripping	70
4.3 Summary	74
CHAPTER 5 CONCLUSIONS AND FUTURE WORK	76
Bibliography	78
Appendix	84

Chapter 1

Introduction

There has been increasing research interest in nanomaterials over the last decades. These Nanomaterials are becoming more and more important, finding applications in several areas such as chemistry and physics [1].

This project aims to produce high aspect ratio Au_{core}-M_{shell} (M = metal) rods of generous yields, measure the optoelectronic properties, compare the properties with theory and later test the rods for electrocatalytic activity. To understand better the topographical, optical properties and shape, characterisation techniques such as UV near -IR spectrophotometry and electron microscopy were employed. The following aspects will be examined briefly in the introduction: nanoparticles, gold nanoparticles and their applications in catalysis, cancer imaging and biosensors. The rest of the thesis will then include a chapter which deals with materials and methods where various methods employed in the fabrication of mono and bimetallic nanoparticles are briefly described. There will be a chapter that details the experimental procedures and methodologies adopted to synthesise monometallic and bimetallic gold nanorods, characterisation and tests run using the AuNRs (gold nanorods) in electro-oxidation reactions. Another chapter for the results and discussions which deals with the results obtained from the experimental and discusses them. And a final chapter will be a summary and conclusion of the project work and possible future work to be undertaken.

1.1 Nanoparticles

A nanometre is a billionth of a meter (10^{-9} m). A nanoparticle is therefore measured in nanometres. There are various shapes which nanoparticles assume such as spherical, hexagonal, ellipsoidal, pentagonal, cylindrical (rod-shaped), cubic, cuboid and triangular.

When used as building blocks to construct complex nanostructures such as nanowires both by themselves and nanoparticles they exhibit properties such as thermodynamic, catalytic, electronic and optical which are often different from those of their corresponding bulk materials [2, 4, 5].

Based on these interesting properties, nanoparticles find applications in fields such as catalysis, biomedicine and electronics, which has made them to be of great current interest and attractive for a wide range of applications [2, 3, 4, 5]. Applications of gold nanoparticles have been on the rise in many areas such as autocatalysis and hydrogen purification [6].

The major factors that determine the catalytic and surface activities of nanoparticles are their shape and crystallographic facets [3], while the optical properties are influenced by the nanoparticle size [3]. One of the important and challenging tasks over the last decades in the synthesis of nanoparticles has been control over their shape and size [3, 12]. These are two levels of sophistications, but through wet chemical synthesis, one can manage to meet these challenges. Nanoparticle size is easily controllable but shape control is always a challenge. This challenge however can be overcome by using an appropriate experimental condition. For instance, if the goal is to make rods, tubes or concentric core-shell structures, one can choose judiciously amongst different experimental conditions and additives to achieve that goal [11].

1.2 Gold Nanoparticles and their optical properties

The use of gold nanoparticles (sols) can be traced back as far as in ancient Egypt when gold sols were first used in staining glass. A solution of gold particles of diameter under 100 nm is wine red in color.

Optoelectronic devices such as transducers have been made particularly from gold nanowires [10]. Gold nanorods find usefulness in optoelectronic devices as well as catalysis, molecular biology and medicine, where much enthusiasm is being generated [5]. El-Sayed and coworkers in a recent work found that gold nanoparticles can be used as labels to target cancer cells [2, 5] owing to their surface plasmon resonance (SPR) enhanced light scattering and absorption [5].

By exercising close control over the aspect ratio (length/width) and shape of gold

nanostructures, their plasmonic properties can be tuned to make them applicable for imaging in the (near infrared) NIR and biosensing. Functionalised gold nanoparticles have been used for saccharide sensing by Geddes and co-workers [13], biotin sensing by Nath and Chilkoti [41] and thrombin sensing by Pavlov and co-workers [30].

Rod-shaped gold nanoparticles, nanorods, show two characteristic absorptions in the UV-Vis NIR at wavelengths in the proximity of 520 nm and 750 nm. The oscillation of conduction band electrons along the width of the rod, otherwise known as the transverse axis, generates the 520 nm peak and that along the longitudinal axis of the rod generates the peak around 750 nm.

1.2.1 AuNPs Size Determination from UV-Vis Spectra

The diameter of spherical gold nanoparticles can be computed from UV-Vis spectra using the formula derived by Wolfgang Haiss and coworkers [14].

They deduced that an absolute error of only 3% can occur when calculating the observed particle diameters, implying that the formula can conveniently be used to compute precise particle diameters ranging from 35 – 110 nm.

The wavelength of the surface plasmon resonance peak (λ_{spr}) is obtained from the UV spectra and used in the computation using the formula [14]:

$$d = \{\ln[(\lambda_{\text{spr}} - \lambda_0) / L_1]\} / L_2 \quad \text{Equation (1)}$$

d = particle diameter

λ_{spr} = wavelength at which the absorption peak occurs on the UV spectra

λ_0 = 512 nm experimentally determined

L_1 = 6.53 experimentally determined

L_2 = 0.0216 experimentally determined

For $d = 35$ nm then,

$$35 = \{\ln[(\lambda_{\text{spr}} - 512)/6.53]\}/0.0216$$

$$\{\ln[(\lambda_{\text{spr}} - 512)/6.53]\} = 0.756$$

$$[(\lambda_{\text{spr}} - 512) / 6.53] = e^{0.756} = 2.13$$

$$\lambda_{\text{spr}} = 525.9 \text{ nm}$$

For $d = 110$ nm,

$$\{\ln[(\lambda_{\text{spr}} - 512)/6.53]\} = 110 \times 0.0216 = 2.376$$

$$[(\lambda_{\text{spr}} - 512) / 6.53] = e^{2.376} = 10.76$$

$$\lambda_{\text{spr}} - 512 = 70.3$$

$$\lambda_{\text{spr}} = 582.3 \text{ nm}$$

The expression can therefore be used to estimate particle diameter only if the wavelength value of the surface Plasmon resonance assumes a value from 525.9 nm to 582.3 nm.

By using fit parameters, they determined from the theoretical values for $d > 25$ nm which are $\lambda_0 = 512$ nm; $L_1 = 6.53$ and $L_2 = 0.0216$, leaving d the particle diameter the only unknown. [14]

The particle diameter of the nanospheres that generated the spectrum in fig 4.1b can be calculated as follows;

$$\lambda_{\text{spr}} = 530 \text{ nm} , L_1 = 6.53 , L_2 = 0.0216$$

$$d = \{\ln[529 - 512/6.53]\}/0.0216 = \ln[17/6.53]/0.0216 = 44.3 \text{ nm}$$

1.3 AuNPs in Cancer Imaging and therapy

Cancer has been and is still responsible for 25% of all deaths in the developed countries. As such, developing a more accurate, sensitive and cost effective method for detecting and treating cancer is a pressing issue [5]. Nanoparticle-biomaterial composites have a tremendous potential in novel methods for detection, characterisation and therapy of cancer, based on their unique optical, thermal and electromagnetic properties.

Optical coherence tomography (OCT) and reflectance confocal microscopy (RCM) are

used in cancer detection based on the imaging of microanatomical features of diseased tissue but their ability to image changes associated with carcinogenesis is limited. Cancer biomarkers and optical contrast agents provide signals specific to molecules in the cancerous tissue, thereby giving both anatomical and molecular features of the disease.

Optical properties of gold nanoparticles leading to surface plasmon resonance-enhanced light scattering and absorption gives them the potential to be used as optical probes and labels for cancer diagnosis [5]. Cervical epithelial cancer cells (SiHa) which are known to overexpress the transmembrane glycoprotein, epithelial growth factor receptor (EGFR) have been imaged in a work by Sokolov et. al by employing immunotargeted Au nanoparticles [5].

Mie theory used to estimate and characterise the optical properties of metal nanoparticles predicts that the optical cross sections of gold nanospheres are of magnitude up to 5 orders higher than those of conventional dyes used. Rhodamine 6G for instance has an extinction coefficient of approximately $1.2 \times 10^5 \text{ M}^{-1} \text{ cm}^{-1}$ while gold nanospheres of diameter 40 nm have a molar absorption coefficient of approximately $7.7 \times 10^9 \text{ M}^{-1} \text{ cm}^{-1}$ both at absorption of 530 nm. This makes Au nanospheres (photostable and non-toxic [5]) superior over Rhodamine 6G (suffers from photobleaching [5]) to be used for biological and biomedical imaging [5]. Furthermore, gold nanoparticles allow a molecular-specific imaging and cancer detection when conjugated to ligands that are specifically targeted to biomarkers on cancer cells [5].

1.4 AuNPs in Biosensors Applications

Biosensors are designed using AuNPs by capping them with a thiolated biomolecule which causes a change in the optical absorption of AuNPs upon identifying the complementary biomolecule [30]. Aptamer functionalized AuNPs bind to thrombin, causing aggregation of gold nanoparticles giving rise to a red shift in the plasmonic peak. A test on the specific binding has been made by exposing aptamer functionalized Au nanoparticles to other proteins (BSA or IgG antibodies) which gave rise to no observable aggregation [30].

The figure below shows a detection pathway of thrombin on surfaces by the catalytic enlargement of thrombin-aptamer functionalized gold nanoparticles [30].

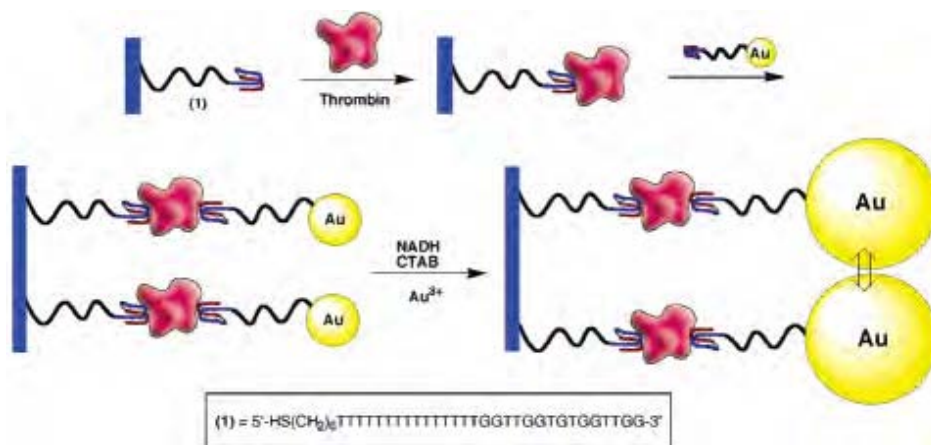


Fig 1.4 Detection of thrombin by aptamer-functionalized AuNPs [30].

In a similar manner, Nath and Chilkoti have used AuNPs to sense biotin. They used γ -APTES to make SAMs on glass, attached AuNPs on them, and then functionalized with MPA. They then functionalized the Au-MPA-APTES with (+)- BTUD. Results from UV-Vis spectra showed a shift and an increase in peak intensity relative to that of non-biotin functionalized AuNPs, confirming biotin binding [41].

1.5 Catalysis

Processes such as hydrogenation, carbonylation, hydroformylation, dehydrogenation, oxidation of petroleum combustion waste gases (catalytic converters for diesel and petrol engines) and more are frequently catalysed by metal particles as a heterogeneous catalyst. The electronic contribution of the metal particles to these catalytic processes is important [31].

In catalysis, bulk gold is usually considered to be weak in chemisorbing and therefore a weak catalyst, but when highly dispersed on a reducible metal oxide as support, the activity of gold nanoparticles in the oxidation of carbon monoxide (CO) increases even at low temperatures [8]. Advances have also been made in electrocatalysis, in the oxygen

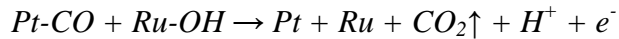
reduction reaction, in which gold nanoparticles deposited on a bulk gold electrode substrate has shown extraordinary activity [8].

The transition metals Pt, Pd, Ru and Rh are well known to catalyze several reactions. A decrease in selectivity and activity due to poisoning is an important issue to address to improve a catalyst's effectiveness. Platinum (Pt) for instance is used as a catalyst in the electrooxidation of methanol (CH₃OH) in the direct alcohol fuel cell (DAFC) technology and in ORR important in areas such as corrosion science and conversion of energy [45].

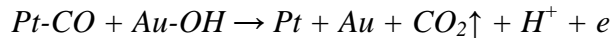
The pure metal Pt catalysts become poisoned by adsorbed CO intermediates and the active sites are blocked. This problem, however, can be solved by using the bifunctional mechanism, which is achieved by alloying Pt with a second metal. The bimetallic catalysts thus generated tolerate CO poisoning [8, 33, 34]. Garcke and co-workers have investigated the bifunctional mechanism using carbon supported platinum and Pt-Ru catalysts [33, 34]. The dehydrogenation processes in the CH₃OH oxidation produce Pt-CO_{ads}. On the other hand, a second metal such as (Ru or Au) contained on the anode reacts with water to produce OH_{ads} [33, 34, 44].



Following the bifunctional mechanism then, the CO species adsorbed on the platinum are oxidised by the following reaction [33, 34]:



For the Au-Pt nanorods, this would be



The catalyst surface is exposed again for catalytic activity as the CO poison is dealt with. Electrooxidation has been carried using HCOOH, CH₃OH and CH₃CH₂OH on some bimetallic catalysts to investigate their catalytic efficiency when alloyed.

1.6 Nanoparticles as catalysts

Catalyst poisoning is an issue that needs to be addressed in order to increase catalytic effectiveness and life of the catalyst. By alloying the precious and expensive metals with gold prevents CO poisoning. Gold makes it possible for CO to be oxidised to CO₂, when alloyed with other precious metals [28]. Gold (Au) alloyed with Pt generates bimetallic Au-Pt catalysts which are effective in the oxygen reduction and methanol (CH₃OH) and formic acid (HCOOH) electrooxidation which find great applications in the fuel cell technology [8,15]. Palladium can be used to catalyze the electrooxidation of formic acid (HCOOH) in the direct formic acid fuel cells (DFAFCs) desirable for the design of compact portable power sources [15]. Formic acid is thought to be an alternative for methanol and hydrogen in fuel cells as it is noted that there are some problems with the latter two with hydrogen difficult to store and methanol having a sluggish anodic oxidation kinetics and innate toxicity [15].

Zhou W. and Lee J. Y. recently reported the electrooxidation of HCOOH over Au-Pd nanoparticles [15]. They ran the experiment using bare gold particles only on carbon, palladium on carbon only and core-shell gold-palladium spherical particles. The scan rate was 5 mV s⁻¹ in their experiment, with potential scans initiated at -0.166 V (vs Ag/AgCl), after 15 min of CO adsorption and 15 min of electrolyte purging with flowing Ar. They observed that the Au-Pd particles were the major contributors towards the electrooxidation of HCOOH and in the oxidation of CO in the CO stripping scans [15], concluding that catalytic efficiency and CO tolerance are tremendously enhanced by the core-shell particles.

1.7 Synthetic Methods

Different methods have been used to generate gold nanoparticles of different aspect ratios. The template, electrochemical reduction and seeded mediated routes are most widely used as they give better yields. The template method involves depositing gold particles electrochemically within the pores of an alumina (Al₂O₃) or a polycarbonate template material followed by re-dispersion [11].

The electrochemical method employs an electrolytic cell with Au as a sacrificial anode and a Pt plate cathode [11]. In the seed mediated method, particles are grown by mixing two separately prepared; seed and growth solutions [11].

For coating of nanoparticles, Roustom B. El and coworkers [8] have deposited bimetallic Pt-Au on boron doped diamond substrate for application to the oxygen reduction reaction [2,8]. They used a sputtering technique to deposit gold on boron-doped diamond. Platinum was later deposited electrochemically on the gold nanoparticles [8].

Bimetallic core-shell nanoparticles can be synthesised directly by several methods such as the *molecular beam* in which atoms are vaporized, nucleated and grown. Under the molecular beam is the condensation metal cluster source which includes the ion sputtering, pulsed arc cluster ion source, laser vaporization and magnetron sputtering processes.

Other synthetic methods that can be employed to synthesise bimetallic nanoalloys are the *chemical reduction* method which involves reducing metal salts [6, 17, 27], reacting preformed clusters in a successive reduction scheme [1, 2] and reducing an appropriate mixture of salts in a co-reduction process [16, 17]. These methods are described further in the following pages.

There is a rich literature on the subject for the project. The interested reader is referred to referenced reviews for more information on the methodologies employed in fabricating nanoparticles and their alloys ; references 1, 2, 3, 8,10 and 11 are a few that cover aspects in the area. The three most widely used synthetic methods reviewed in the literature are briefly described below.

1.7.1 The Template method

Small amounts of Ag or Cu is sputtered on a nanoporous template made of alumina (Al_2O_3) or a polycarbonate to provide a conductive film.

Gold particles are deposited electrochemically within the pores. The template synthesised gold particles are then re-dispersed in water or an organic solvent, followed by

stabilization with a polymer. Size control can be achieved [11] and desired length of rod can be obtained by varying the quantity of charge used for deposition [10].

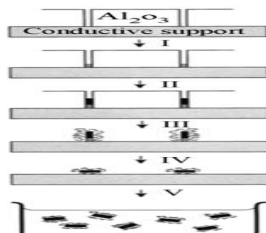


Fig 1.7.1 Schematic of nanoparticle synthesis by template route [11].

1.7.2 The Electrochemical Method

The electrochemical method [16, 17] can be used to generate metal atoms from the bulk metal by electrodeposition at liquid-liquid interfaces.

In a work by Reetz and Helbig an electrochemical method was proposed to oxidise the bulk metal and reduce the metal ions to prepare nanoparticles stabilized by tetraalkylammonium salt, with particle size selectivity controlled by the current density [17].

An electrolytic cell set up consists of two metal electrodes of the bulk metals from which atoms are created to form the nanoparticle.

Bimetallic nanoparticles such as Pd-Pt, Ni-Pd, Fe-Co, Fe-Ni can be prepared electrochemically [16, 17].

This involves inserting metal plates of the two bulk metals into an electrolyte, which both serve as anodes. The electrolyte contains a salt of tetraalkylammonium which acts as a stabilizer. The cathode is a platinum plate.

The metal ions are oxidised to their corresponding ions at the anode, and the Pt cathode produces electrons. The metal ions are then reduced by these electrons to the metal atoms, which aggregate to form the bimetallic nanoparticles, which are stabilized from further aggregation by the tetraalkylammonium salt in the electrolyte [17].

Figure 1.7.2.1 below [17] is a schematic representation of the single electrolytic cell used to generate bimetallic nanoparticles electrochemically. This method has also been used by Wang and coworkers to produce high yields of gold nanorods stabilized by CTAB which also served as a supporting electrolyte, with a sacrificial Au anode and a Pd

cathode [9].

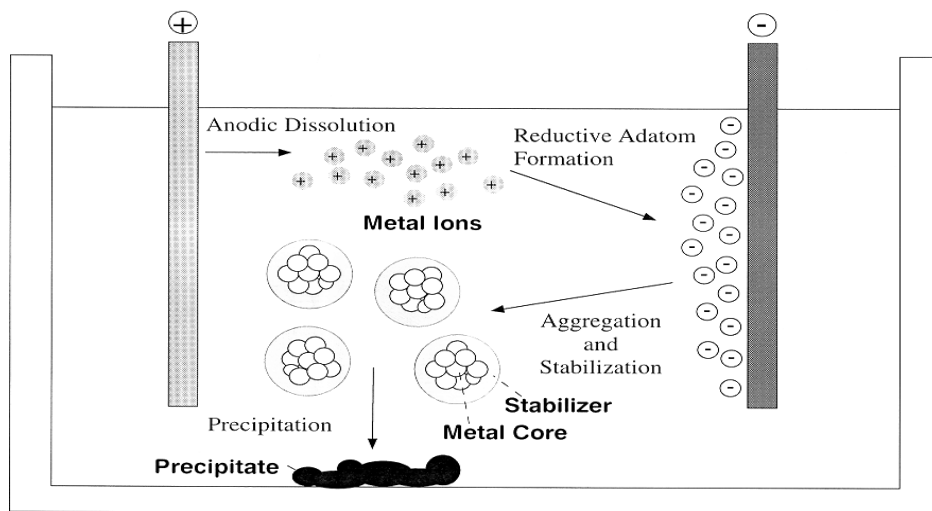


Fig 1.7.2.1 A schematic showing showing the formation scheme of electrochemically produced metal nanoparticles [17].

This method can also be used to fabricate nanoparticles, both monometallic and bimetallic in solutions.

To synthesise a monometallic nanoparticle, an electrolytic cell is made up of a sacrificial Au anode, Pt cathode and an electrolyte made by mixing cationic surfactant $C_{16}TAB$ with small amount of tetradodecylammonium bromide TCAB, a cosurfactant. A silver plate is gradually immersed behind the Pt cathode, this helps increase the yield and aspect ratio but how it does it is not known [11]. The cell is placed in an ultrasonic bath [11] at $36^{\circ}C$. At the anode, gold ions are produced which react with the bromide ions from CTAB to form $AuBr_4^-$. The cationic surfactants then complex the $AuBr_4^-$ and transport it to the cathode where electrons reduce the gold, followed by nucleation and sonication to break the rod off the cathode surface if that is where reduction occurs. The rods produced are stabilized by the CTAB. A schematic representation of the electrolytic cell is shown in fig 1.7.2.2 below.

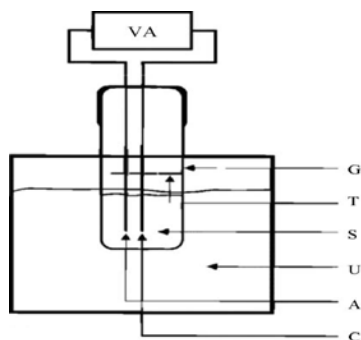


Fig 1.7.2.2 Schematic of the electrochemical set-up for the preparation of gold nanorods.

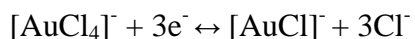
VA=power supply; G=glassware electrochemical cell; T= teflon spacer; S=electrode holder; U= ultrasonic cleaner; A=anode; and C=cathode [11].

1.7.3 The Seeded Mediated Method

This method has been used as far back as the 1920s to grow monodispersed colloid particles by chemical reduction of metal salts [11].

For the growth of gold nanorods, two solutions- a seed and a growth solution- are prepared.

Gold salt is mixed with the surfactant then reduced with a strong reducing agent such as NaBH_4 to Au (0) to get the seed solution.



A growth solution is prepared with CTAB and gold salt. A mild reducing agent such as ascorbic acid reduces Au^{3+} to Au^+ in the presence of CTAB according to the equation below [11].



This implies that no gold particles are formed in the growth solution until mixed with the seed solution. This solution provides extra electrons from their excess to reduce the Au (I) to Au (0) and initiate growth of particles and rods.

1.7.4 Thermal Decomposition of Transition-Metal Complexes

Organometallic transition metal complexes and clusters containing the two metals can be decomposed thermally to produce high yields of bimetallic nanoparticles in the presence of stabilizing ligands such as polyvinylpyrrolidone (PVP).

This method would be exemplified by bimetallic nanoparticles synthesised recently by Thomas, Johnson, and co-workers [16].

Organometallic precursor clusters with carbonyl and phosphine ligands anchored within silica micropores were heated in vacuum conditions to about 473 K for two hours. Metal atoms aggregate on cooling to form bimetallic nanoparticles stabilized by the ligands.

Examples of bimetallics produced includes $\text{Ru}_{12}\text{Ag}_4$, $\text{Ru}_{12}\text{Cu}_4$ and Ru_6Sn [16].

1.7.5 Synthesis in Molecular Beams

Bimetallic nanoalloys can be obtained by producing atoms of the monometallic targets by vaporization with molecular beams (Fig. 1.7.5.1). These atoms condense and nucleate into clusters. More atoms are then added to the already formed ones enabling them to grow. The small clusters containing the two target metallic elements then aggregate to form the bimetallic nanoalloy [16].

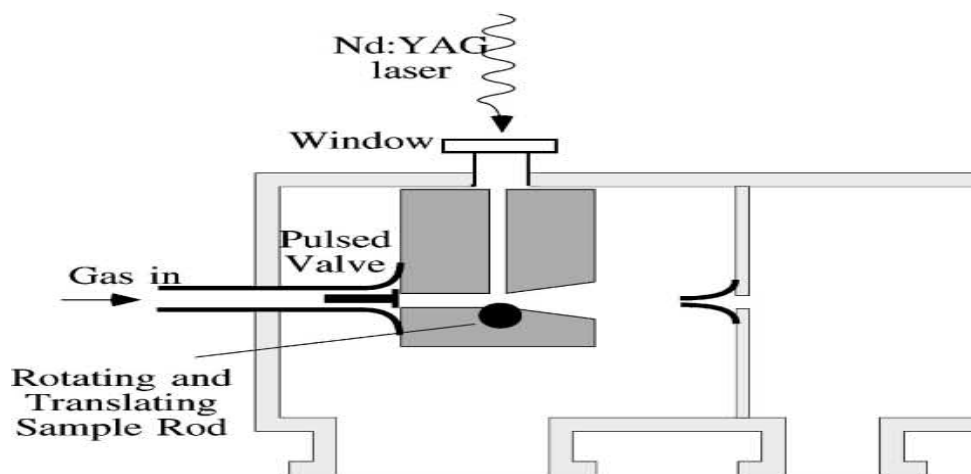


Fig 1.7.5.1 Laser beam source for evaporation of monometallic targets [18].

The target monometals can be vaporized by using a laser beam as illustrated by Figure 1.7.5.2.

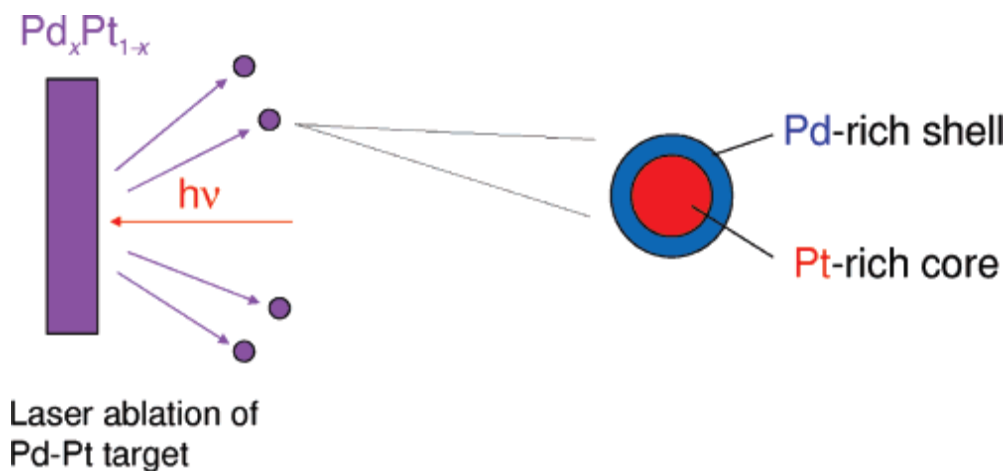


Fig 1.7.5.2 Formation of Pt_{core}-Pd_{shell} particles by laser ablation of Pd-Pt alloy rod [16].

There is a pulsed arc ion source [16, 18] where an electrical discharge is passed through them, elucidated by the following diagram

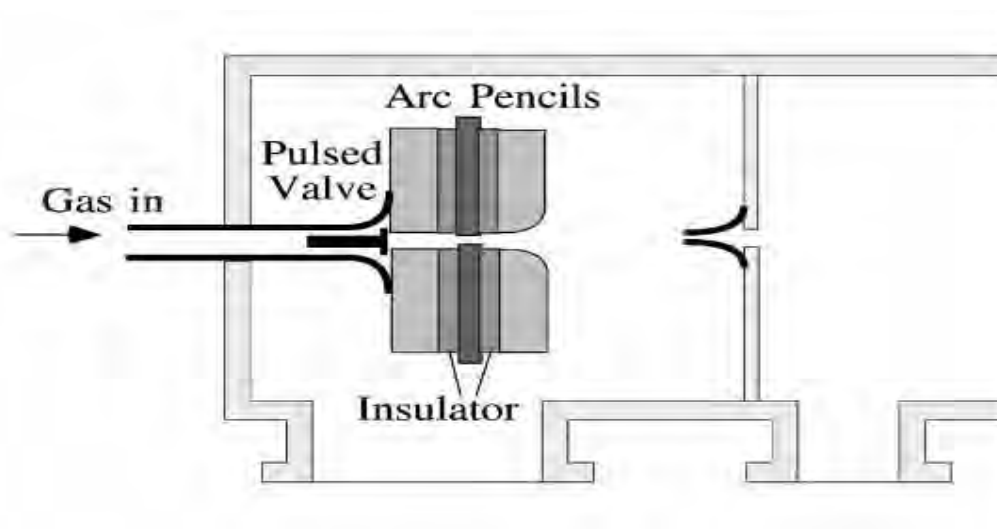


Fig 1.7.5.3 Schematic of the pulsed arc cluster ion source [18].

or an ion sputtering in which the monometallics are bombarded with Kr⁺ or Xe⁺ gas ions at high energies of about 30 keV and a current of about 10 mA.

Liquid nitrogen is used for cooling and aggregation follows (see Fig 1.7.5.4).

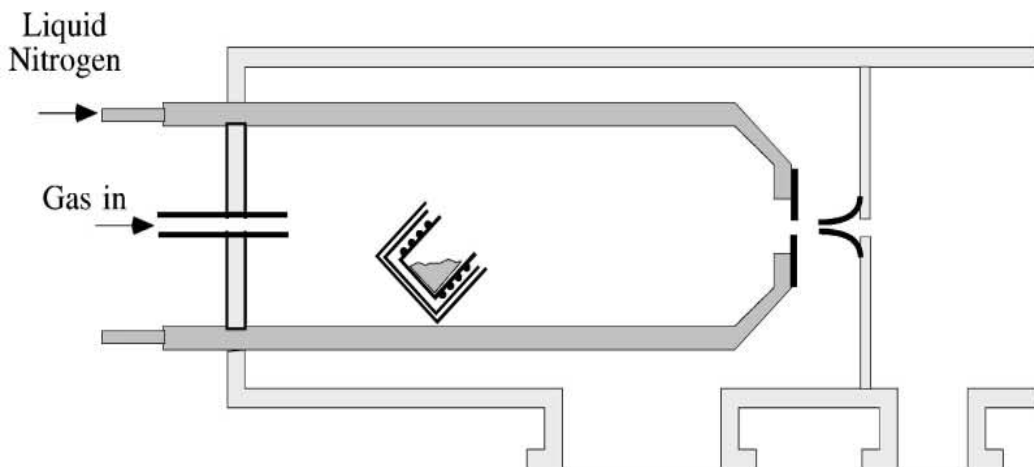


Fig 1.7.5.4 Source for gas aggregation [18].

$\text{Pt}_{\text{core}}\text{-Pd}_{\text{shell}}$ nanoparticles have been synthesised by laser ablation of a Pd-Pt alloy rod using the Nd-YAG laser (see Fig 1.7.5b) [16, 26].

1.7.6 Synthesis by Co-Reduction

This is a chemical method which can be used to generate nanoalloys and at the same time control the chemical core-shell ordering using a surfactant.

The method involves reducing salts of the metals in solution with reducing agents such as sodium borohydride NaBH_4 .

The metal salt is reduced to generate metal atoms which then collide in solution with metal atoms, or clusters to form an irreversible seed of metal nuclei on which other clusters will grow [19]. The metal with a higher redox potential preferentially precipitates and the other then precipitates on it giving a core (higher potential metal) shell (lower redox potential metal) arrangement.

An example of a nanoparticle prepared by this method is the $\text{Ag}_{\text{core}}\text{-Pd}_{\text{shell}}$. Palladium has a more positive redox potential (a higher electron affinity), a smaller atomic radius, a higher cohesive energy, a higher surface energy and higher electro negativity than silver which normally would give a $\text{Pd}_{\text{core}}\text{-Ag}_{\text{shell}}$ arrangement with palladium occupying the core position [16]. The ordering however can be reversed by co-reducing them in the presence of ammonia. This leads to a stronger binding between NH_3 and palladium

(which has a more positive redox potential) thereby stabilizing the reverse core-shell clusters [16]. Having a higher electronegativity, Pd has a higher electron affinity than Ag and therefore will readily bind to a nucleophile (NH₃ in this case) and be reduced. The diagram below illustrates the synthetic pathways of the chemical metal salt reduction process [19].

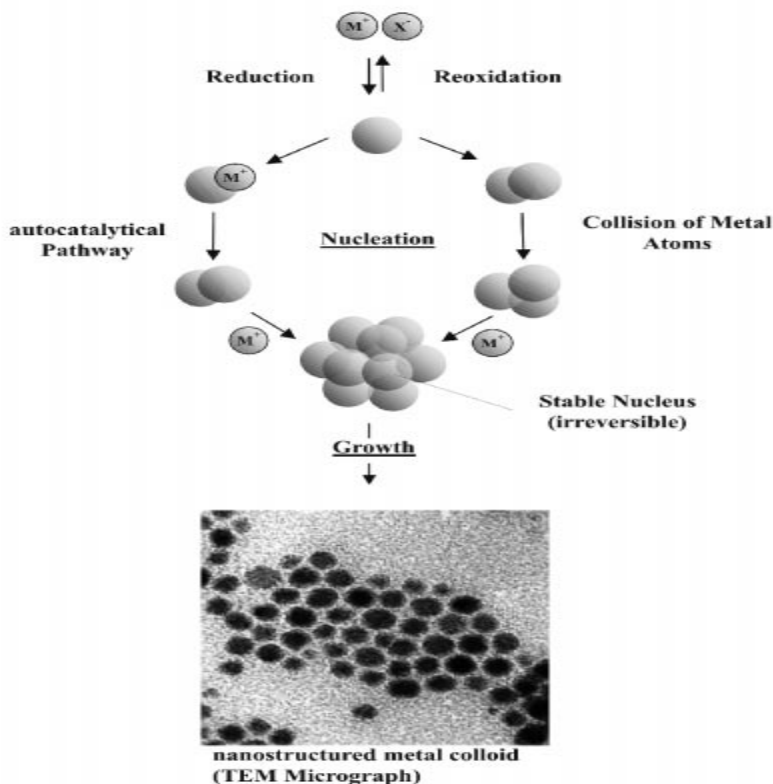


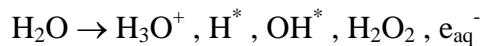
Fig 1.7.6 Formation of nanostructured metal colloids by the salt reduction method [19]

1.7.7 Radiolysis

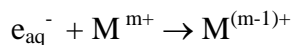
Bimetallic transition metal clusters can be generated efficiently by reducing metal ions in aqueous solution by radiolysis [16, 20].

Ag-Pt nanoclusters have been prepared by radiolysis of aqueous solutions prepared with AgNO₃, Ag₂SO₄, H₂PtCl₆, K₂PtCl₄, and 2-propane [9].

The aqueous solution is exposed to gamma irradiation to produce solvated electrons from water radiolysis as follows [20]:



The solvated electrons produced reduce the metal ions to the atoms according to the equations [20]:



and



Coalescence of the metal atoms then occur to form aggregates [20]



In this synthetic method the more noble metal is normally reduced preferentially but factors like gamma ray dose which determines the rate of radiolysis, the relative concentrations of the two metals, the nature of the ligands coordinated to the metal ions and the inter-ion electron transfer determine if nanoalloyed particles or core-shell clusters would be formed [16].

The chemical ordering then can be controlled or determined by the dosage of the gamma rays.

A high dose of gamma irradiation can be supplied if mixing is desired with a few exceptions like Ni-Pt, and Pt-Ag where mixing is favored at low gamma dose rates and it goes with atomic ordering.

Other examples of nanoalloys produced by this method are the Ni-Pt, Ag-Au, Cu-Ag which have been deposited from Ag halide emulsions [16].

1.7.8 Sonochemical Synthetic Method

This method involves subjecting aqueous solutions of the monometallic ions to high intensity ultrasound radiation.

Core-shell Au-Pd [16] and Fe-Co [21] nanoalloys have been synthesised sonochemically. Fe-Co nanoalloy synthesis involved irradiating solutions with relative concentrations of $\text{Fe}(\text{CO})_5$ and $\text{Co}(\text{CO})_3\text{NO}$ [21].

A high intensity ultrasonic probe was used to irradiate the solutions in dry decane, at 273 K, and under argon for 3 hours.

Irradiation led to the formation of black powders which were filtered and washed in a glove box.

Fe-Co nanoalloy was produced after treatment with hydrogen H₂ [21].

For the synthesis of Au_{core}-Pd_{shell} which was a recent finding by Kan et al., successive deposition in the sonochemical generation of core-shell nanoalloy is preferred to simultaneous deposition [16]. This is as a result of the influence of the influence by the characteristics of the sonochemical experiment, which include microjet stream and effective stirring [16].

1.7.9 Ion Implantation

The ion implantation method involves the use of high energy (approx. 100 keV) metal ion beams to sequentially implant two different metal ions in silica to obtain bimetallic nanoalloys [16, 22, 23, 24].

Ion implantation has been used to synthesise Au-polyimide nanocomposite films [24], indium nanoclusters [22], and Ag-Au, Cu-Pd, Cu-Au nanoalloys [16, 23].

Au-Cu and Pd-Cu nanoalloys were synthesised at the INFM laboratories in Legnaro in Italy by sequentially implanting the Au/Cu and Pd/Cu metal ions in sliced silica using an M⁺ ion beam of 90 keV, 190 keV and 130 keV for Cu, Au and Pd respectively, using a current density of under 2 μA cm⁻² and implantation fluence of 3 x 10¹⁶ ions cm⁻² [23].

In order to increase the probability of alloy formation, the most reactive ion species was the last to be implanted.

The next step after implantation was the annealing process and this was done by heating the two systems in a reducing condition using a 1:24 mixture of H₂ and N₂ for 1 hour at a temperature of 1173 K to form the crystalline nanoalloys [23].

1.7.9.1 In-Vivo Biogenesis

This is a biosynthetic method in which metal ions are reduced biologically by microorganisms to the zerovalent metal [16, 25].

Ni-Ti clusters were synthesised using a 5 mg mL⁻¹ suspension of processed powdered milled alfalfa in an ultrasonic bath to reduce Ti⁴⁺ and Ni³⁺ into clusters of Ti-Ni.

The 5 mg mL⁻¹ alfalfa suspension and a buffer solution were mixed and centrifuged in an

ultrasonic bath [25]. The function of the buffer was to control the pH.

Already prepared solution mixture of known concentrations of Ti^{4+} and Ni^{3+} ions from their corresponding complex salts was added to the alfalfa/buffer centrifuged mixture.

An ultrasonic bath was used to homogeneously mix the two solutions followed by a 30 min centrifugation.

The resulting mixture was then left to stand for 2 hrs at room temperature. The reaction mixture was separated after a 30 min centrifugation to obtain a colloidal suspension of Ni-Ti which was left to stand for 2 days [25].

Cell bound Pd nanoparticles were also made by Mackaskie and co-workers. They reduced aqueous Pd (II) to Pd (0) using bacterial hydrogenases. The Pd nanoparticles obtained are said to be very effective in reducing chromium from the +6 to +3 state. This reduction is not effectively done by chemically reduced palladium. Such bio-formed Pd nanoparticles find important applications in bioremediation of industrial wastes and Bio-Pd⁰ particles for hydrogen fuel cell applications [40].

Chapter 2

Experimental Techniques

2.1 Electron microscopy

Electron microscopy is an experimental imaging technique which employs the use of high energy electrons generated from a source and accelerated to the sample. The operating principle is similar to that of a light microscope with the difference that high energy electrons are used for imaging instead of light.

There are two types of electron microscopes used for imaging.

These are the transmission electron microscope (TEM) and the scanning electron microscope (SEM). Both techniques are used to characterise nanoparticles.

2.1.1 Transmission electron microscopy (TEM)

This characterisation method is used to obtain images of nanoparticles and determine their sizes.

In a TEM, the electron beam from an electron source made of tungsten or LaB_6 passes through a sample which must be ultra thin, interacting with it on their way through [35]. The transmitted electrons then form an image on an imaging device, with the help of specific lenses, which gives information about the sample.

Various signals are obtainable from this microscopic technique used to form images.

The signals include: transmitted electrons, inelastically scattered electrons which give kikuchi patterns, elastically scattered electrons which give dark field images and characteristic x-rays used for chemical analyses.

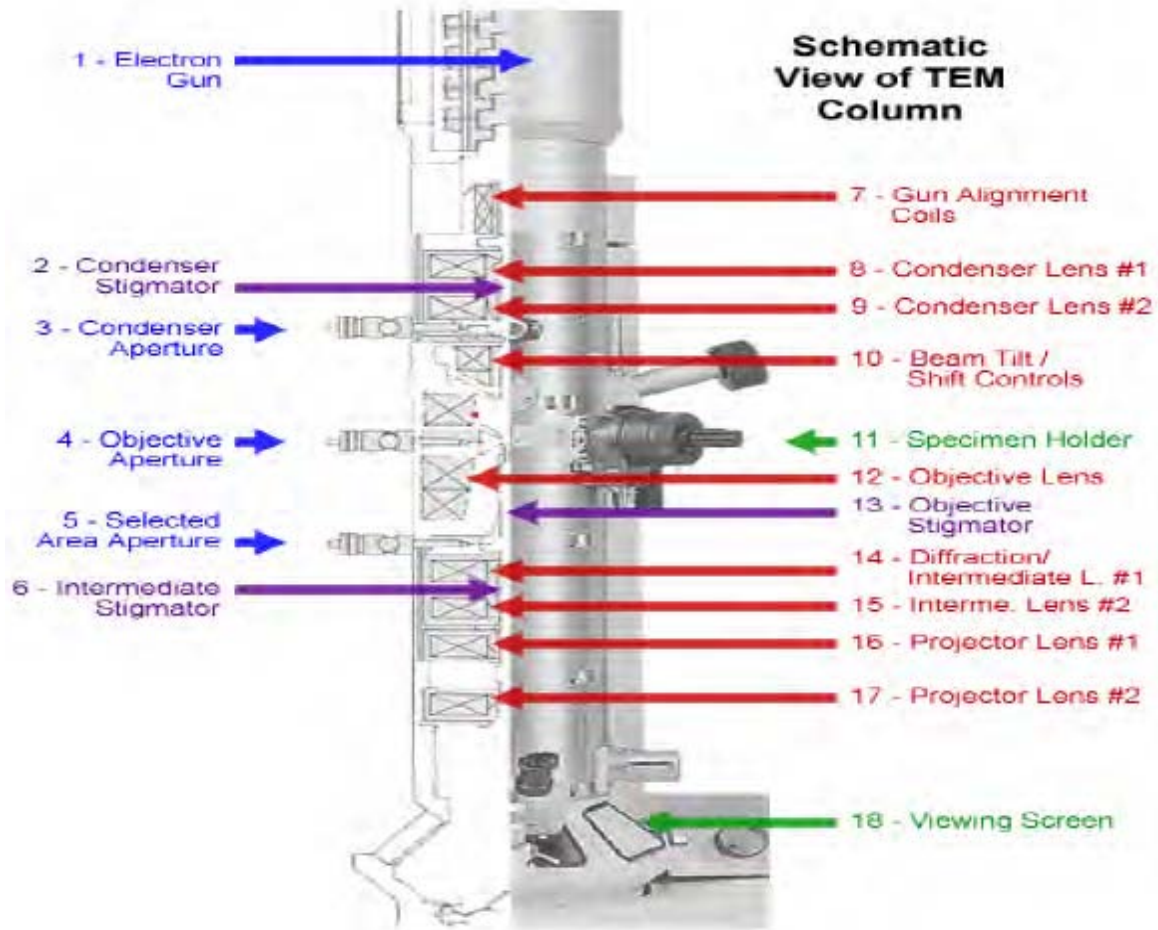


Fig 2.1.1 A schematic showing the various components of a Transmission Electron Microscope (lecture notes)

2.1.2 Scanning electron microscopy (SEM)

These signals include: the secondary electrons (true electrons) [36], back scattered electrons (BSE), Characteristic x-rays, light (cathodoluminescence), specimen current, auger electrons and Transmitted electrons [36].

The individual signals arise as a result of a particular interaction between the incident electron beams with the nanoparticle specimen under examination thereby providing structural information about the nanoparticles in the specimen [37].

The diagram below is a schematic showing what happens when the incident electrons interact with the sample.

When the electron beam strikes the sample, both **photon** and **electron** signals are emitted.

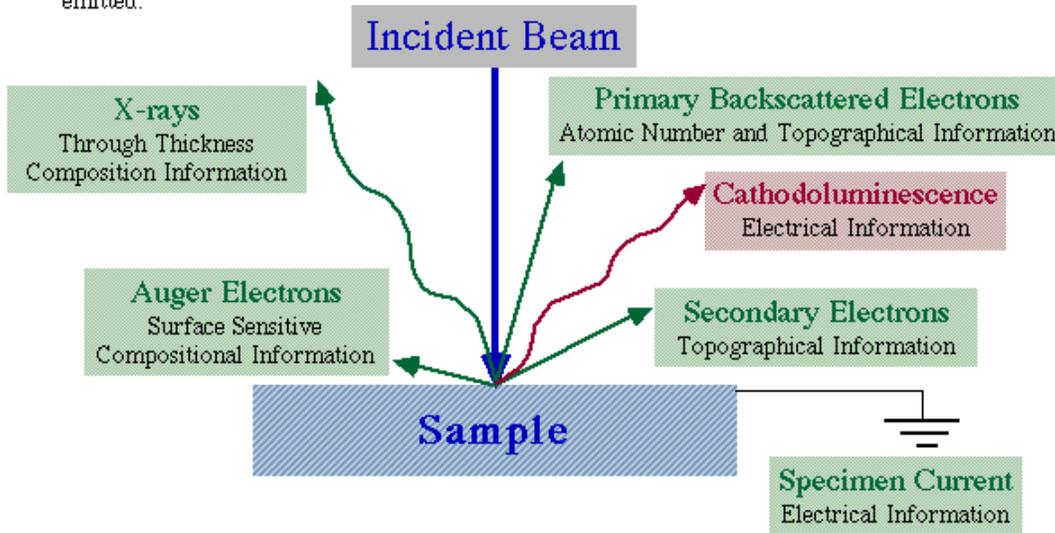


Fig 2.1.2 Schematic showing the various signals obtained when an electron beam interacts with a sample in an SEM (lecture notes)

2.2 Ultraviolet-Visible near infrared spectrophotometry (UV-Vis NIR)

This is a measurement technique which involves the spectroscopy of photons in the ultraviolet and visible region of the EM spectrum. Spectroscopy is the use of visible light that has been dispersed for instance by use of a prism according to wavelengths. A photon will be defined here as a form of EM radiation.

Absorption measurement of the UV and visible radiation by species in solution is a quantitative analytical method. This is one of the most widely used analytical method in laboratories [42].

For a complete analysis to be done, a sample with suitable absorbing species is first made. With the knowledge of the wavelength region in which the species absorb, the next step is to select a suitable wavelength range to ensure an accurate measurement.

The third point is to determine the ratio of the light intensity transmitted through the analyte to that of the reference solution. These bases of measurement are governed by the Beer-Lambert law which is defined thus:

$$A = \log (I_0/I) = -\log (T) \quad \text{Equation (2)}$$

A = absorbance

T = transmittance.

I_o = intensity of incident light

I = intensity of transmitted light

In this technique, a spectrophotometer with either single beam or double beam is used in measurements. The analyte is most often in liquid form, though sometimes solid surfaces may be analysed.

This technique is used to characterise AuNPs in homogeneous solutions.

The spectrometer consists of five component areas [42]:

- the radiation sources which cover the required wavelength range
- the monochromator to select a narrow band of wavelengths
- the sample cell compartment with holders for the sample and blank cuvettes
- the photodetector with devices to measure the intensity of the light transmitted through the analyte and blank in the cells
- the display and chart recorder which record the quantity measured in a suitable form.

The sample cell used in this instrument is made of silica of 1 cm path-length and a volume of 4 cm³.

2.3 Electrochemistry

Electrochemistry is the study of chemical reactions taking place in a solution involving charge transfer. The reactions occur on the interface between an electron conductor (electrode) and an ionic conductor (solution), which is in contrast to many chemical measurements involving homogeneous bulk solutions [38]. The electron conductor can be a metal or semiconductor (electrode) and the ionic conductor is the electrolyte. This study involves the transfer of electrons between the electrode and the electrolyte, qualifying the electrode surface as a junction between an ionic and an electronic conductor.

There are practically two classes of electrochemical cells.

- Galvanic electrochemical cells which are used to produce electricity and

- Electrolytic cells which consume external electrical energy.

Potentiometric and potentiostatic measurements are the two principal types. At least two electrodes and an electrolyte are needed in either of the two, and a combination of these three constitutes an electrochemical cell.

The two types of electrodes are the working and the reference electrode.

The working electrode, otherwise known as the indicator electrode, responds to the target analytes and the reference electrode operates at a constant potential independent of the properties the solution exhibits.

- a.) In potentiostatic techniques where the potential is controlled, charge transfer occurs at the electrode-solution interface, based on no zero current situations or dynamic situations. In this technique, the potential of the electrode is used to drive an electron transfer reaction which produces a current that is measured [38].
- b.) The potentiometry technique on the other hand is a zero current or static technique. Here, the potential established across a membrane is measured and information about the composition of the sample is obtained.

For high selectivity to be imparted, different types of membrane materials have been developed which possess different ionic recognition processes [38].

2.3.1 Cyclic Voltammetry

Cyclic voltammetry is a measurement technique used to acquire qualitative information about electrochemical reactions. It is the most widely used technique in that category. This technique has the ability to provide considerable information on the kinetics of heterogenous electron transfer reactions, adsorption processes and on thermodynamics of redox processes within a very short time.

In this technique, the potential of a stationary working electrode in an unstirred solution is scanned linearly using a triangular waveform.

A potential is applied to the electrode, and the potentiostat measures the current resulting from this applied potential during the potential sweep. The cyclic voltammogram often abbreviated CV, is the plot of the resulting current versus the potential [38].

An example of a reaction that can generate a CV is an electro-oxidation reaction.

Chapter 3

Experimental

3.0 Materials and methods

Cetyltrimethyl ammonium bromide ($C_{16}TAB$) $C_{19}H_{42}BrN$ known also as CTAB; (Acrōs), sodium borohydride $NaBH_4$; (Riedel-de Haën), silver nitrate $AgNO_3$ (Sigma Aldrich), tetrachloroauric acid (49 wt.% gold) $HAuCl_4 \cdot xH_2O$; (Alfa aesar), trisodium citrate $Na_3C_3H_5O(CO_2)_3$; (Alfa aesar), potassium tetrachloropalladate K_2PdCl_4 (Alfa Aesar), copper (II) sulfate pentahydrate $CuSO_4 \cdot 5H_2O$; (Fluka), potassium tetrachloroplatinate K_2PtCl_4 (46.87 wt% Pt); (Alfa aesar), sodium hexachlororhodate (17.27 wt% Rh); (Alfa aesar), ascorbic acid $C_6H_8O_6$ (Acrōs), Carbon Black VULCAN XC72 (Cabot Corp.) and Nafion (Sigma Aldrich) were the compounds used.

Water used throughout was purified by a MilliQ Granulator System (resistivity of 18.2 $M\Omega$ cm, TOC \leq 4 ppb).

All glassware was cleaned thoroughly by boiling for 1 hr with a 50:50 mixture of concentrated sulphuric and nitric acid, followed by thorough rinsing with milli-Q water to eliminate any possible metal contaminant.

UV-Vis spectra were measured with a double beam Camspec M550 model UV-vis spectrophotometer in silica cuvettes of path length 1 cm. A double beam spectrophotometer with Tungsten-Halogen and Deuterium light sources, Littrow type monochromator with 1200 lines/mm grating, Silicon Photodiodes and a wavelength range of 190 – 1100nm was used to analyse all samples in this work.

STEM and SEM measurements were with an aberration-corrected JEOL 2100F operating at 200KV, with a FEG electron source. Electrochemical reactions were performed on an Autolab potentiostat/galvanostat and E&G Princeton Applied Research potentiostat/galvanostat model 273A.

3.1 Synthesis of Gold nanorods

Gold nanorods were synthesised using the approach published by Pérez-Juste and co-workers [11]; a modification of the approach by Nikoobakht and El-Sayed [2], which was

also used later.

Two solutions were prepared, one seed solution and one growth solution.

The seed solution was made up of a mixture of CTAB and tetrachloroauric acid in water and sodium borohydride as a reducing agent. The concentrations of gold and CTAB in the final solution were 0.00025 M and 0.1 M, respectively.

3.1.1 Preparation of Seed solution

A 100 ml aqueous solution containing HAuCl_4 (0.00025 M) and CTAB (0.1 M) was prepared in a conical flask at room temperature. 6 ml of a freshly prepared, ice cold NaBH_4 (0.0189 g in 50 mL H_2O = 0.01 M) solution was then added to the seed solution and heated at 44°C while stirring for 15 minutes. Heating ensured the removal of excess sodium NaBH_4 . The color changed from orange to brownish yellow.

3.1.2 Preparation of Growth solution

A 250 ml aqueous solution containing HAuCl_4 (0.0005 M), CTAB (0.01 M) and AgNO_3 (0.00004 M) was prepared in a 250 ml volumetric flask.

3.1.3 Growth of Nanorods

For the growth of nanorods, 10 ml of the growth solution was placed in each of five 20 ml vials.

Next, 0.07 mL of 0.1 M ascorbic acid was added into each solution and thoroughly mixed. The color of the solutions changed from orange to colorless. The following volumes of seed solution were then added into the resulting 5 solutions in the vials: 0.006 mL, 0.012 mL, 0.024 mL, 0.050 mL and 0.150 mL.

Gold nanorods started growing within 10 to 20 minutes as the solutions gradually turned blue. The solutions were left undisturbed for 96 hours, after which time UV-Vis spectra were measured. Nanorods grow by the following mechanism (see Fig 3.1.3). Gold ions attached to the CTAB micelles are transferred to the growing seed particles controlled by the doublelayer interaction [11].

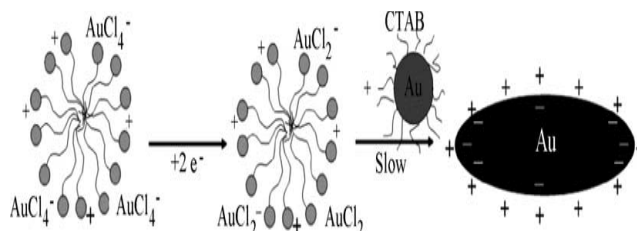


Fig. 3.1.3 Transport of Au ions bound to C16TAB micelles to growing seed particles [11]

3.1.4 Coating Au Rods with Pd (bimetallic rods)

Core-shell gold-palladium nanorods were generated following a modified wet chemical synthetic recipe by Jia-wen Hu and co-workers. The source for palladium in the synthesis was K_2PdCl_4 and not H_2PdCl_4 .

Palladium coated gold nanoparticles/nanorods were prepared as follows:

A portion (3 mL) each of the 5 batches was centrifuged at 3000 rpm for 1 hour to remove excess CTAB and nanospheres. The supernatant was carefully removed with a pipette. The pure gold nanorod precipitate was re-dispersed in milliQ water made up to 1.5 mL (7.5×10^{-6} moles Au).

Next; 1.5 mL of the previously prepared 1 mM K_2PdCl_4 (1.5×10^{-7} moles Pd) was added to each Au nanorod solution and mixed. This was followed by the addition of 3 mL of freshly prepared 0.1 M ascorbic acid.

3.1.5 Coating Au Rods with Rh (bimetallic rods)

Gold rods were coated with rhodium in a similar manner as with palladium. A 1 mM solution of sodium hexachlororhodate ($Na_3RhCl_6 \cdot 12H_2O$) was prepared by dissolving 0.086 g of the salt in 25 mL ultra pure water. Next, 2 mL of the prepared Au NRs solution was mixed with 2 mL of the Rh solution and properly mixed. 1 mL of freshly prepared ice cold $NaBH_4$ (0.01 M) was then added. The colour of the solution darkened indicating formation of Rh particles. UV-Vis measurement was taken an hour later to examine the spreading of Rh on the Au rods. Later, 1 mL of the Au@Rh rod solution was properly mixed with 1 mL of Rh solution followed by the addition of 1 mL of 0.01 M of freshly prepared ice cold $NaBH_4$. UV-Vis measurement was carried out on the resulting solution to see how well the Au rods were covered.

Rhodium nanoparticles were also synthesised by reducing 3 mL of the solution with 1.5

mL of the freshly prepared NaBH_4 solution. The colour changed from light pink to pale black on addition of NaBH_4 , indicative of particle formation. UV-Vis measurement was also carried out on the particles.

3.1.6 Coating Au Rods with Pt (bimetallic rods)

Bimetallic Au-Pt rods were made in aqueous solution with ultra pure water. A platinum solution of concentration 1 mM was prepared by dissolving 0.01335 g Potassium tetrachloroplatinate (II), K_2PtCl_4 salt in 15 mL ultra pure water.

Next, 1.5 mL of the already made Au NRs solution was placed in a 10 mL vial. This was followed by the addition of 1.5 mL of the pale yellow platinum salt solution. The solutions were properly mixed by swirling and left to stand for a few minutes. 1 mL of 0.01 M ice-cold freshly prepared NaBH_4 solution was then added and mixed. The solution turned to grey indicating the reduction of Pt to form particles.

UV-Vis NIR measurements were made 20 hours later.

An additional layer of platinum was added on the Au@Pt rods by adding 1mL Pt salt solution followed by reduction with 0.5 mL of, yet again, a freshly prepared, ice-cold NaBH_4 (0.01 M) solution. UV-Vis measurements were measured two hours later.

3.2 Synthesis of Citrate stabilised Au nanospheres

Citrate-stabilised spherical gold nanoparticles were synthesised and used to monitor how changes in the UV-Vis NIR spectra occurred when different volumes of the sol were added to a fixed volume of a palladium solution. The recipe by Kundu et al. [32] was followed with a slight modification.

To prepare the citrate stabilised gold sol, 5 mg of gold salt (HAuCl_4) was dissolved in milliQ water and made up to 50 mL, giving a concentration of 2.5 mM. 4 mg of trisodium citrate salt $\text{Na}_3\text{C}_3\text{H}_5\text{O}(\text{CO}_2)_3$ was also dissolved in milliQ water.

The faint yellow gold solution was heated to boiling in a pyrex glass conical flask in a fume cupboard. The citrate solution was then added to the boiling solution while stirring.

The colour gradually changed from faint yellow to clear, to grey, to purple and finally to wine red. Heating and stirring was continued for 30 minutes, after which the solution was

left to cool to room temperature and the volume made up to 50 mL to compensate for water lost by evaporation.

3.2.1 Coating AuNSs with Pd (bimetallic AuNSs) Au-Pd bimetallic

A palladate solution was prepared by dissolving 0.05g of K_2PdCl_4 salt in 50 mL of MilliQ water making it 1mM.

5 mL of the K_2PdCl_4 solution was placed in each of five 20 mL labelled vials and placed in an ice bath. Different volumes (10, 5, 2.5, 1.25 and 0.25 mL) of the gold sol were then added to the vials and stirred. This gave Pd-Au molar ratios of 0.2, 0.4, 0.8, 1.6 and 8 respectively. Particle diameter of those produced by Kundu et al. [32] measured between 40-45 nm. The gold nanospheres obtained experimentally in this work have average diameters in that range as computed later using the formula by Haiss et al. [14].

Next, 1.5 mL of a 0.1 M ascorbic acid $C_6H_8O_6$ solution was added to each and stirred. The colour of the solutions changed to brownish black.

UV-Vis spectra of the five Au-Pd particles, the gold sol and the palladium solution were later measured (see figure 4.1b).

3.2.2 Characterisation of Particles STEM Studies

Silicon wafers were used for observation in the STEM. A drop of the sample was placed on the wafer with a syringe, left under the microscope overnight to dry and then observed.

3.2.3 Coating Au Rods with Pt electrochemically by Cu UPD

The underpotential deposition procedure during which a displacement reaction occurs is used to deposit platinum on gold nanorods. This was carried out using two approaches: firstly an Ag wire was used and then a glassy carbon as working electrodes.

With the Ag wire as working electrode, the Au nanorods previously synthesised were coated with platinum by underpotential deposition of copper on the silver electrode. Copper was first deposited on the rods electrochemically and then displaced by platinum. Copper II sulfate pentahydrate; $CuSO_4 \cdot 5H_2O$ (Fluka) solution 1 mM and K_2PtCl_4 salt

solution (1 mM) were prepared in a volumetric flask and vial respectively.

The Ag electrode was derivatised with the prepared AuNRs solution using the dithiol.

A conventional three electrode cell was used. The derivatised electrode was placed in the cell containing 0.05 M H₂SO₄. The counter electrode was a Pt wire and the reference electrode was a calomel electrode. After purging in argon for 30 minutes, 10 scans were run in 0.05 M sulfuric acid.

Another cell was prepared containing the CuSO₄ solution and all the electrodes were rinsed and transferred to this cell. It was again purged in argon for 30 minutes.

A Cu adlayer was deposited electrochemically on the AuNRs by holding the potential at -0.12 V vs. SCE for 40 minutes.

The Ag electrode with Au-Cu rods was then dipped in the platinum salt solution and purged for 10 minutes. A CV was run again using the Ag electrode, in 0.05 M sulfuric acid to investigate for Pt oxidation and reduction peaks. Scans were performed at a rate of 0.05 V s⁻¹.

An Au NR/Carbon mixture of 80 wt% C/20 wt% NRs was prepared. Firstly, 1g of carbon black was cleaned. This was done by refluxing in HNO₃ for 50 minutes then rinsed several times on a filter paper with ultra-pure water. The clean carbon was placed in a beaker and dried in an oven overnight.

10 mL of 0.0005 M Au NR solution was centrifuged, the supernatant removed with a pipette and the precipitate re-dispersed in ultra-pure water, made up to 0.5 mL. The Au NR solution was then mixed with 0.0008 g of the clean carbon black and 0.01 mL of nafion. The mixture was sonicated for 90 minutes at 22 °C to get a homogeneous Au NR/carbon black ink.

The electrode was prepared by dropping a small quantity of the ink on the 2 mm (area = 0.03143 cm²) glassy carbon electrode and dried with flowing inert argon. A small quantity of nafion was dropped on the dried ink to stabilize it on the electrode. This was again dried in flowing argon.

Deposition of copper and subsequent replacement by Pt was done as described above.

3.2.4 Catalysis

High purity sulphuric acid H_2SO_4 (~100%); (ADH Aristar) was purchased from VWR, methanol CH_3OH (99.9%); (Sigma-Aldrich) and formic acid HCOOH (puriss. p.a., ~98%); (Fluka) was purchased from Sigma-Aldrich.

3.2.4.1 Electrooxidation of Formic Acid and Methanol on Au@Pd and Au@Pt NRs

Before commencement of electrochemical measurements, the 3-electrode electrochemical cell, platinum wire counter electrode and other glass accessories were thoroughly cleaned as previously described. The gold (area = 0.0314 cm^2), glassy carbon (area = 0.071 cm^2) and platinum (area = 0.0314 cm^2), electrodes were polished before use using levigated deagglomerated alpha alumina (Al_2O_3) powder micro-polish of 1.0, 0.3 and 0.05 micron in that order, for 5 minutes each, thoroughly rinsed with ultra pure water and then soaked in ultra pure water for another 15 minutes to ensure removal of alumina.

The gold electrode was further cleaned by cycling (in 0.05 M H_2SO_4) between the hydrogen evolution and oxygen evolution potentials until a reproducible CV was obtained. The electrode was then rinsed with ultra pure water, dipped in 1,9-nonanedithiol and left overnight. This was slightly rinsed with ethanol and placed in an aliquot of the previously synthesised gold palladium core-shell nanorods and left overnight. The electrode was then rinsed with ultra pure water. For the attachment of Au@Pt NRs for investigation of methanol electrooxidation, a similar procedure was followed.

A 0.05 M sulphuric acid solution was prepared by weighing out 4.904 g of the pure acid into 1L volumetric flask containing ultra pure water and made up to the 1000 mL mark. The acid should be added to water and not the other way round, to prevent evolution of acid mists. In a similar manner, 0.23015 g of HCOOH was made up to 100 mL electrolyte to get a 0.05 M solution.

A methanol solution of 0.1 M was also made from 0.81 g (99.9% CH_3OH) in 50 mL sulfuric acid.

In order to expose the catalytic material surface, a cyclic voltammogram was carried out first in sulphuric acid (0.05 M) for 2 cycles, then carried out in a mixture of HCOOH

(0.05 M) and H₂SO₄ (0.05 M).

Electrooxidation of formic acid (HCOOH) was also investigated on bulk gold and bulk platinum electrodes for comparison.

Methanol electrooxidation was investigated over Au@Pd, Au@Pt and Au and Pt electrodes, for comparison.

Electrochemical measurements were performed using a conventional 3-electrode electrochemical glass cell controlled by Autolab potentiostat/galvanostat. The reference electrode used was an Hg/Hg₂SO₄, with a platinum wire as the counter electrode. The working electrode was a polycrystalline gold disc (area = 0.0314 cm²) pasted with the catalyst material by means of the 1,9-nonane dithiol linker.

A 0.05 M solution of sulphuric acid was used as the supporting electrolyte and the electrochemical test was carried out first in the supporting electrolyte only and with 0.05 M formic acid.

A scan rate of 0.05 Vs⁻¹ or 0.1 Vs⁻¹ was employed depending on the experiment, then with a potential range of -0.64 to 1 V against the Hg/Hg₂SO₄ reference electrode. The cell is represented by the figure below.

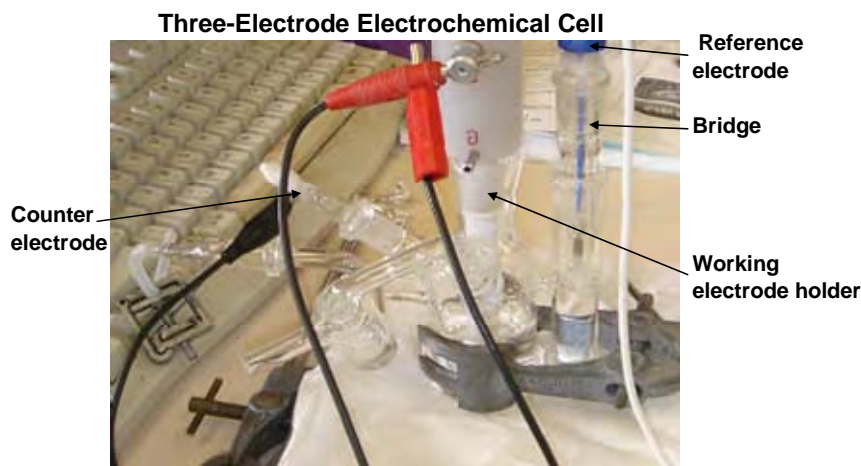


Fig 3.2.4.1 A three-electrode electrochemical cell

3.2.4.2 CO Stripping on Au@Pd and Au@Pt Nanorods

The Au@Pd nanorods were attached to a gold working electrode with 1,9-nonane dithiol linker. A Pt wire and Hg/Hg₂SO₄ served as counter and reference electrodes respectively. The electrochemical cell set up contained a 0.05 M sulfuric acid electrolyte. The solution was purged with flowing argon for 30 minutes. Besides rendering the system oxygen free, the rod surfaces were also cleaned to expose the Pd catalytic sites. Carbon monoxide (CO) was then bubbled through the solution at an open circuit for 30 minutes to get CO adsorbed on Pd sites. The cell was left to stand for 10 minutes. The solution was again purged with argon for 15 minutes to get rid of excess CO. Potentiostatic scans were then run before placing in 0.05 M HCOOH + 0.05 M H₂SO₄ for electrochemical measurements to be done.

For CO stripping on Au@Pt NRs, the electrode prepared on glassy carbon containing the Au@Pt NRs obtained by the Cu UPD was used.

The procedure described above was followed for the CO stripping experiment using Pt wire and SCE as counter and reference electrodes. Scans were done at 50 mVs⁻¹.

3.2.4.3 Oxygen reduction by the RDE on Au@Pt NRs

ORR measurements were carried out using the CTV101 Speed Control Unit radiometer with a speed range of 0-5000 RPM. The radiometer was coupled to the Autolab PGSTAT12 and ORR was done at 100, 400, 900, and 1600 RPM. Firstly, the prepared electrode in 0.05 M H₂SO₄ was purged in flowing Ar for 30 minutes and a scan run to confirm the presence of the Pt/C catalyst material on the electrode. The solution was then saturated with O₂ by bubbling oxygen through for 30 minutes and a scan taken for comparison to the CV of the Pt/C in H₂SO₄ Ar saturated. The solution was re-saturated with O₂ and ORR measurements performed at 100 RPM. The procedure was repeated at speeds 400 rpm, 900 rpm and 1600 rpm. All measurements were done using a 2mm diameter glassy carbon as working electrode, an SCE reference electrode and a Pt wire as counter electrode. RDE measurements were carried out at a scan rate of 20 mVs⁻¹.

4.0 Results and Discussion

4.1 Synthesis and characterisation

4.1.1 AuNRs synthesis

In synthesising metal nanorods, most of the methods used suffer from limitations in either the yield or materials used [7].

Nikkoobakt and El-Sayed [9] used the seeded mediated approach in which rods of different aspect ratios were synthesised by varying the concentration of AgNO_3 .

The set of UV-Vis spectra below (fig. 4.1.1.1a) from experimental work is representative of one set of rods synthesised by the seeded mediated method using the modified Nikkoobakt and El-Sayed method, keeping the concentration of AgNO_3 constant.

The spectra (fig 4.1.1.1a and 4.1.1.1b) show absorption of AuNRs of length 75 ± 5 nm and width 15 ± 5 nm (dimensions measured from STEM images), with aspect ratios up to 4+, which can be seen clearly from STEM images of uncoated AuNRs (fig. 4.1.1.2).

Two-peaked spectra arise due to transverse plasmon electronic oscillations at wavelengths $\lambda=549$ nm to 580 nm, and $\lambda=719$ nm to $\lambda=756$ nm from the longitudinal oscillations.

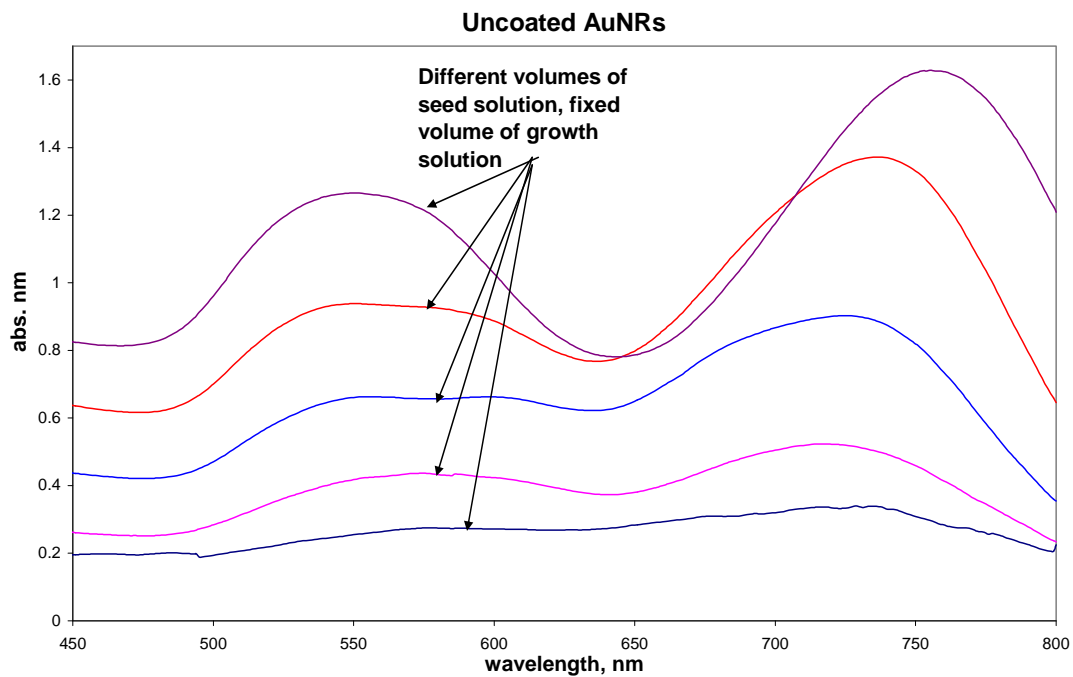


Fig 4.1.1.1a UV-Vis spectra of gold nanorods with aspect ratios of up to 4.03 as indicated by STEM images.
The aspect ratio increases from the bottom spectrum to the top.

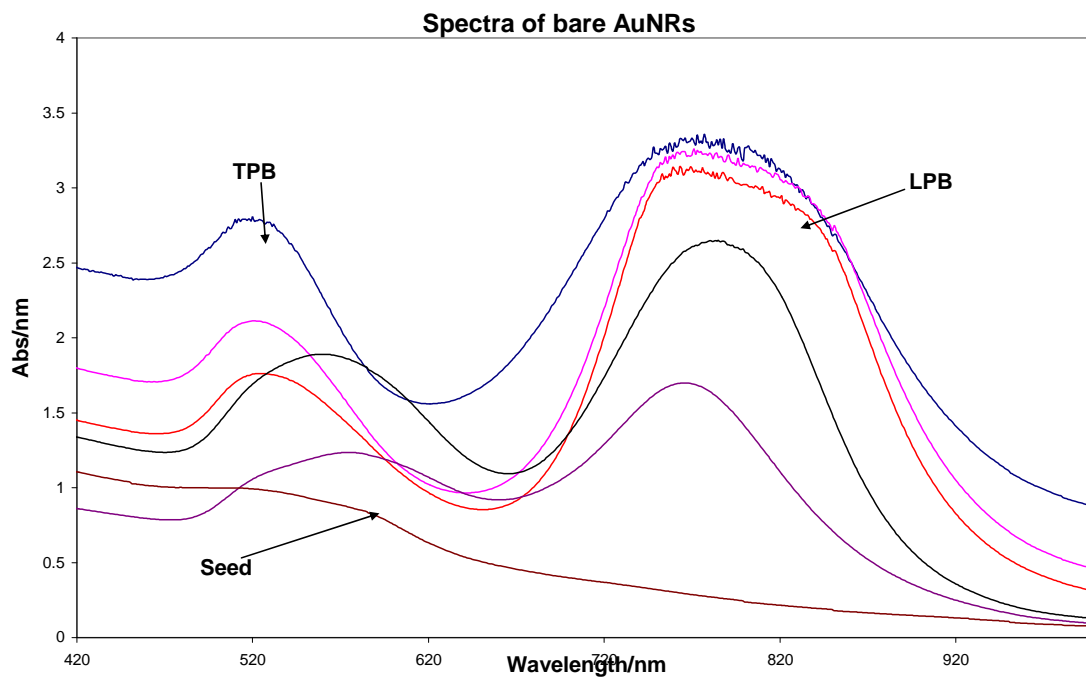


Fig 4.1.1.1b UV-Vis NIR spectra of Au rods with aspect ratio >4
The aspect ratio increases from the bottom spectrum to the top.

The spectrum with two maxima (549 nm and 756 nm) comes from gold rods with highest aspect ratios of approximately 4.

In a separate synthesis experiment, another batch of AuNRs was successfully synthesised and the UV-Vis NIR spectra measured after four hours. The spectra above (fig. 4.1.1.1b) are representative of AuNRs with aspect ratios greater than 4.

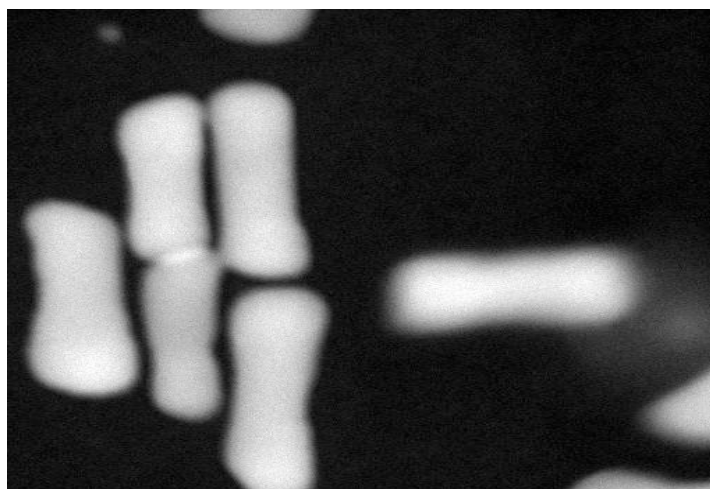


Fig 4.1.1.2 STEM images of bare gold nanorods, aspect ratio appr. 4

Based on the collective oscillation of electrons in the conduction band, gold nanorods would have two absorption bands: the longitudinal Plasmon along the long axis of the rod which appears at a higher λ (peak maximum 719-756 nm) and the transverse plasmon bands along the transverse axis (549 nm to 580 nm referring to fig 4a) of the rod [9]. Figure 4.1.1.1b shows characteristic absorption bands at wavelengths 520–576 nm for the transverse spectra and 767–789 nm for the longitudinal spectra.

The literature states that the percentage purity however is often low (<20%) as particles of different shapes such as spheres and nanoprisms form together with rods in the solution mixture (see fig 4.1.1.3) [29].

Therefore, rods of different aspect ratios ranging from slightly greater than 1 to about 4-4.5 were experimentally produced in this work as indicated by the STEM micrographs. The absorption maximum at 549 nm (transverse) has only small shift but that at 756 nm (longitudinal) exhibits a significant red shift (fig 4.1.1.1a). Rods that generated these

spectra were thinner and therefore had the highest aspect ratio in that batch. The most blue shifted bands may represent absorption by both nanospheres and transverse electronic oscillations. It is worth noting that nanospheres only have one oscillation [9]. Absorption along the transverse axis and of nanospheres appears at a shorter λ , red shifted. The position of the absorption band on the EM spectrum depends on the aspect ratio of the rods and very long rods with high aspect ratios can even have bands reaching the near IR [11]. Longer and thinner rods (high aspect ratios) would have a blue shift and shorter and thicker, low aspect ratio rods would have a red shift.

The literature based on past work states that percentage purity is often low due to the formation of by-products.

Khanal and Zubarev [29] in a recent work stated that the percentage purity of nanorods is often $< 20\%$ and adopted a method for purification.

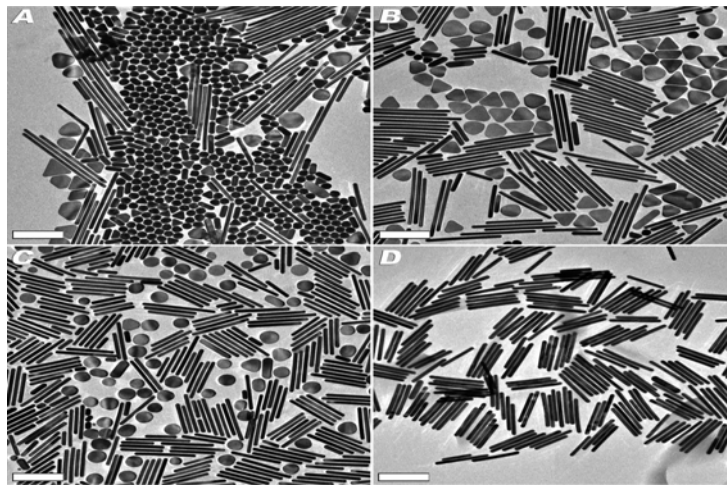


Fig. 4.1.1.3 [29] shows how low the fraction of rods is when synthesised

From personal experience, success in obtaining nanorods begins with cleaning procedures and avoidance of contaminants. Impurities will impair the growth of gold nanorods, as such from weighing to making of solutions, very clean spatulae, weighing boats etc. should all be very clean. The use of aluminium foil to weigh out sodium borohydride should be avoided as it will attack aluminium. Clean glass weighing boats should be

used. In the present work, yields of rods before purification of >50% were achieved, which is an improvement on the literature report. Centrifugation of these products successfully removed nanospheres but a few star-shaped particles remained.

4.1.2 Au nanospheres synthesis and coating

Citrate-stabilized gold nanospheres with an average diameter of approx. 44.3 nm were obtained. The average size was computed from UV-Vis spectra using the formula developed by Wolfgang Haiss and coworkers [14]. This is an approximation and there is no back up image of these particles.

Generally, the size of the particles formed in solution, be it rods, spheres nanowires or nanocubes, depends on the concentration of the capping agent. This decreases with increase in capping agent concentration.

The citrate-stabilised particles were coated with palladium as a test of the method before applying it to rods. The spectra below in fig 4.1.2 show both the pure Au particles and the coated particles. It is evident from the spectra that the Au-Pd particles show from very weak absorptions to almost no absorption at all, as palladium would absorb below 300 nm.

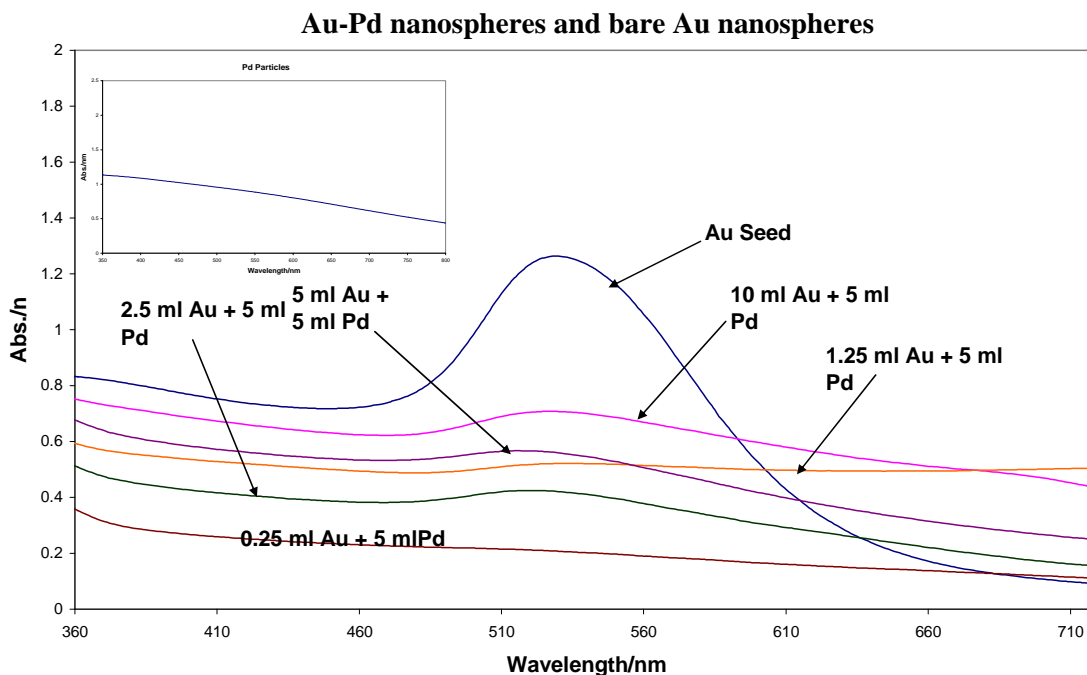


Figure 4.1.2 UV-Vis spectra of palladium coated gold nanospheres of $d = 44.3$ nm

Referring to fig. 4.1.2 above, the surface plasmon resonance peak at wavelength 529 nm with an absorbance maximum at 1.26 nm is characteristic of the nanospheres in the citrate stabilised gold-only sol.

When different volumes of the sol were added to 5 mL of palladium then reduced with ascorbic acid, it was observed that the amplitude of the peak was reduced. This observation could be explained by the fact that the electronic oscillation in the conduction band was dampened. This shows that the gold particles have been shielded by the Pd. The thicker the palladium coat on the gold particle, the lower the peak's amplitude becomes and at some point it flattens out. This drop in amplitude is good evidence that a core-shell Au-Pd bimetallic nanoparticle has been formed. The inset on Fig 4.1.2 is the UV-Vis spectrum of Pd particles in the wavelength range 350-800 nm. Pd does not show any absorption in this region confirming that the absence of Au SPR is due to Pd overlayers.

4.1.3 Palladium coated AuNRs

UV-Vis spectra of all the five coated samples of the batch were measured alongside the uncoated solutions and are presented in fig 4.1.3.1 below. Figure 4.1.3.2 is an excerpt from fig 4.1.3.1 which shows the spectrum of palladium particles, one solution of pure Au rods and another of the same solution that has been coated with palladium, and also an illustration of the origin of the peaks from the longitudinal and transverse plasmonic resonances. Similarly to the case of nanospheres, the absorption maxima are not present for Au-Pd rods, indicating that the Au rods have also been covered with Pd.

The STEM image presented in fig. 4.1.3.3 provides further evidence that the AuNRs synthesised were successfully coated with Pd. The contrast of the image enables us to see the gold core and the palladium shell distinctively. The very white features that can be seen are the gold NRs and the light grey shells surrounding them is the Pd.

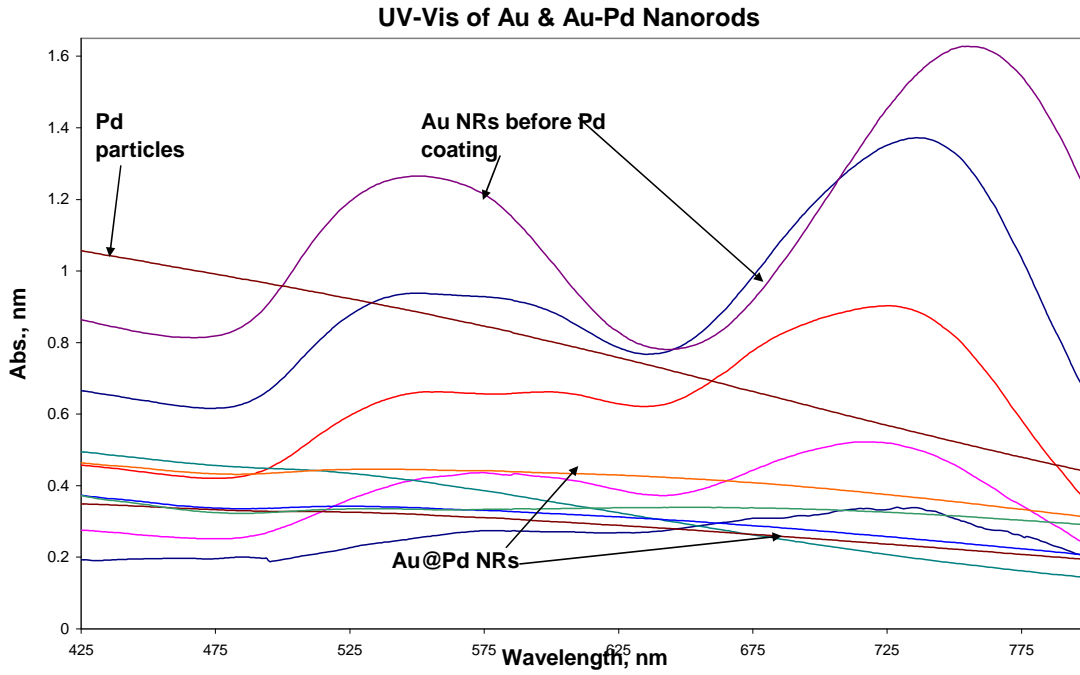


Fig 4.1.3.1 UV-Vis spectra of pure AuNRs and Au@Pd AuNRs showing how the absorption by Au disappears with deposition of Pd

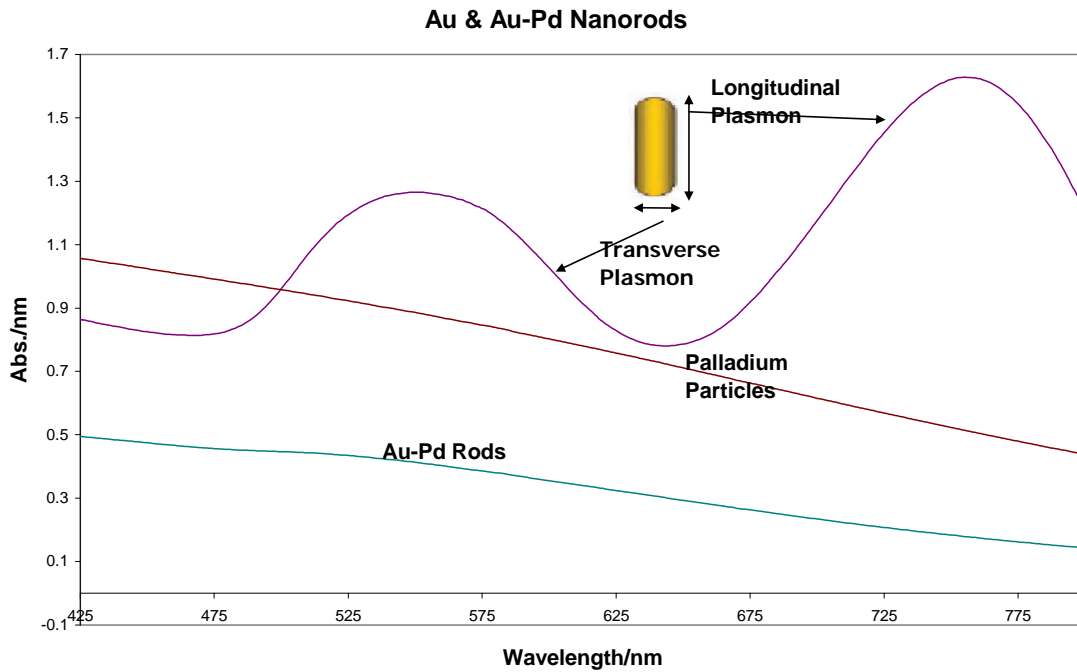


Figure 4.1.3.2 showing the absorptions of AuNRs, Au@Pd rods and Pd nanoparticles

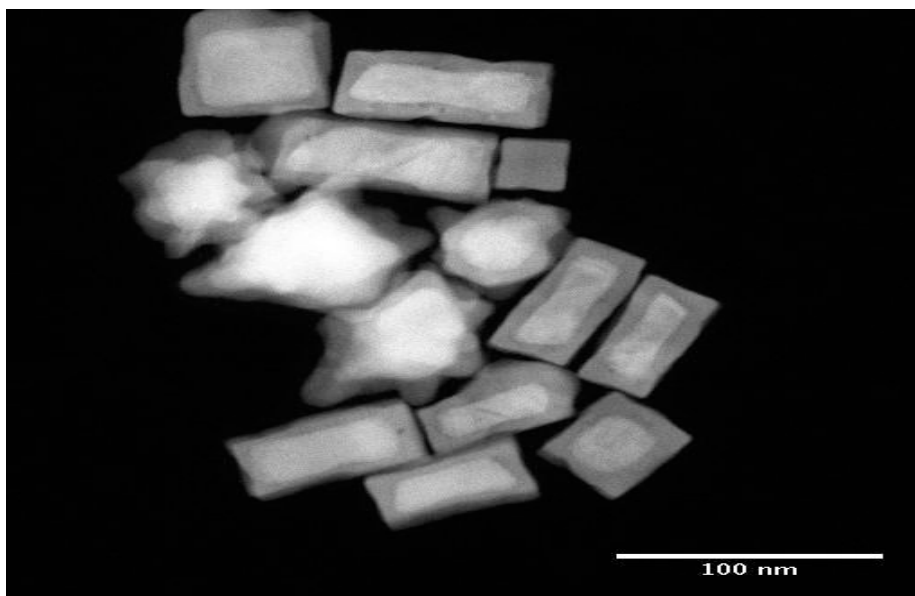


Fig 4.1.3.3 STEM image of Au NRs coated with Pd. The rods are completely covered with Pd.

4.1.4 Coating AuNRs and Au@Pd NRs with Rh

The spectra obtained from the UV-Vis measurements (Fig 4.1.4) clearly show that the gold rods were completely covered by rhodium. The spectrum with two clear peaks (black) is from the as-prepared Au NRs solution. A portion of the same solution was used to prepare the Au-Rh core-shell rods.

Very weak longitudinal and transverse absorption peaks could still be seen for a 50-50 mixture of Au and Rh (dark blue spectrum). To clarify any confusion that may arise, it should be mentioned that rhodium particles do not absorb anywhere in the 400-900 nm wavelength range of the EM spectrum; as such, any peak arising from Au-Rh or Au-Pd rods is from gold only. The spectra in fig. 4.1.4 are indicative of a thin layer of rhodium, thin enough for Au to show an SPR response.

As the rhodium layer was made thicker by increasing the mixture ratio to a 67 % (Rh)-33 % (Au) by volume (1 mL Au, 2 mL Rh), the shell became thick enough to completely shield the Au. 2×10^{-5} moles Rh and 5×10^{-5} moles Au were present. As a result, there was no characteristic absorption peak (green spectrum) because the Au was incapable of showing an SPR.

By the same coating procedure, a tri-metallic Au-Pd-Rh was synthesised by depositing Rh on Pd in the Au@Pd NRs to obtain Au-Pd-Rh. There is no STEM image for the tri-

metallic, but the UV-Vis spectra did not show any absorption by Au. This, however, is not enough evidence that Rh was deposited on Pd especially as UV-Vis of Au@Pd will have no characteristic SPR for Au in that wavelength range. Further experiments will be needed to determine whether the Rh was deposited on the Au-Pd.

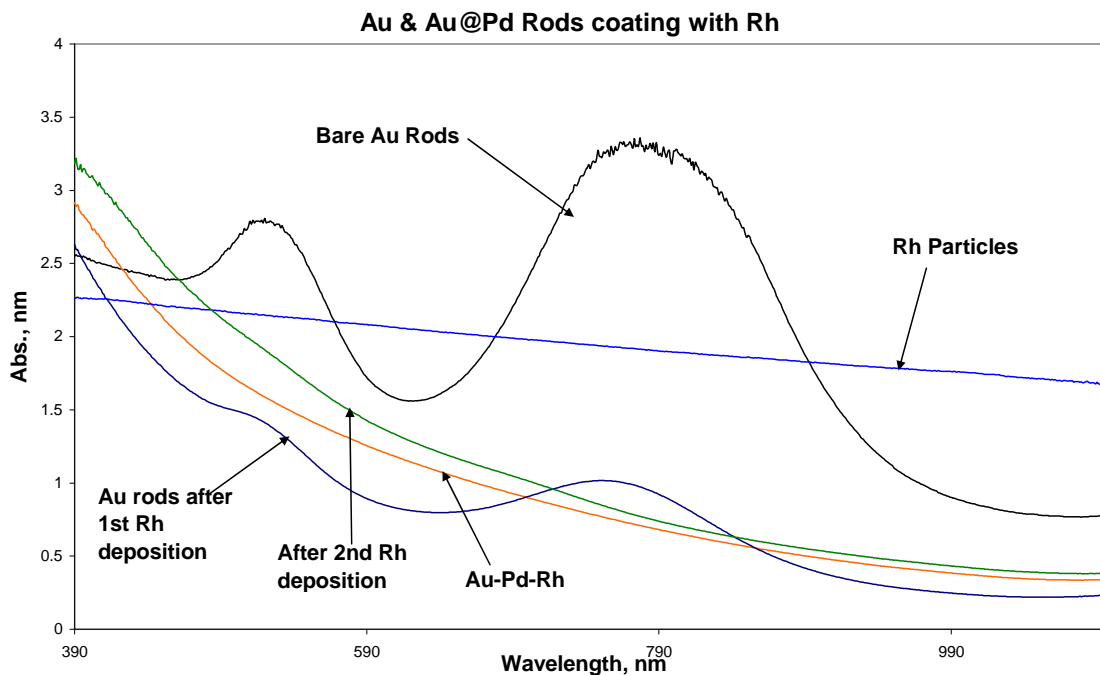


Fig 4.1.4 UV-Vis spectra of bare AuNRs, Rhodium coated AuNRs and Rh particles

4.1.5 Coating Au NRs with Pt in aqueous solution

The UV spectra presented in Fig 4.1.5 were obtained from the as-made Au rod solution, Pt particles solution and Au-Pt solution. It was observed that the gold rods were coated by a thin layer of platinum, as interpreted from the Au-Pt spectrum. This is explained by the fact that there were still longitudinal and transverse peaks present, indicating a weak absorption by the gold rods. After a second Pt deposition (final volume 2.5 mL Pt solution and 1.5 mL Au solution) was made, there was no absorption by Au observed. The peaks completely disappeared and the spectrum resembles that of Pt nanoparticles. This would suggest that the rods were now coated in Pt.

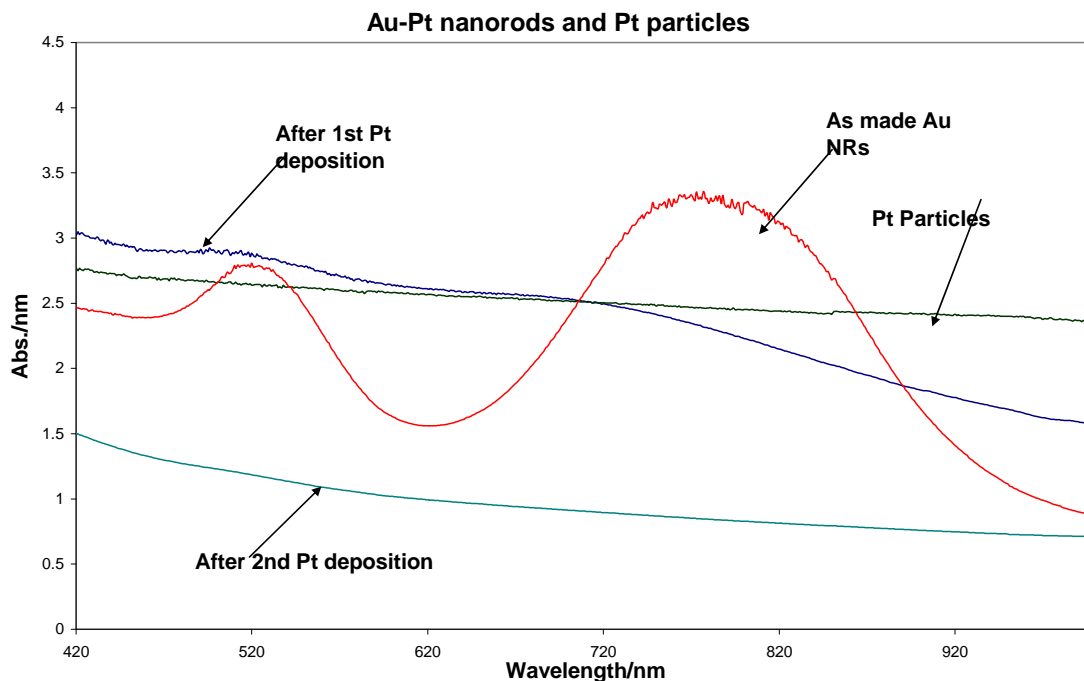


Fig 4.1.5 UV-Vis spectra of as-made Au NRs and successively Pt-coated Au NRs

Deposition of Pt on AuNRs was successful as can be seen on Fig 4.1.5. The spectrum after a second deposition closely resembles that of Pt particles suggesting that the SPR of AuNRs was dampened by Pt overlayer.

4.1.6 Coating Au NRs with Pt by the displacement deposition process: UPD of Cu

These rods were prepared as described in section 3.1. Fig 4.1.6.1 is the cyclic voltammogram obtained of the Au@Pt modified Ag electrode in 0.05 M sulfuric acid. If a Pt wire is used as electrode, it will be hard to tell if the CV is from the bulk Pt or from the Pt particles. The forward scan produced an oxidation peak and the backward and negative scan produced a reduction peak at around 0.41 V which is characteristic of a Pt oxide (PtOx) reduction peak. The appearances of the peaks for PtOx formation in the forward scan and Pt oxide reduction in the negative scan is evidence that Cu was displaced by Pt.

The displacement occurs via the spontaneous oxidation of the Cu adlayer by PtCl_4^{2-} ions according to the following equation:

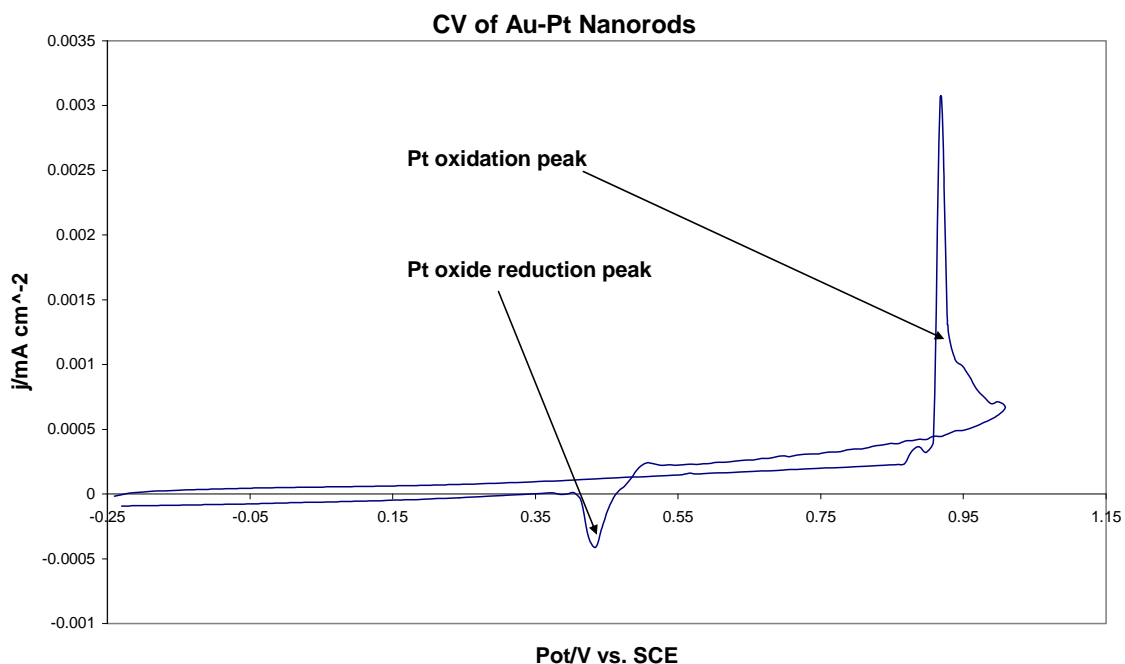
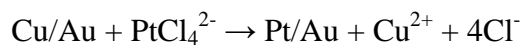


Fig 4.1.6.1 Cyclic voltammogram of Au@Pt attached to a Ag wire electrode in 0.05 M H₂SO₄. Scan rate: 0.05 V s⁻¹

A similar experiment was performed for AuNRs immobilized on C. Fig 4.1.6.2 is a CV of the AuNRs in 0.05 M H₂SO₄ and Fig 4.1f3 is a CV carried out in 0.05 M H₂SO₄ + 1 mM CuSO₄. The UPD peak is observed at 0.056 V. For the deposition of platinum on AuNRs, the Cu adlayer was used as a precursor. Cu was deposited onto the AuNRs at 0.056 V, which corresponds to the marker on Fig 4.1.6.3. After Cu deposition, the modified Au/Cu/C electrode was placed in de-aerated K₂PtCl₄ solution.

The voltammetry of the resulting electrode in 0.05 M sulfuric acid is shown in Fig 4.1.6.4.

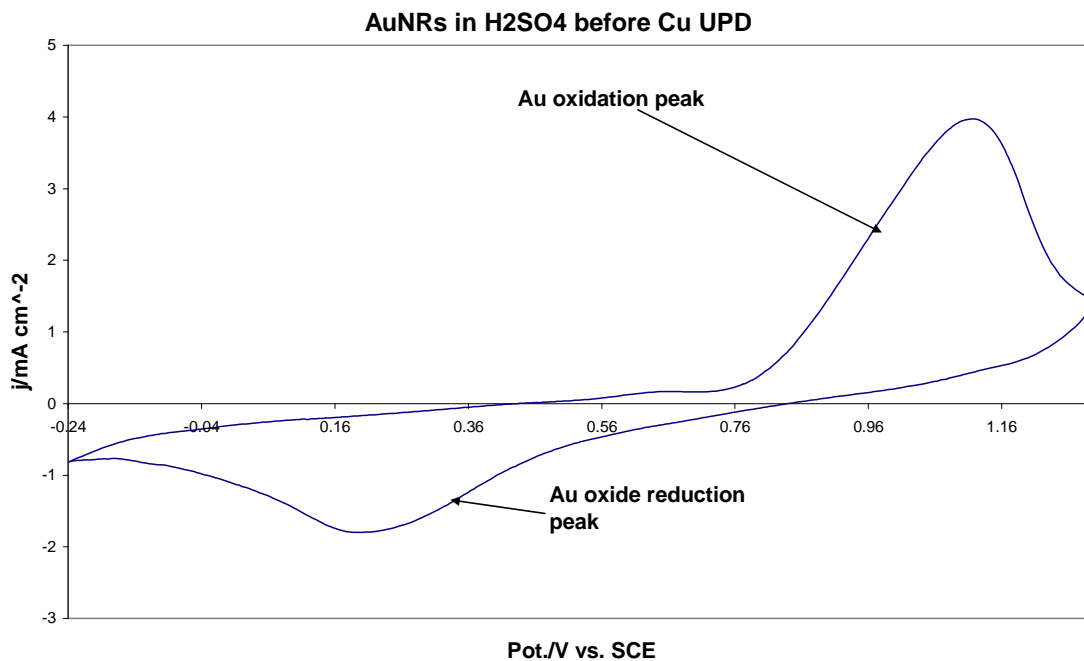


Fig 4.1.6.2 Cyclic voltammogram of Au NRs in 0.05 M H₂SO₄. Scans performed using a glassy carbon electrode. Scan rate: 0.05 V s⁻¹

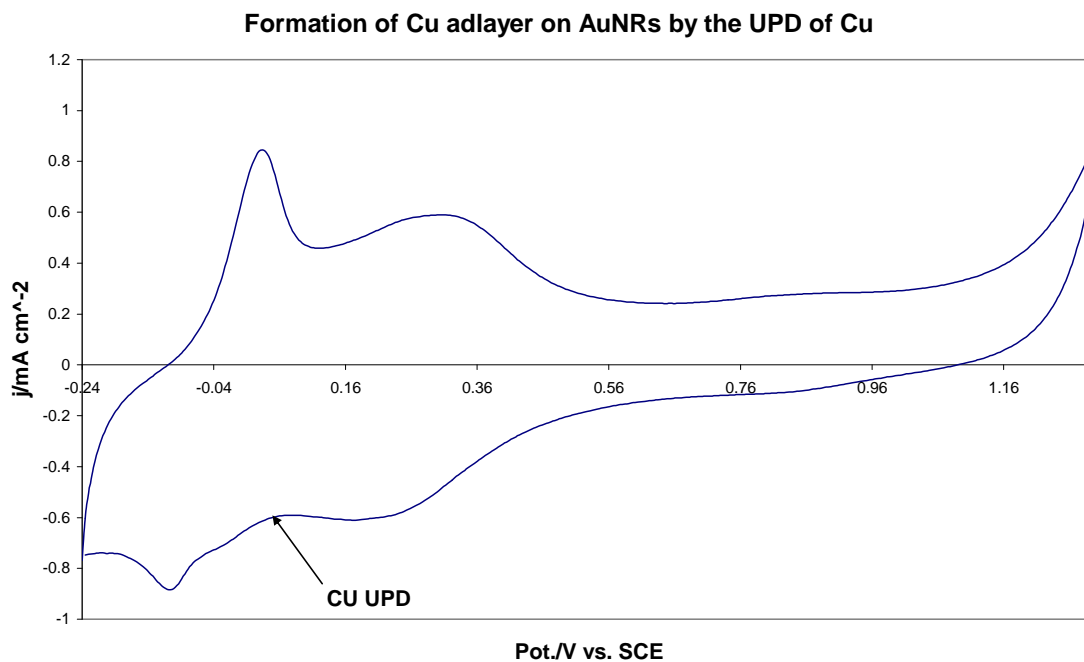


Fig 4.1.6.3 Cyclic voltammogram for Cu deposition on AuNRs recorded in 1 mM CuSO₄ in 0.05 M H₂SO₄. Scans performed on a glassy carbon electrode. Scan rate: 0.05 V s⁻¹

At positive potentials (Fig. 4.1.6.3) the AuNRs are oxidised in the positive sweep. The Au oxides are reduced in the negative sweep. Both the reduction and oxidation peaks here (Fig. 4.1.6.3) are small compared with polycrystalline Au, but the features are apparent. The two symmetric peaks in the low potential region around 0.22 V both in the positive and negative sweeps correspond to the formation and the dissolution of the monolayer of copper.

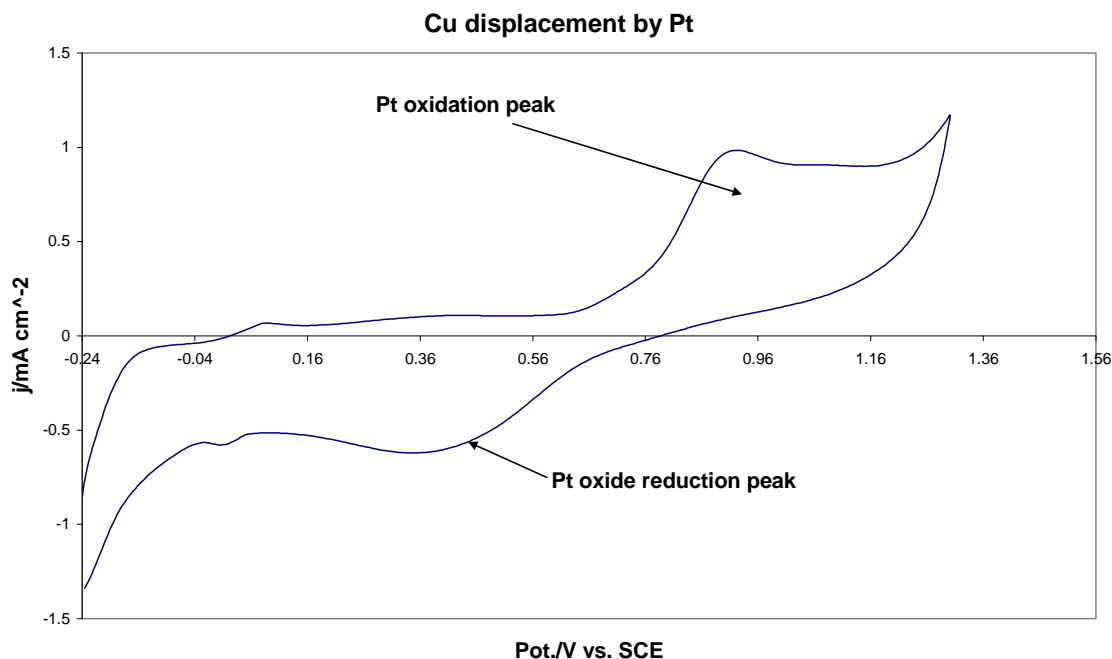


Fig 4.1.6.4 Cyclic voltammogram of Au@Pt in 0.05 M H₂SO₄. Scans performed on a glassy carbon electrode. Scan rate: 0.05 V s⁻¹

The features in the CV of Fig 4.1.6.4 are somewhat broader than for polycrystalline Pt but some evidence of H_{ads/des} and oxide formation and reduction is apparent.

4.2 Electrochemistry

4.2.1 Electrochemical Surface Characterisation

This section presents the results of electrochemical measurements that were carried out on the nanoparticles. Before proceeding to presenting the electro-oxidation results, CVs in 0.05 M H₂SO₄ of the working electrode materials used are presented. All CVs were recorded at a scan rate of 50 mV s⁻¹ with Hg/Hg₂SO₄ reference electrode and Pt wire as

counter electrode.

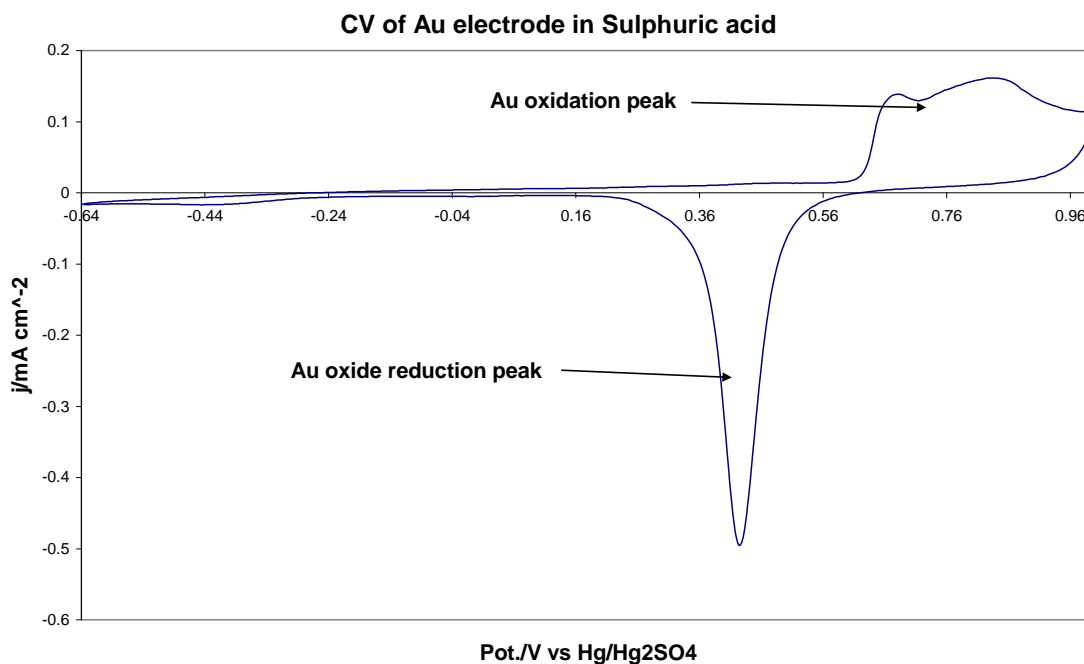


Fig 4.2.1.1 CV of Au electrode in 0.05 M H₂SO₄, scan rate 0.05 V s⁻¹

Oxide layer forms on polycrystalline Au in the forward scan (Fig 4.2.1.1) producing a current of about 1.5 mA cm⁻² of gold surface. The Au oxide is reduced in the negative sweep producing the peak around 0.4 V. The size of the reduction peak suggests that all or almost all of the oxide formed is reduced, as is the case for polycrystalline Pd (Fig 4.2.1.2) and Pt (Fig 4.2.1.3). There is no hydrogen desorption or adsorption peak observed, suggesting that the gold surface is not a good adsorbent for hydrogen.

In the case for palladium (Fig 4.2.1.2), distinct H_{ads/des} peaks are seen in the positive and negative sweeps.

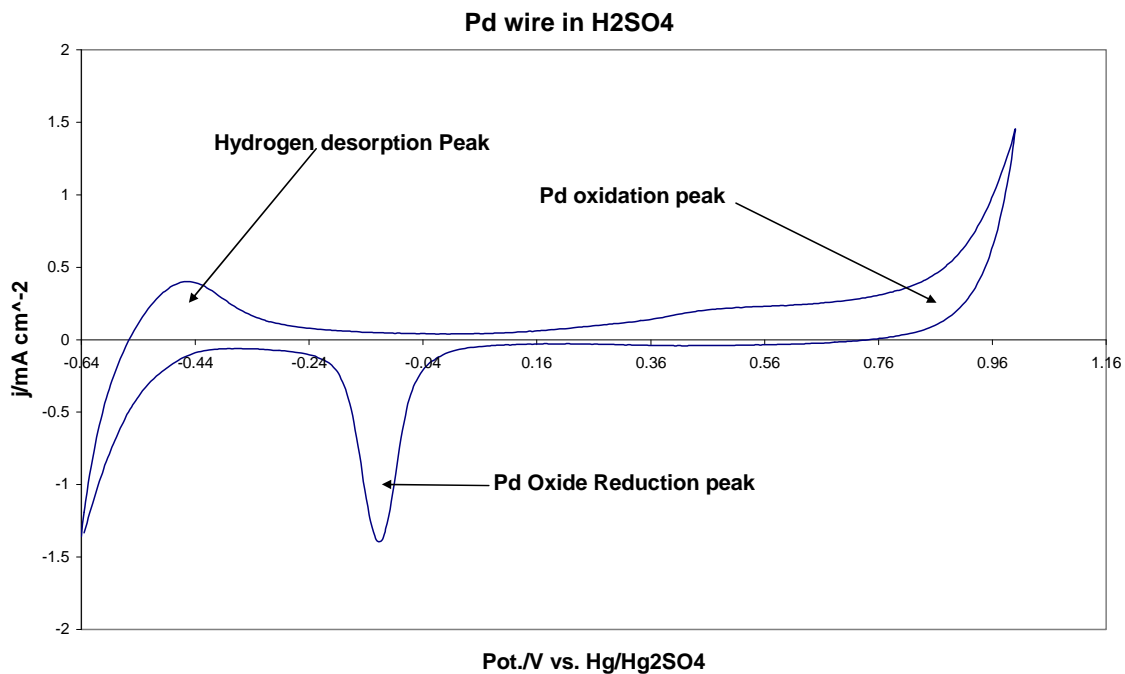


Fig 4.2.1.2 CV of Pd wire in 0.05 M H₂SO₄, scan rate 0.05 V s⁻¹

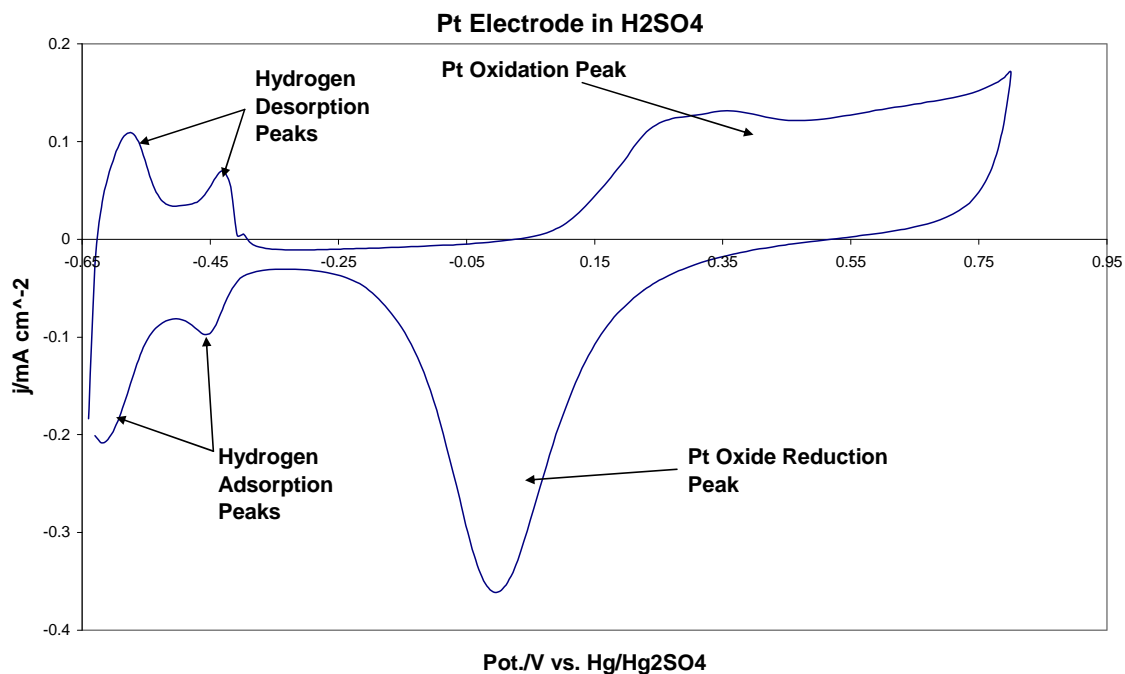
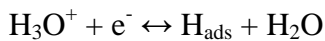


Fig 4.2.1.3 CV of Pt electrode in 0.05 M H₂SO₄, scan rate 0.05 V s⁻¹

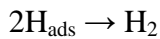
Fig 4.2.1.3 is the CV evolution of polycrystalline Pt in 0.05 M H₂SO₄. Two characteristic

peaks are observed for the desorption of hydrogen in the positive sweep and two H adsorption peaks in the negative sweep. This is because in the case of Pt, two H species are involved in the adsorption/desorption processes. These are the UPD H which occurs at a potential less positive (-0.56 V) and terminal H observed at a potential less negative (-0.42 V) in the positive sweep as illustrated by Fig 4.2.1.3 [46].

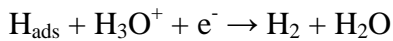
Desorption of hydrogen from metal surfaces in general is accepted to take place in two steps. A hydronium ion is first discharged to give adsorbed hydrogen atom H_{ads} , a step known as Volmer step, which is reversible. Adsorption occurs in the negative sweep.



This is followed by either the Tafel step or the Heyrovsky step. In the former, two H atoms combine to form H_2 .



In the latter, a H_{ads} reacts with H_3O^+ ion in solution to give H_2 and H_2O [46].



In the positive sweep, hydrogen is desorbed.

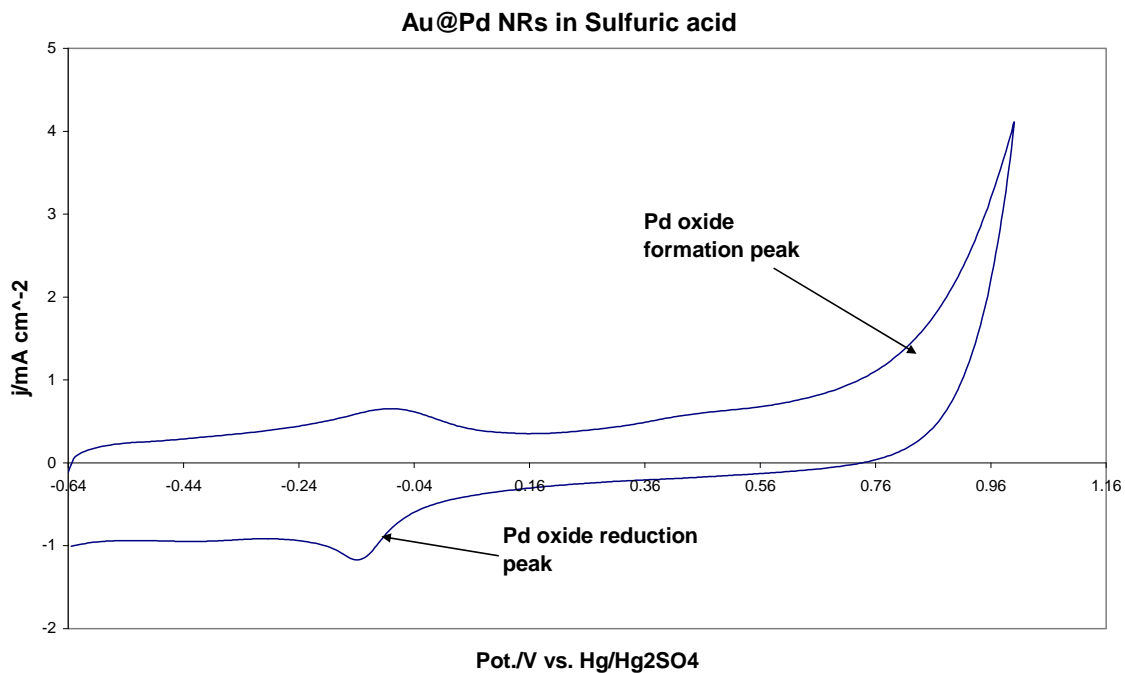
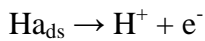


Fig 4.2.1.4 CV Au@Pd/C NRs in 0.05 M H_2SO_4 , scan rate $0.05 V s^{-1}$

The CV in fig 4.2.1.4 was evolved from Au@Pd/C NRs in 0.05 M H₂SO₄. It shows no gold features which suggest that Au is covered with Pd. As opposed to polycrystalline palladium, the thin Pd films on AuNRs show no hydrogen adsorption peak, but there are weak features corresponding to the formation and reduction of palladium oxide.

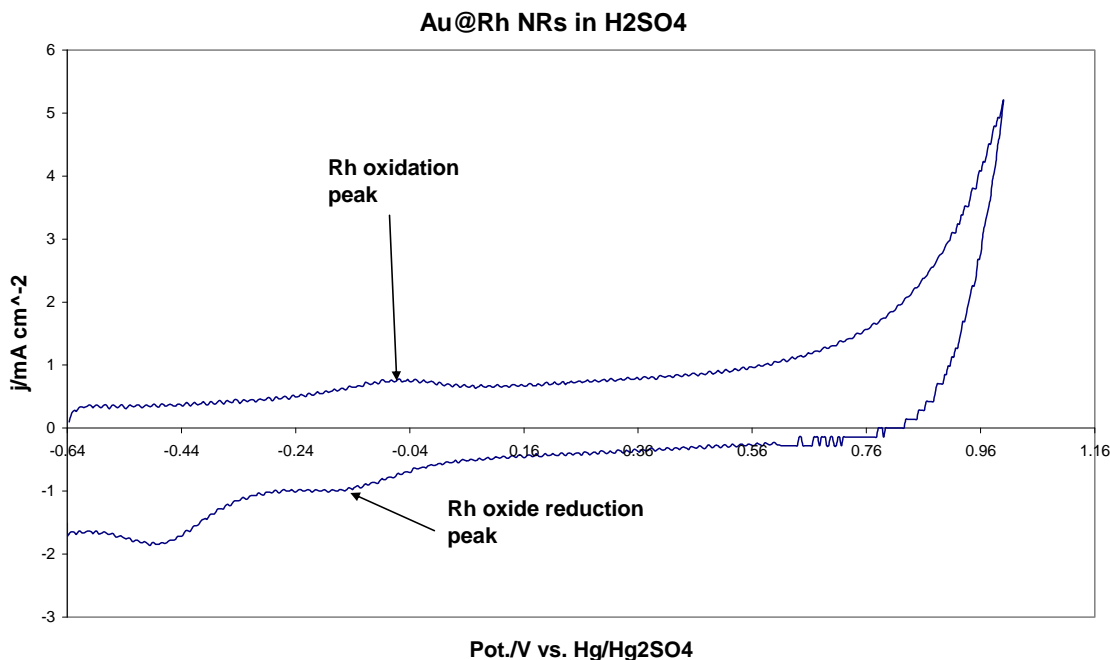


Fig 4.2.1.5 CV Au@Rh/C NRs in 0.05 M H₂SO₄, scan rate 0.05 V s⁻¹

Fig 4.2.1.5 is a cyclic voltammogram of Au@Rh/C NRs in 0.05 M H₂SO₄. The CV shows no Au features, again suggesting that the gold nanorods were covered by Rh. This, in combination with the UV-Vis spectra of the Rh-coated Au NRs is concrete enough proof that Au NRs were covered in Rh.

4.2.2 EO of FA on Au@Pd NRs, Pd particles, bulk Au, Pd wire, bulk Pt & Au@Pt NRs

The results obtained from the formic acid electro-oxidation on Au@Pd NRs are presented in figures 4.2.2.1 and 4.2.2.2.

The peak at about 0.8 V in the forward scan is from the oxide layer on Pd, which is reduced on the backward scan giving rise to the reverse peak.

Looking at Fig. 4.2.2.1, one can see distinctive current peaks with maxima around 0.0 V and 0.08 V. In the forward scan, formic acid electro-oxidation started at a potential of about -0.4V giving a peak with current density of about 0.6 mA cm^{-2} reaching a maximum of about 2.31 mA cm^{-2} . There are two peaks in the forward scan occurring at 0.0 V and 0.3 V.

The oxidation of HCOOH can follow the dual-pathway. There is the direct pathway in which HCOOH is directly oxidised to CO_2 and the indirect pathway through adsorbed intermediates.

In the direct pathway, HCOOH is completely dehydrogenated to CO_2 .



In the indirect pathway, one H is abstracted from HCOOH to form an unstable formate anion, which almost immediately decomposes. This is the indirect oxidation pathway [48]



Now, the peak at 0.0 V is the hydrogen abstraction peak and the second is the decomposition of the intermediate.

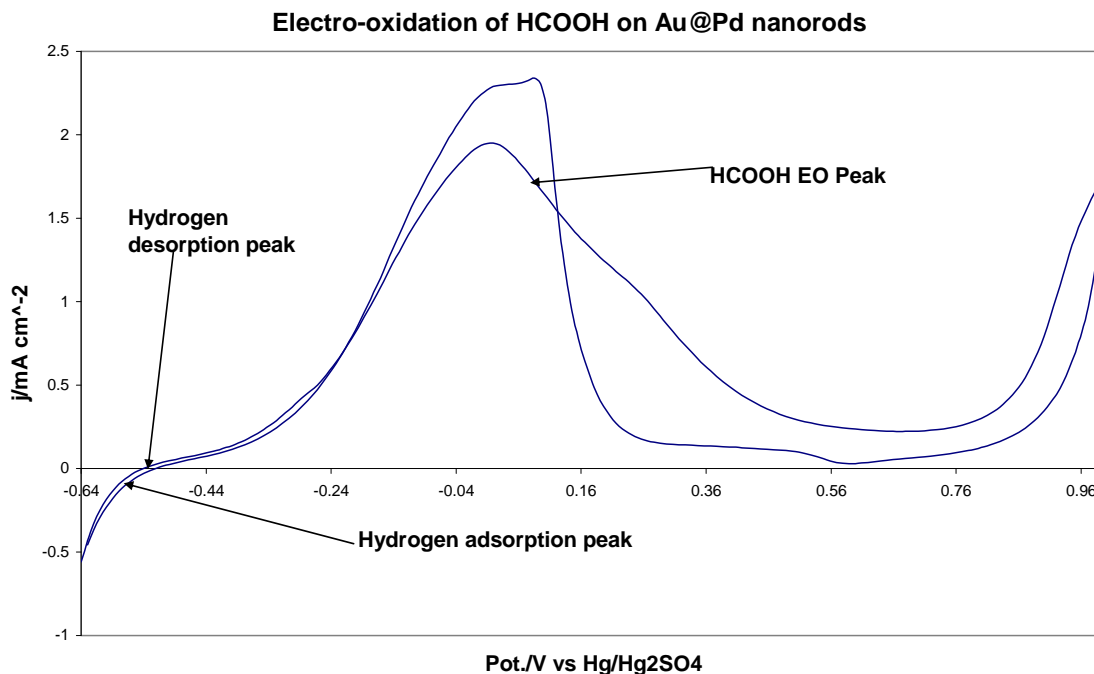


Fig. 4.2.2.1: Formic acid electro-oxidation on the as made Au@Pd NRs pasted on a Au electrode with the help of 1,9-nonane dithiol linker. Scan was initiated at -0.64V vs Hg₂/HgSO₄ ref. electrode, in a 0.05 M H₂SO₄ electrolyte. Scan rate: 0.1 V s⁻¹.

Fig 4.2.2.2 is a CV obtained from the FA electro-oxidation on centrifuged Au@Pd NRs solution. The Au@Pd film thickness on the Au electrode increased by making the catalyst solution about 10 times (5 mL to 0.5 mL) more concentrated. This, as can be clearly seen on the CV (Figs 4.2.2.2 and 4.2.2.3), increased the current produced to 5 times compared to the as-prepared Au@Pd, upon electro-oxidation of formic acid. There were more Au@Pd NRs therefore present to participate in the electrochemical reaction.

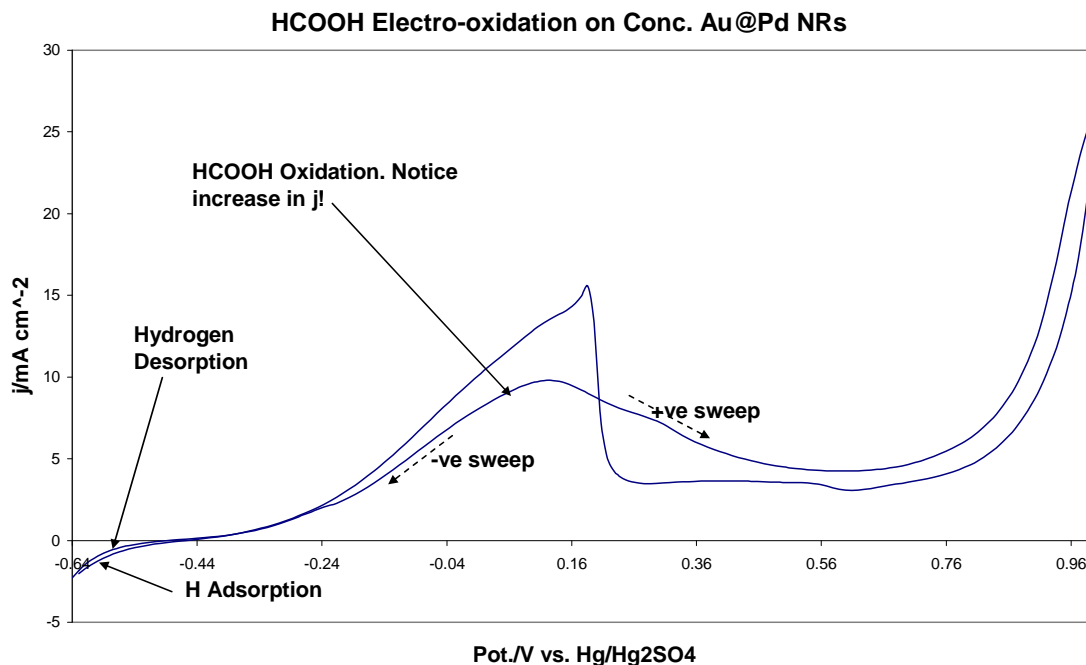


Fig. 4.2.2.2: Formic acid electrooxidation on centrifuged Au@Pd NRs, again pasted on a Au electrode with the help of 1,9-nonane dithiol linker. Scan was initiated at $-0.64\text{V vs Hg}_2/\text{HgSO}_4$ ref. electrode, in a $0.05\text{ M H}_2\text{SO}_4$ electrolyte. Scan rate: 0.1 V s^{-1} .

For the purpose of clarity and ease in comparison, the CVs on electro-oxidation of HCOOH on the as-made Au@Pd NRs and the centrifuged Au@Pd NRs have been presented on the same pair of axes. This is presented in figure 4.2.2.3.

**Comparison between the as-made Au@Pd & conc. Au@Pd NRs towards
EO activity of FA**

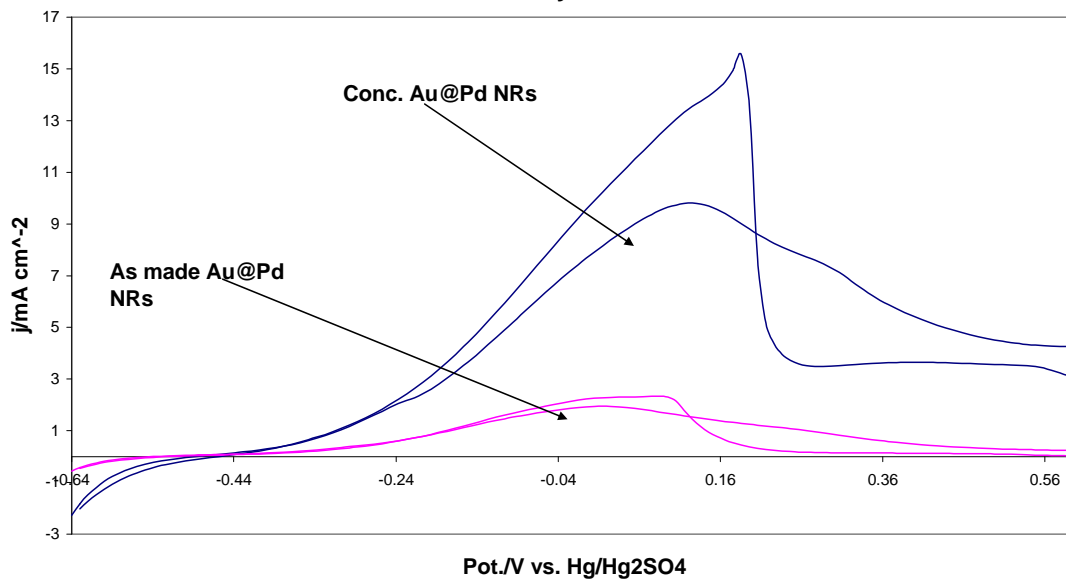


Fig. 4.2.2.3: Figs 4.2.2.1 plotted together with 4.2.2.2 for simplicity

Fig. 4.2.2.4 is the CV from electro-oxidation on Pd NPs. A very small and almost negligible FA oxidation peak appeared at about 0.4 V, which started around 0.025 V, ending up with an oxide formation on Au.

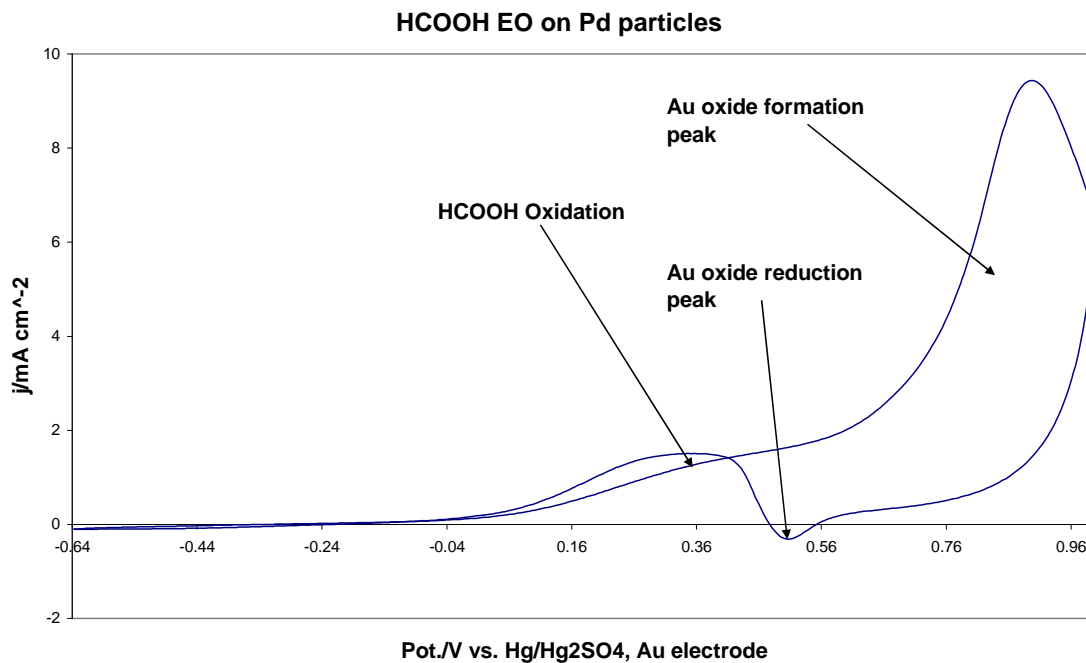


Fig. 4.2.2.4: Formic acid electro-oxidation on Pd NPs, again pasted on a Au electrode with the help of 1,9-nonane dithiol linker. Scan was initiated at $-0.64\text{V vs Hg}_2/\text{HgSO}_4$ ref. electrode, in a $0.05\text{ M H}_2\text{SO}_4$ electrolyte. Scan rate: 0.05 V s^{-1} .

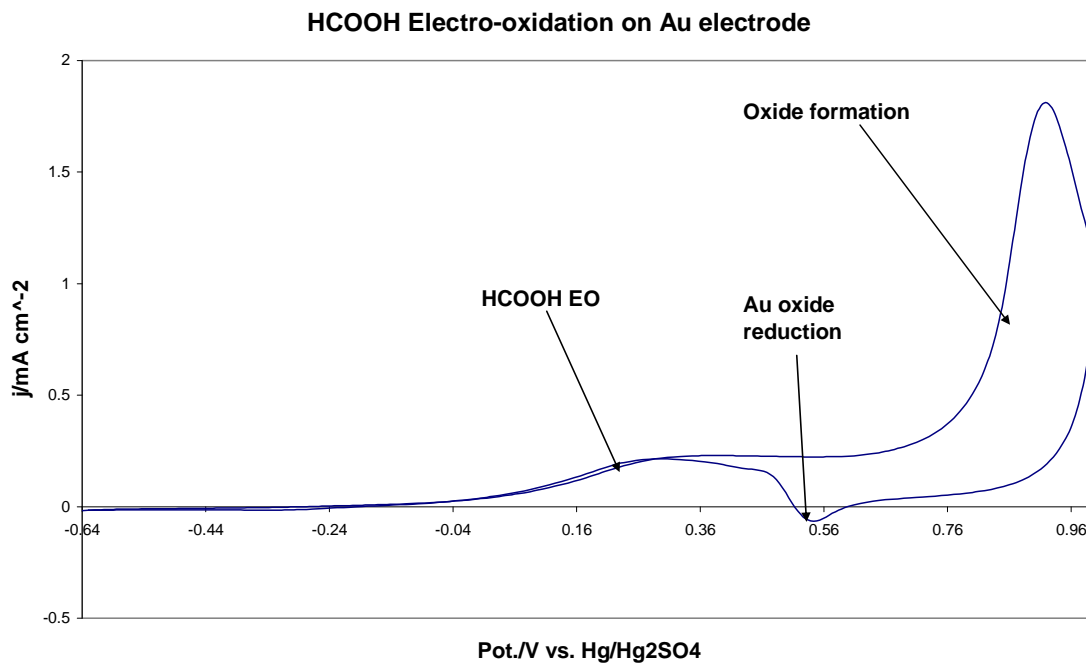


Fig. 4.2.2.5: HCOOH electrooxidation on Au electrode. Scan was initiated at -0.64V vs.

Hg₂/HgSO₄ ref. electrode, in a 0.05 M H₂SO₄ electrolyte. Scan rate: 0.05 V s⁻¹.

With the results of these separate scans, it is clear that there is very negligible or no contribution of polycrystalline Au towards the electro-oxidation of formic acid on Au@Pd NRs.

On the other hand, monometallic palladium particles contributed absolutely nothing towards the electro-oxidation of HCOOH (Fig. 4.2.2.4). The features of the HCOOH on Pd CV are similar to those on Au electrode. This infers that the Pd particles did not adhere onto the Au electrode, meaning the CV was almost entirely dominated by the Au electrode. A similar result was obtained with the Pd-free gold electrode (Fig. 4.2.2.5). Very small, near negligible current was produced. The adsorption/desorption of hydrogen in the lower potential region is absent, also suggesting the absence of Pd particles.

Fig. 4.2.2.5 is the cyclic voltammogram from the electro-oxidation of HCOOH on bulk Au at room temperature. There is a very weak current peak that occurred around 0.3-0.4 V. This is attributed to a negligible activity of gold towards HCOOH electro-oxidation. This, as also observed by Zhou and Lee [15], is due to the fact that formic acid could not be adsorbed on gold for electro-oxidation to occur.

Why the core-shell structure is effective in electro-oxidation and CO-tolerant has sometimes been attributed to electronic effects where the Au-core interacts with the Pd-shell electronically, and sometimes also to the bifunctional mechanism. In the latter case, Au will react with water to form Au-OH_{ads}, which then reacts with the Pd-CO_{ads} formed to release Pd [33, 34].



The Pd shell in this work is rather thick but it is not impossible that some alloying would take place on prolonged electrochemical cycling.

In the electrooxidation of HCOOH on Au@Pd, two things happen in oxidising HCOOH. Two parallel reaction pathways are distinguished; the fast and slow. In the fast reaction

pathway, HCOOH gets oxidised rapidly to CO₂ and H⁺ through a short-lived and weakly bound anhydride intermediate, generating some electrons. The slow pathway involves the formation of CO on Pd catalytic sites, and H₂O.

The fast reaction pathway would be preferred since no CO is formed and hence there is no sluggishness in the reaction kinetics. Electronic effects are believed to weaken binding to CO [15].

Lee and Zhou have characterised the Au@Pd by XPS [15]. They found that there was a weak negative binding energy shift in photoemission peak of the 3d-orbital of Pd. This gave rise to more surface oxidation of Pd in the Au@Pd. They related these phenomena to Au donating d-electrons to the Pd metal and the thin Pd shell structure. This interaction between the Au-core and the Pd shell is most probably what contributes in weakening the CO adsorption strengths in the Pd-CO_{ads} thereby releasing the Pd sites.

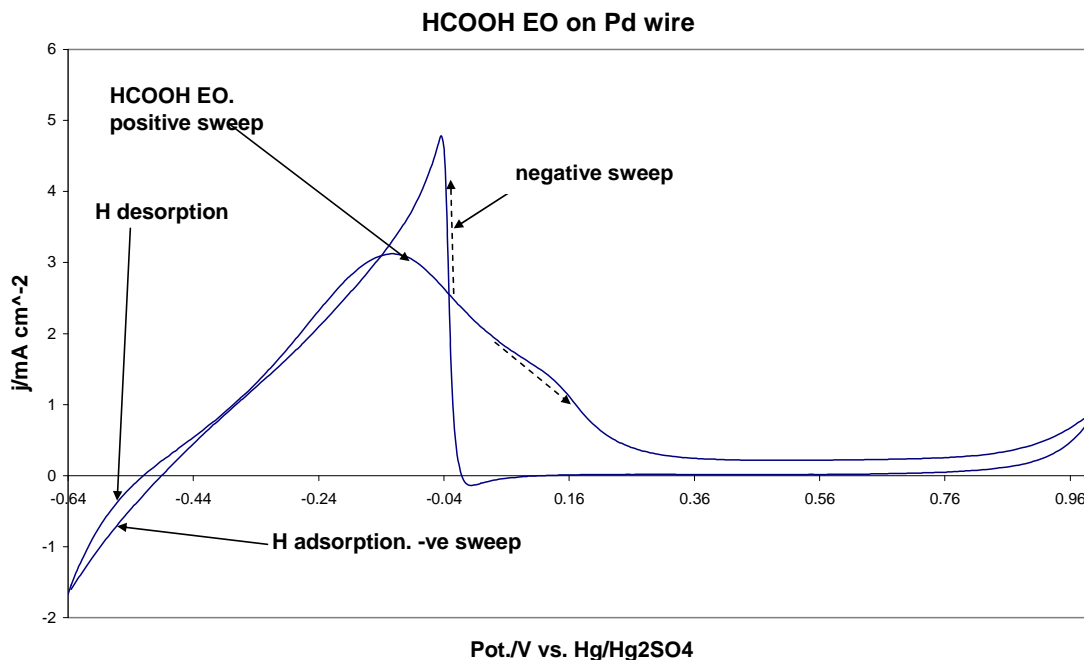
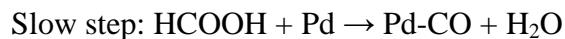
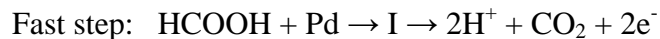


Fig. 4.2.2.6: HCOOH electro-oxidation on Pd wire. Scan was initiated at -0.64V vs Hg₂/HgSO₄ ref. electrode, in a 0.05 M H₂SO₄ electrolyte. Scan rate: 0.05 V s⁻¹.

Palladium wire, though, produced much more current (fig 4.2.2.6), although the Au@Pd NRs outperformed even this in terms of catalyst stability during the electro-oxidation of HCOOH. It was observed that the catalytic stability of Pd wire dropped quite early compared to the Au@Pd NRs which showed increase in current and stability up to 220 scans.

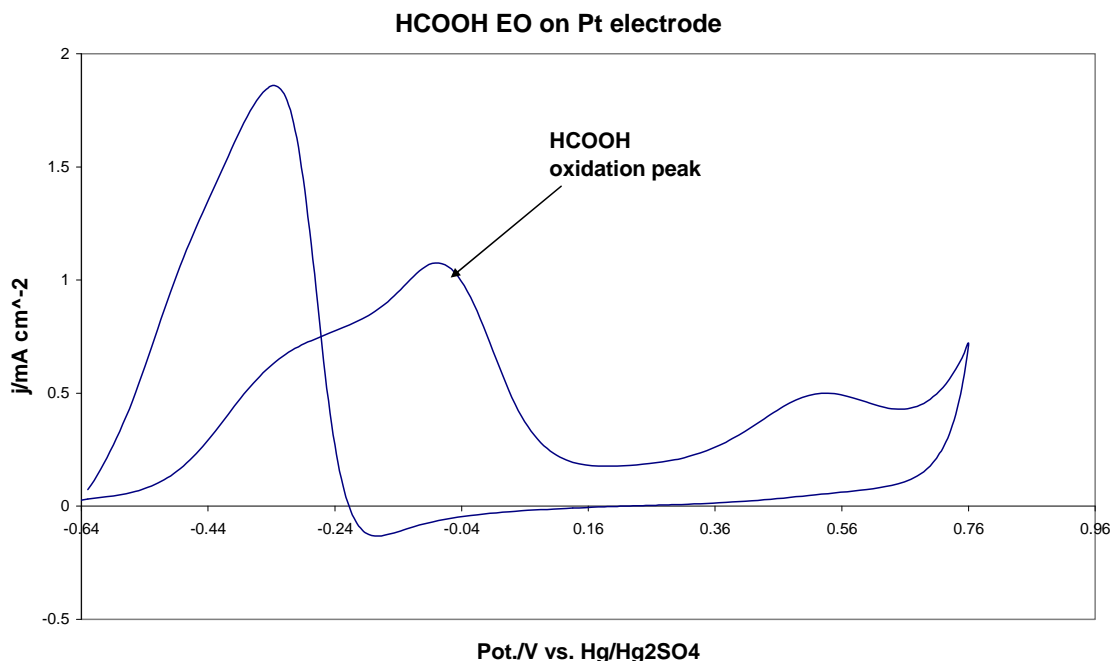


Fig. 4.2.2.7: HCOOH electrooxidation on Pt electrode. Scan was initiated at -0.64 V vs Hg/Hg₂SO₄ ref. electrode, in a 0.05 M H₂SO₄ electrolyte. Scan rate: 0.05 V s⁻¹.

Investigation of FA EO on polycrystalline Pt is shown in the CV on figure 4.2.2.7. It was observed that the catalytic activity of Pt dropped quickly in HCOOH suggesting accumulation of CO_{ads}. The maximum current produced per unit centimetre was 1.08 mA. This is only about one-ninth that produced by the centrifuged Au@Pd NRs and only about half that produced by the as-made Au@Pd NRs.

Figure 4.2.2.8 is the CV of HCOOH electro-oxidation on the UPD produced Au@Pt NRs. Oxidation of formic acid is observed from the peak at 0.59 V, which was only observable during the first five scans. Then after, there was no HCOOH oxidation peak. All the other features on the CV resemble those of polycrystalline Pt in 0.05 M H₂SO₄ in

figure 4.2.1.3. The peaks for the oxide formation on Pt and for the Pt oxide reduction are very small, implying there was very little oxide formed on the Pt sites. The peak at 0.59 V may be ambiguous as it may either be FA oxidation and Pt oxide formation peaks combined or oxide formation. Further experiments will be needed to confirm the origin of the current.

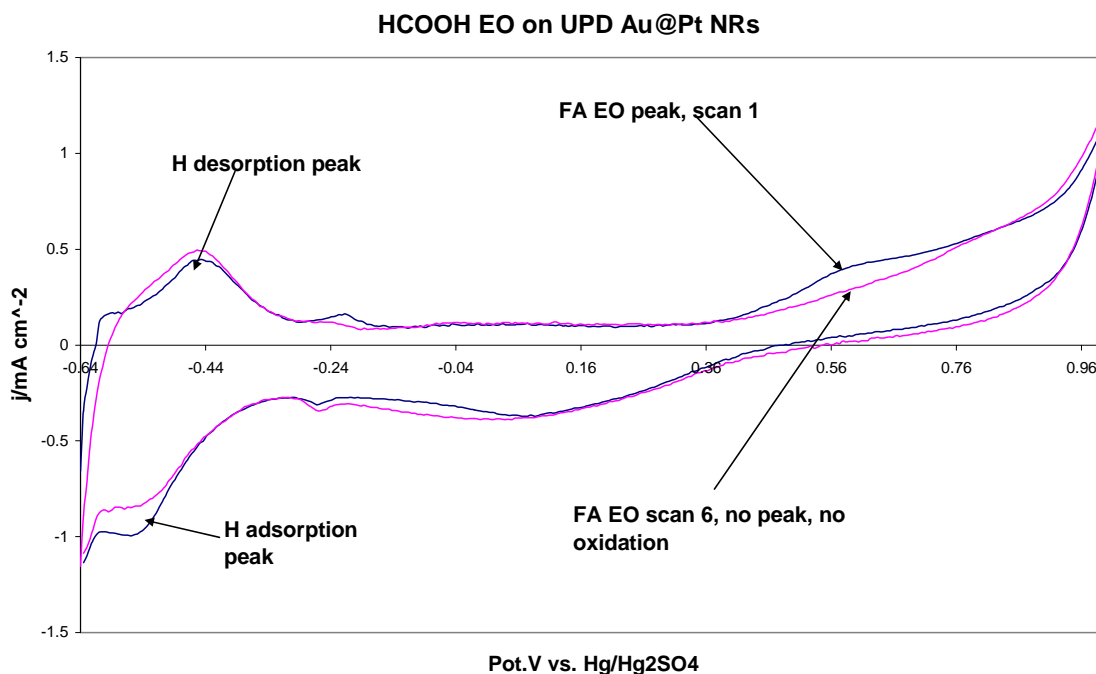


Fig. 4.2.2.8: CV of HCOOH electro-oxidation on Au@Pt obtained by Cu UPD. Scan was initiated at -0.64 V on Glassy carbon vs Hg/Hg₂SO₄ ref. electrode, in a 0.05 M H₂SO₄ electrolyte. Scan rate: 0.05 V s⁻¹.

Catalyst stability was investigated by monitoring the catalytic activities of the various catalysts with number of scans during the electro-oxidation of HCOOH.

For the electro-oxidation of 0.05 M HCOOH in 0.05 M H₂SO₄ on the Pt electrode, it was observed that the catalytic activity of the active sites on the Pt gradually depreciated. Depreciation was indicated by the gradual drop in current produced just after the fourth scan (there was an increase from first to fourth). Fig 4.2.2.7 is the CV obtained from scans using Pt.

4.2.3 Electro-oxidation of Methanol (CH₃OH)

Methanol electro-oxidation was investigated over Au@Pt, Au@Pd, Au@Rh and, Pt electrode and Pd wire. The potential scans are represented by the CVs below (figs 4.2.3, 1 - 4).

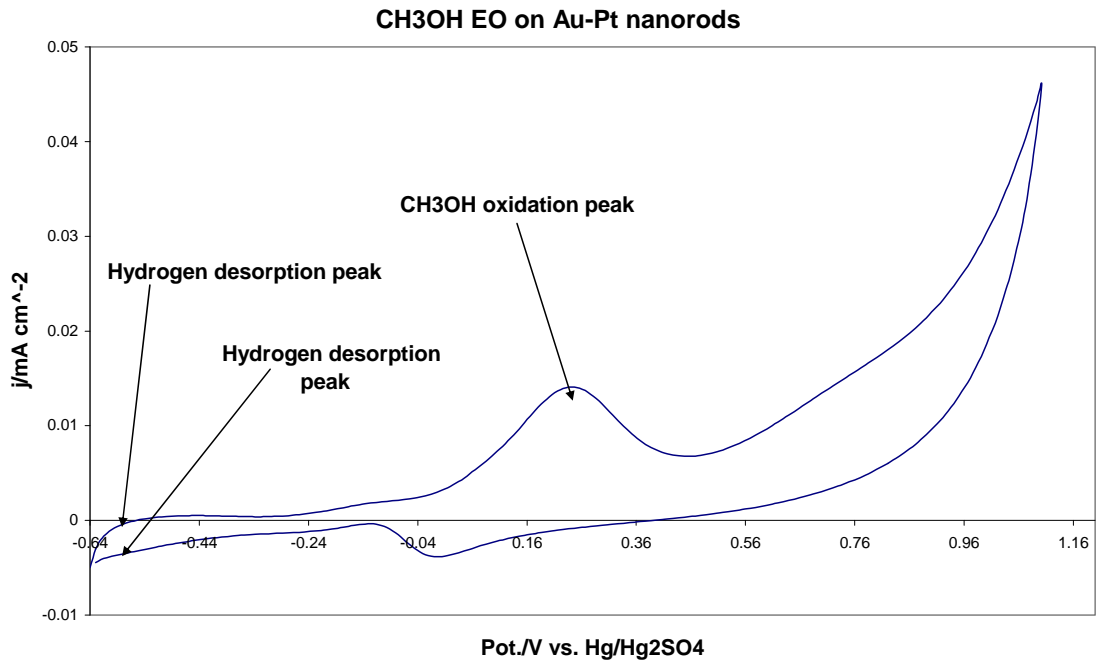


Fig 4.2.3.1: CV of 0.1 M methanol on Au@Pt nanorods in 0.05 M H₂SO₄ on Au electrode vs Hg/Hg₂SO₄ reference and Pt wire counter electrode. Scan rate: 0.05 V s⁻¹

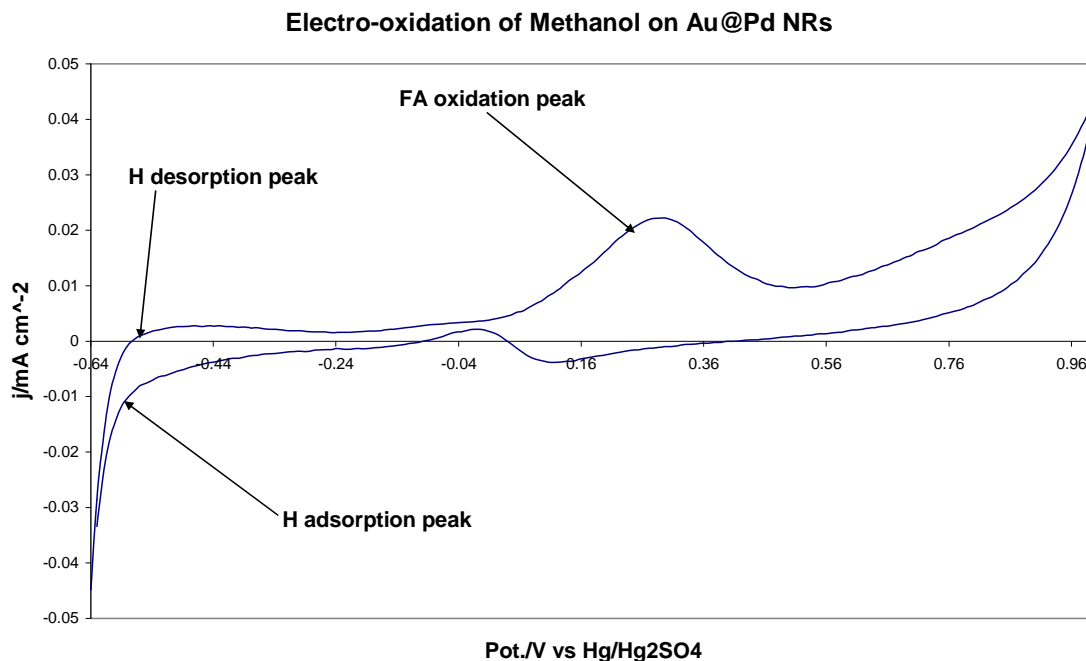


Fig 4.2.3.2b: CV of 0.1 M methanol on Au@Pd nanorods in 0.05 M H₂SO₄ on Pt electrode vs Hg/Hg₂SO₄ reference and Pt wire counter electrode. Scan rate: 0.05 V s⁻¹

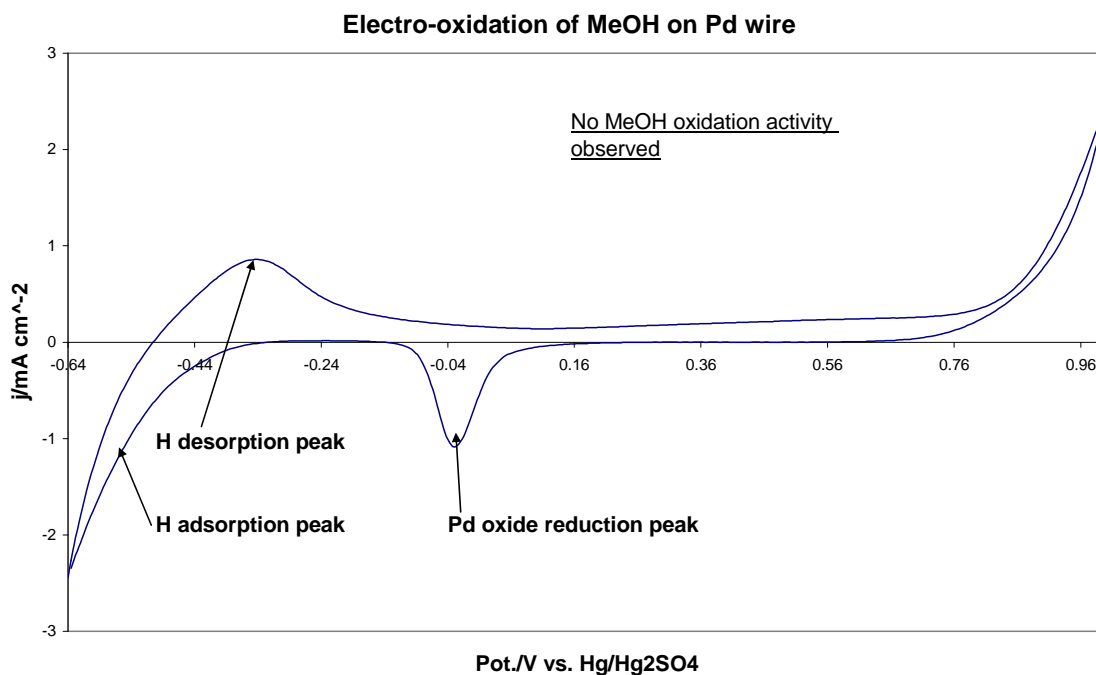


Fig 4.2.3.3: CV of 0.1 M methanol on Pd wire in 0.05 M H₂SO₄ vs Hg/Hg₂SO₄ reference and Pt wire counter electrode. Scan rate: 0.05 V s⁻¹

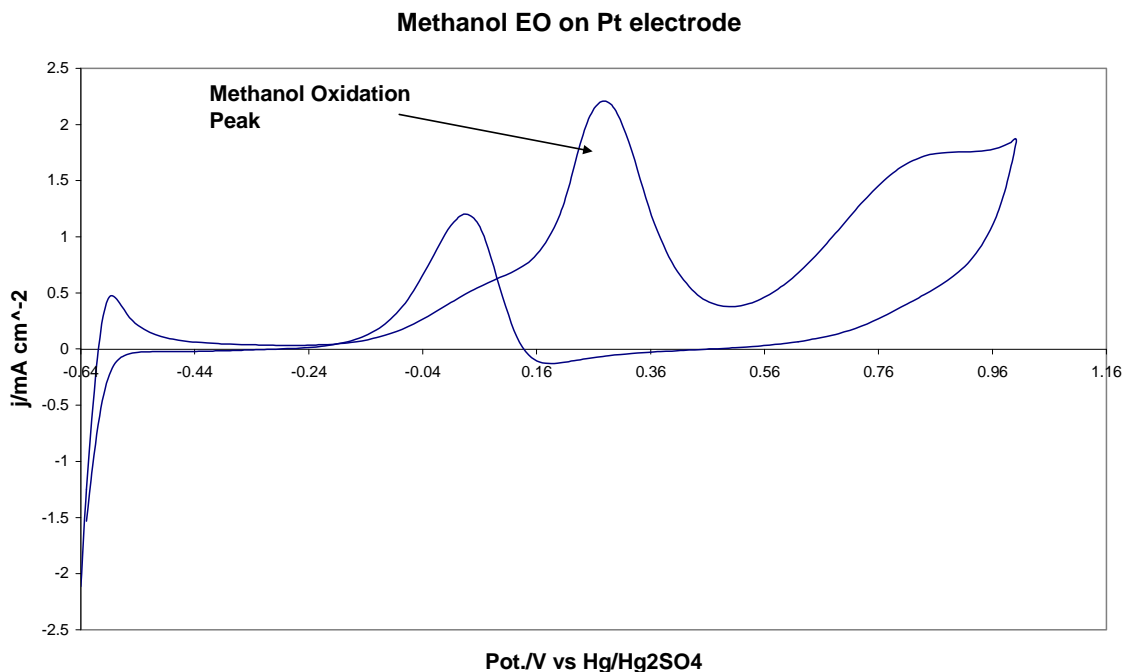


Fig 4.2.3.4: CV of 0.1 M methanol on Pt electrode in 0.05 M H₂SO₄ vs Hg/Hg₂SO₄ reference and Pt wire counter electrode. Scan rate: 0.1V s⁻¹

Potential scans in the forward direction was initiated at -0.64 V where the cycle was ended. At the beginning of the scan on Au@Pt, hydrogen is adsorbed on the Pt sites indicated by the small hydrogen peak shown. During the scan, oxide layers form on the Pt sites of the rods and are reduced in the backward scan. Methanol starts to be oxidised at a potential of about 0 V, producing an anodic peak current which increased up to a maximum of 2.2 mA cm⁻² in the eleventh scan and stayed stable for several scans after. As mentioned earlier in the introduction, methanol is innately toxic and has sluggish reaction kinetics. These are likely to be the reasons why the electro-oxidation of CH₃OH on Au@Pt only yielded a small current compared to that generated by HCOOH electro-oxidation on Au@Pd nanorods. HCOOH, HCHO and adsorbates such as -(COH)_{ads}, (-HCO)_{ads}, (-COOH)_{ads}, (CH_xOH)_{ads}, and CO (both bridged and linear bonded) form during the electro-oxidation of methanol [43]. Formic acid is in a more oxidised state than methanol and is likely to form less CO during the oxidation reaction. For comparison, fig 4.2.3.4 above is a CV of platinum electrode in 0.1 M CH₃OH + 0.05 M H₂SO₄. Platinum works well as an anode catalyst in the electro-oxidation of methanol but it becomes poisoned very easily by adsorbed CO species.

Methanol electro-oxidation was also investigated on Au@Pd nanorods. Fig 4.2.3.2 is the CV obtained from the scans which show that methanol was oxidised on Au@Pd. Since a platinum working electrode was used for the electro-chemical reaction and platinum on its own oxidises methanol, the Au@Pd nanorods were retested for methanol electro-oxidation on an Au electrode, which does not oxidise methanol. This was to confirm that the contribution towards the electro-oxidation of methanol came from the Au@Pd NRs. The CVs obtained from over twenty scans showed no indication of methanol electro-oxidation. It therefore means that the Pt electrode contributed towards the electro-oxidation of methanol in the results presented by the CV of fig 4.2.3.2, especially as the oxidation occurred at the same potential as in the case with Pt electrode, and the features are similar to those of bulk Pt. This is further supported by figure 4.2.3.2 above, which shows no methanol oxidation on bulk Pd.

This experiment was repeated with the Au@Pd NRs supported by carbon black pasted on the glassy carbon electrode. Interestingly enough, the Au@Pd/C then oxidised methanol (see fig 4.2.3.5).

This means that the Au@Pd NRs did not properly adhere to the electrode when the dithiol was used. The thiol groups therefore may have been oxidised. Carbon attachment is thus the preferred method for our nanorods.

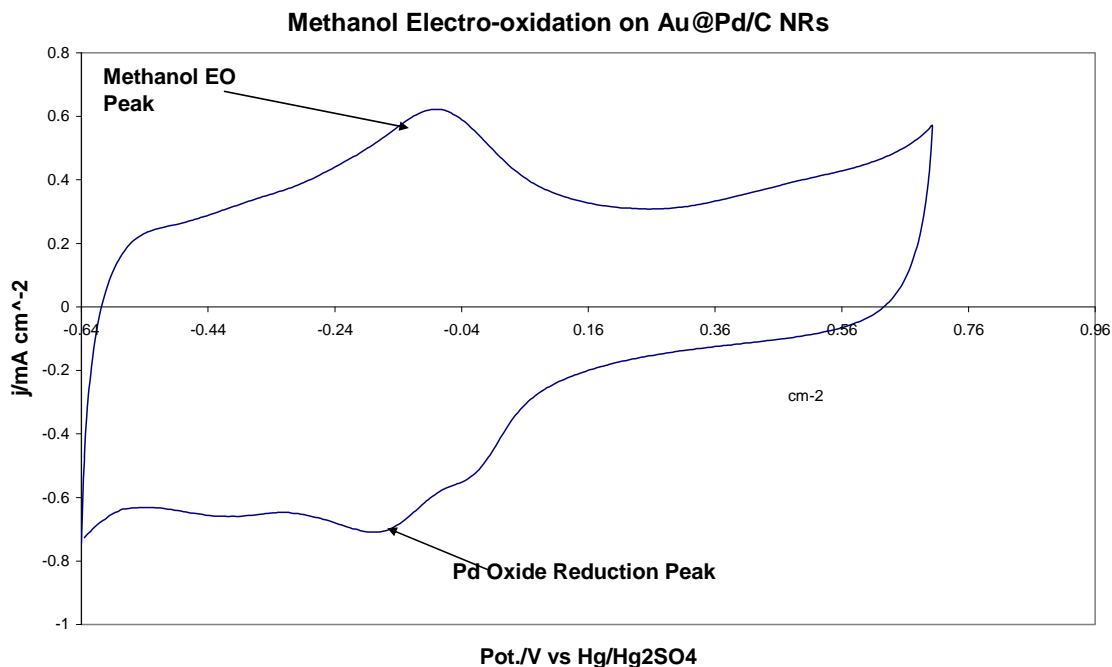


Fig 4.2.3.5: CV of 0.1 M methanol on Au@Pd/C in 0.05 M H₂SO₄ vs Hg/Hg₂SO₄ reference and Pt wire counter electrode. Scan rate: 0.05 V s⁻¹

As described earlier in the case of HCOOH electro-oxidation on Au@Pd, electronic effects enhance the catalytic activity. In the case of Pt in Au@Pt, both the bifunctional mechanism and electronic effects could contribute in CO tolerance. Gold will easily react with water to form Au-OH_{ads}, which will then react with the Pt-CO_{ads} formed to remove the CO species and release the Pt active catalyst sites. This takes place at a potential lower than that of pure Pt [44]. It is more likely that Au is exposed in this system as Pt is known to form clusters rather than smooth atoms thereby allowing access of the reactants to the Au-core surface. Should that be the case, then the bifunctional mechanism becomes applicable. However, electronic effects may also contribute to the observed results.

In order to investigate the stability of the mono- and bi-metallic catalysts, as was done in the case of HCOOH, over 400 scans were made on each during methanol electro-oxidation. It was observed that the current produced during electro-oxidation of methanol on the bimetallic core-shell Au-Pt (though smaller), was stable longer than the monometallic Pt which gradually dropped after 460 scans. This shows that electronic

effects based on the core-shell structure of Au-Pt helps stabilise Pt as a catalyst, viz. the bi-functional mechanism explained earlier. By observation, the catalytic activity of platinum by comparison drops faster in the electro-oxidation of formic acid, far faster than is the case with methanol.

4.2.4 Oxygen Reduction Reactions (ORRs)

4.2.4.1 ORR on Au@Pt/C NRs

Before ORR was performed on the Au@Pt NRs, a scan was done first in an O₂-saturated H₂SO₄ solution.

The CV below (fig. 4.2.4.1.1) shows a characteristic cathodic peak in the vicinity of 0.4 V which is a reduction peak of Pt oxide formed during the forward scan. This is evidence that Pt has taken the place of Cu on the Au rods to form Au-Pt NRs. A further scan of the electrode after purging in flowing O₂ yields a slightly more negative cathodic peak indicating reduction of O₂. O₂ can be reduced once the surface oxides are removed.

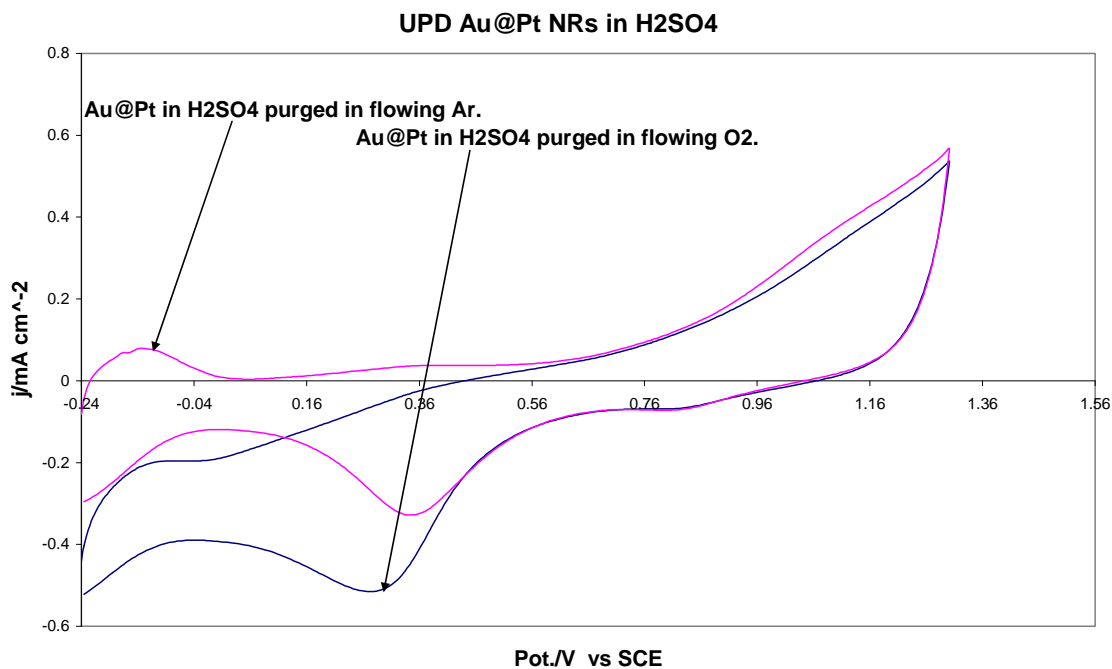


Fig 4.2.4.1.1: Cyclic Voltammograms of Au@Pt/C in Ar purged and O₂ saturated 0.05 M H₂SO₄ solutions. Glassy carbon vs SCE. Scan rate: 0.05 V s⁻¹

For ORR, scans were performed at rotating speeds of 100, 400, 900 and 1600 rpm. Figure

4.2.4.1.2 presents the results. The calculated rate constant for the reaction k_c was $9.95 \times 10^{-6} \text{ cm s}^{-1}$. The surface area used for the calculations was the electrode area of 0.071 cm^2 . A limiting current is not reached in this case.

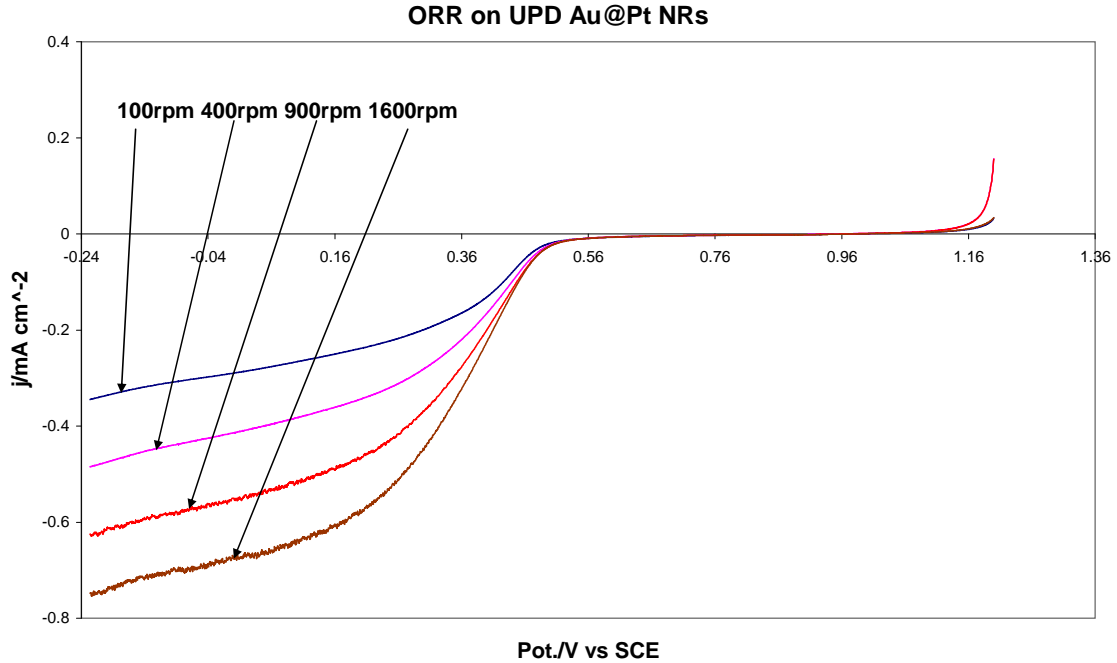


Fig 4.2.4.1.2: ORR on Au@Pt/C in O_2 saturated $0.05 \text{ M H}_2\text{SO}_4$ at different rotating disk speeds, on glassy carbon. Scan rate: 0.002 V s^{-1}

4.2.4.2 ORR on Au@Rh/C NRs

A similar RDE experiment was carried out on the Au@Rh NRs. Figures 4.2.4.2.1 and 4.2.4.2.2 present the results of these ORR experiments. Scans were performed in a similar way as was with Pt. Unlike the case with Pt, the Au@Rh system displayed a limiting current. A current-potential curve in the mixed kinetic control region was used to analyse the reaction kinetics.

Koutecky-Levich plots were used to derive the rate constants and the number of electrons was calculated from the expression:

$$b = 0.62nFS c_{\text{O}_2} (D_{\text{O}_2})^{2/3} \nu^{-1/6}$$

Equation 4 [47]

b is the Levich slope

n is the number of electrons

F is Faradays constant = 96485 C mol^{-1}

S is the surface area

$D_{O_2} = 1.93 \times 10^{-5} \text{ cm}^2 \text{ s}^{-1}$ [47]

$c_{O_2} = 1.22 \times 10^{-6} \text{ mol cm}^{-3}$ [47]

$\nu = 8.93 \times 10^{-3} \text{ cm}^2 \text{ s}^{-1}$ [47]

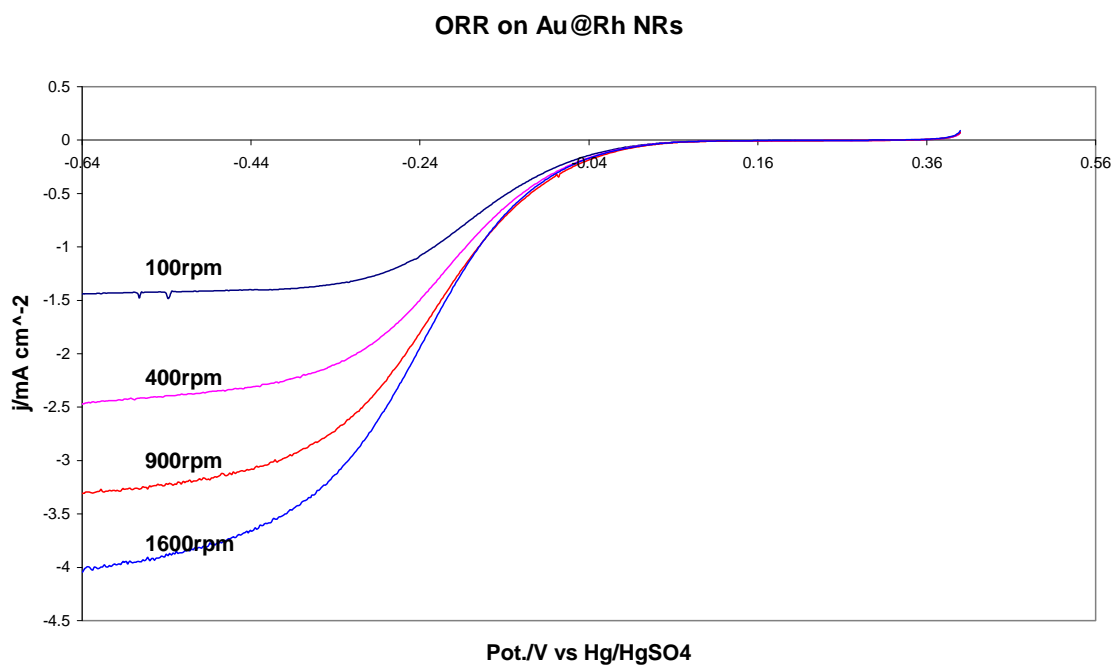


Fig 4.2.4.2.1: ORR on Au@Rh/C in O_2 saturated $0.05 \text{ M H}_2\text{SO}_4$ at different rotating disk speeds, on glassy carbon vs Hg/Hg₂SO₄SCE. Scan rate: 0.002 V s^{-1}

Koutecky-Levich Plot for ORR on Au@Rh Rxn 1

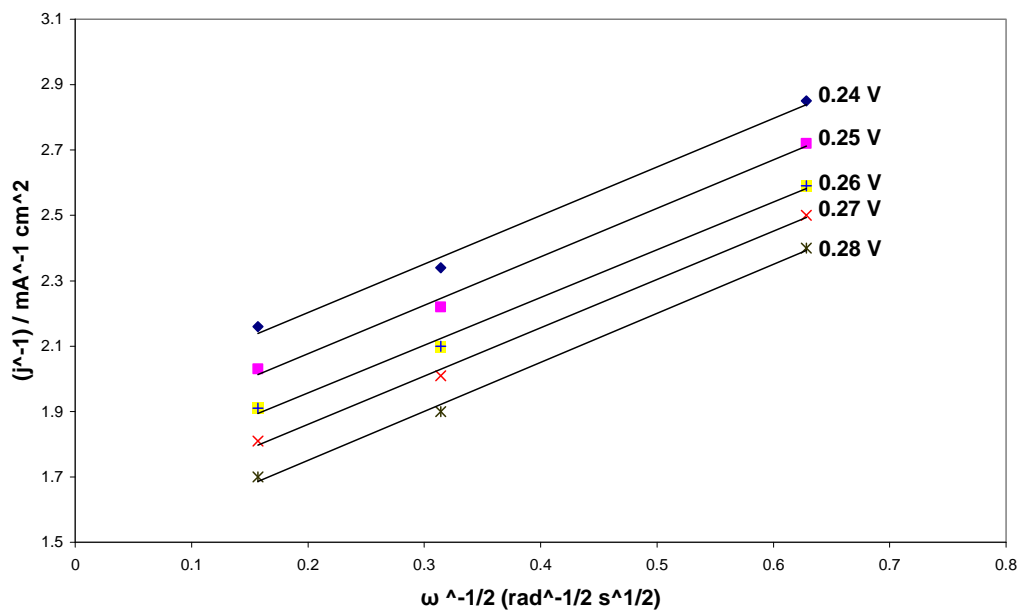


Fig 4.2.4.2.2: Koutecky-Levich plots for ORR expt.1 in O₂-saturated 0.05 M H₂SO₄ on Au@Rh NRs at different rotating disk speeds, on glassy carbon vs SCE. Scan rate: 0.002 V s⁻¹

Figure 4.2.4.2.2 displays the Koutecky-Levich plots for the first ORR performed on Au@Rh/C NRs. From the slope 1.487 mA cm⁻² rad^{-1/2}s^{1/2}, the number of electrons transferred was evaluated using the Levich equation, equation (a) above as 5. The rate constant k_c for the reaction was found to be 1.2×10^{-5} cm s⁻¹.

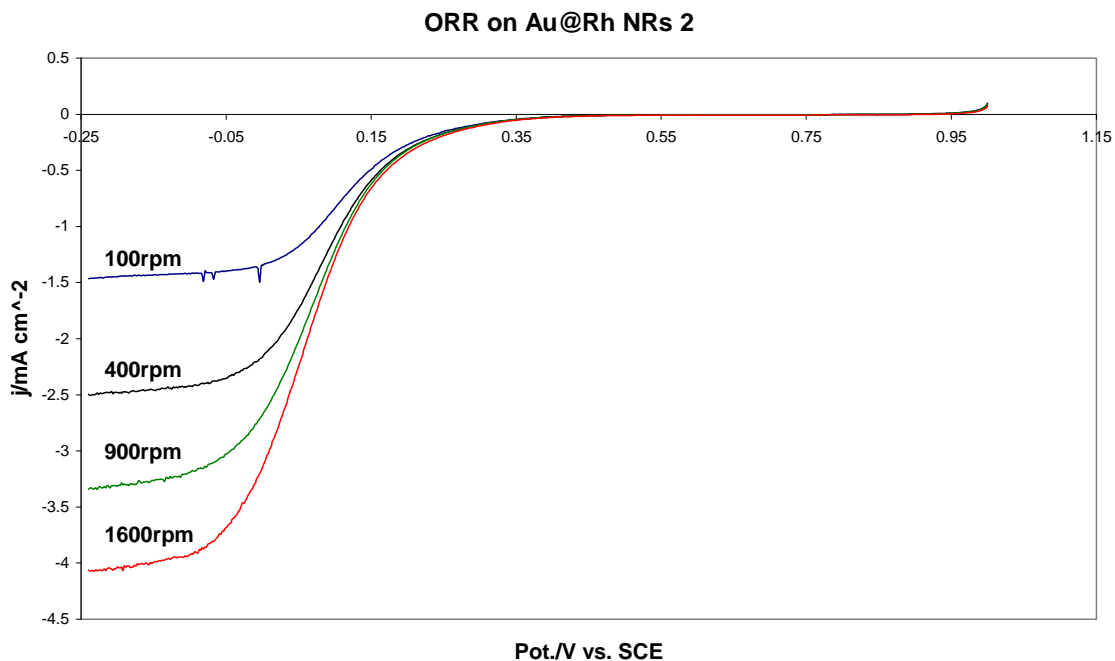


Fig 4.2.4.2.3: ORR on Au@Rh/C in O₂ saturated 0.05 M H₂SO₄ at different rotating disk speeds, on glassy carbon vs SCE. Scan rate: 0.002 V s⁻¹

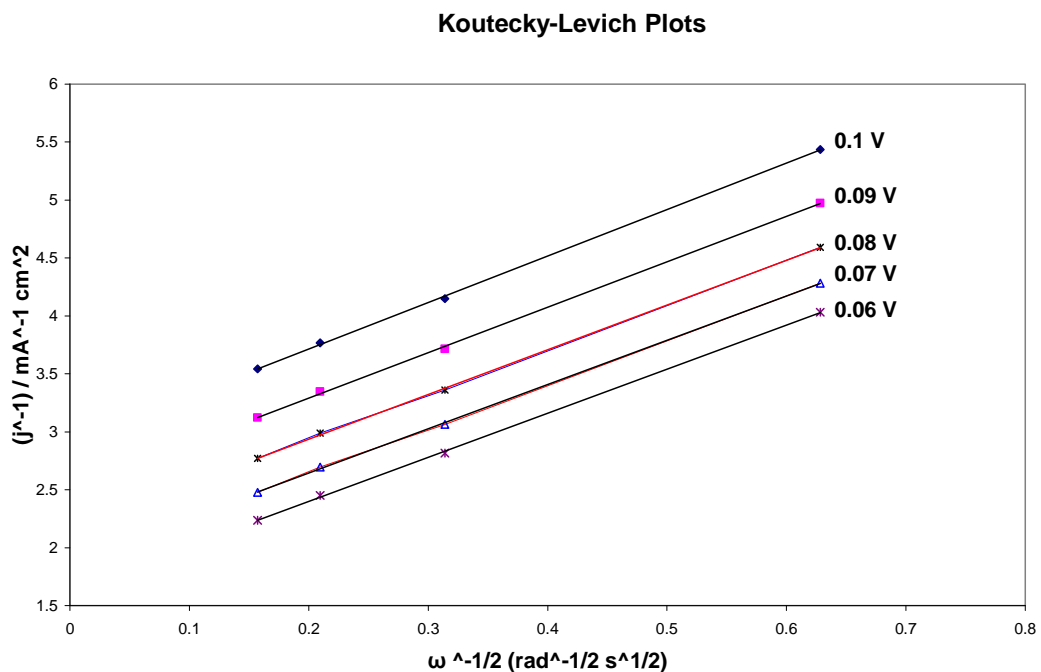


Fig 4.2.4.2.4: Koutecky-Levich plots for ORR expt.2 in O₂-saturated 0.05 M H₂SO₄ on Au@Rh NRs at different rotating disk speeds, on glassy carbon vs SCE. Scan rate: 0.002 V s⁻¹

Figure 4.2.4.2.4 displays the Koutecky-Levich plots for the second ORR performed on Au@Rh/C NRs (Fig 4.2.4.2.3). The Koutecky slope of $4 \text{ mA cm}^{-2} \text{ rad}^{-1/2} \text{ s}^{1/2}$ was used to determine the number of electrons transferred during the reaction. From the Levich equation, equation (a) above, the number of electrons transferred was 2 and the rate constant k_c determined for the reaction was $1.4 \times 10^{-6} \text{ cm s}^{-1}$. If more time had been available, more experiments would have been carried out to narrow the error obtained in the calculation of the number of electrons transferred.

If the number of electrons was in fact 4 in each case, the average k_c would be $6.7 \times 10^{-6} \text{ cm s}^{-1}$.

4.2.5 Carbon monoxide (CO) Stripping

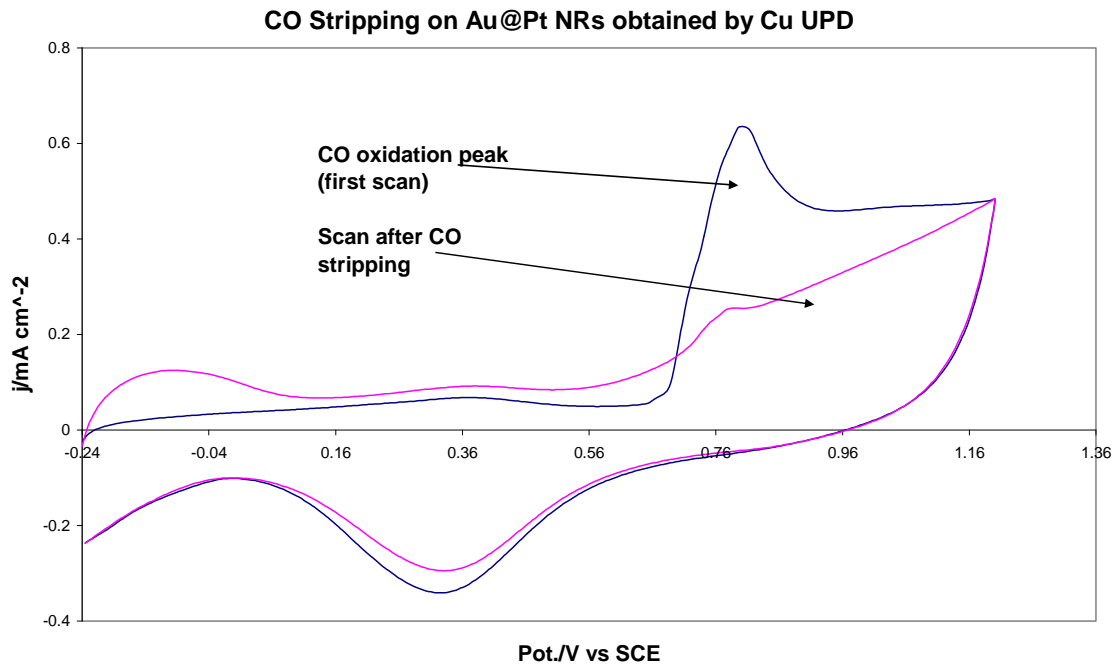


Fig 4.2.5.1: CO stripping CV on Au@Pt/C NRs on glassy carbon Vs SCE. Scan rate 0.05 m V s^{-1}

Figure 4.2.5.1 above is a CV for the oxidation of CO by Au@Pt NRs. The first scan showed a characteristic peak at 0.8 V producing a current density $j = 0.6 \text{ mA cm}^{-2}$. The second scan (purple line) showed almost exclusively features of Pt oxide formation and reduction, indicating that the CO had been oxidised to CO_2 .

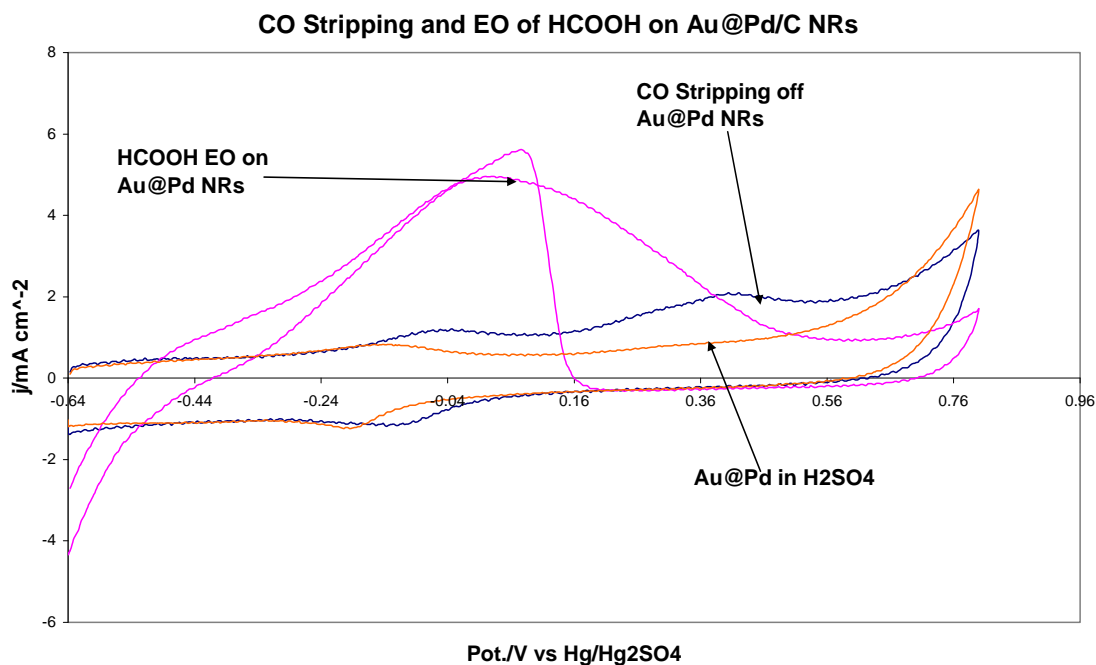


Fig 4.2.5.2: CO stripping and HCOOH EO CV on Au@Pd/C NRs on glassy carbon . Scan rate 0.05 V s^{-1}

CO-stripping on Au@Pd/C represented on fig 4.2.5.2 is analogous to that on Au@Pt on figure 4.2.5.1. After the CO was stripped-off, the electrode was used to oxidise HCOOH. The purple plot shows the electro-oxidation of HCOOH at 0.033 V in the positive-going producing a current of 4.9 mA cm^{-2} of electrode surface. The current produced is almost twice that produced by the thiol immobilised Au@Pd (Fig. 4.2.5.1), suggesting that the catalyst material is better immobilised in nafion stabilised-carbon black.

In a similar sequence, CO and HCOOH were oxidised on Au@Rh/C NRs. The results are presented in figure 4.2.5.3 below. The oxidation of CO started at 0.22 V , reaching a peak current density of 3.55 mA cm^{-2} at 0.28 V .

The electrode was analysed for HCOOH EO. The orange plot shows the EO of HCOOH which produced a peak with a maximum at 0.22 V and a current of 2.7 mA cm^{-2} .

The fact that Au@Rh NRs did oxidise CO and HCOOH adds to the UV-Vis evidence for Au-coverage by Rh.

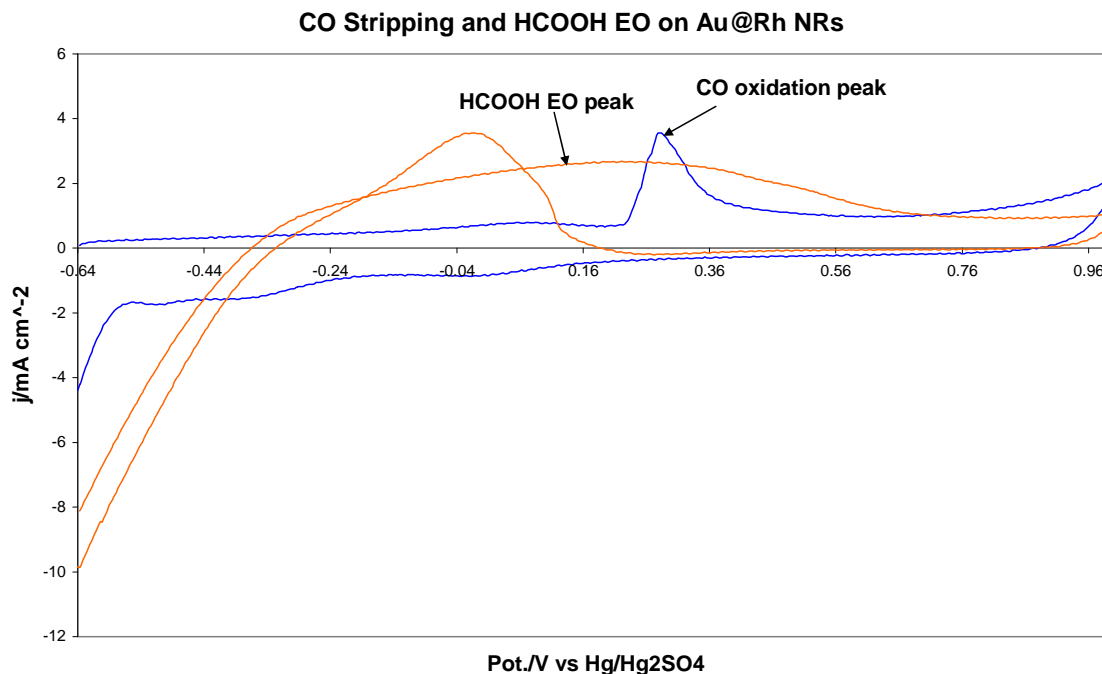


Fig 4.2.5.3: CO stripping and HCOOH EO CV on Au@Rh/C NRs on glassy carbon. Scan rate 0.05 V s^{-1}

Figure 4.2.5.4 below is a combined CV of CO stripping and HCOOH EO on Au@Pd NSs. This experiment was performed in order to investigate how well core-shell Au-Pd NSs compare to core-shell Au-Pd NRs.

The results show that oxidation of CO started at -0.1 V and reached a maximum at 0.1 V , producing a current of 0.2 mA cm^{-2} . HCOOH oxidation started at 0.09 V , producing a current of 0.143 mA cm^{-2} in the positive going.

The results clearly show that the loading of Au@Pd NRs was more successful than that of their Au@Pd NSs counterparts. The catalytic activity towards the HCOOH oxidation seems to be greater for NRs. It was intended to use the CO stripping measurements to determine surface area but the peaks are rather broad and difficult to deconvolute from the charging current and other oxidation currents at more positive potentials. Further investigations could be carried out with more time, varying the upper limit of the CV and the CO deposition conditions (e.g. adsorbing at different applied potentials).

For an analysis of the peaks observed in the negative-going on a majority of the systems, Weaver et al. attributed it to a recovery of the attenuating current in the oxidation peak

region [49]. Therefore, we think the peak is possibly due a recovery of the catalyst surface due to the decomposition of the adsorbed species and oxides.

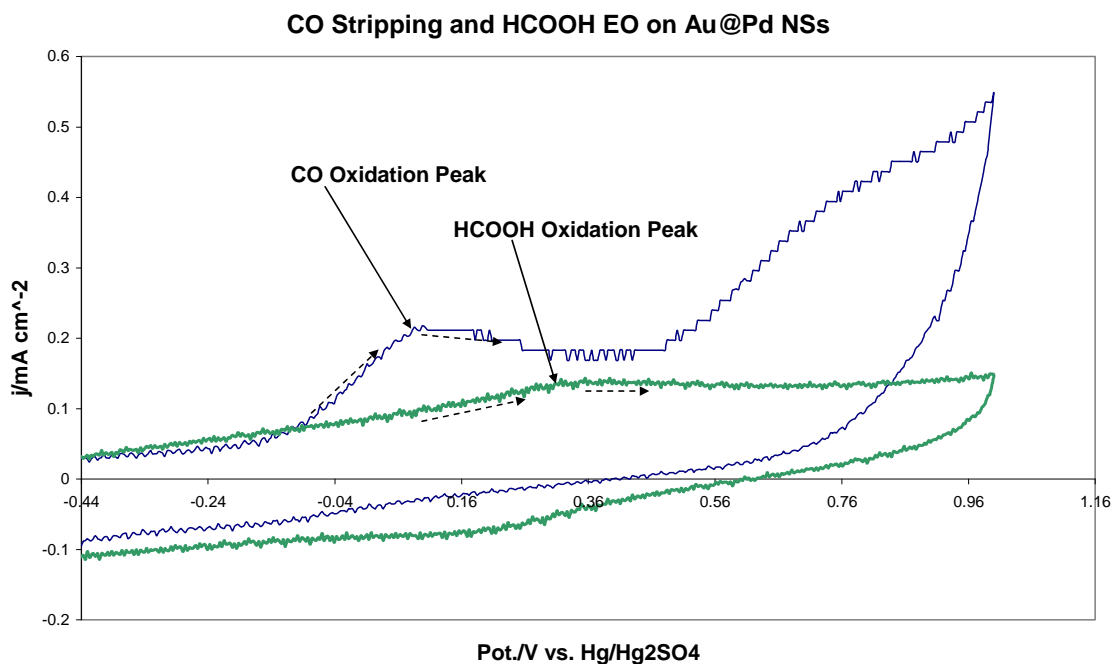


Fig 4.2.5.4: CO stripping and HCOOH EO CV on Au@Pd/C NSs on glassy carbon. Scan rate 0.05 V s^{-1}

CO oxidation was investigated on AuNRs immobilised on carbon black. Figure 4.2.5.5 is a resultant CV of the stripping. Oxidation of the adsorbed CO started at 0.14 V producing a small peak with maximum at 0.26 V. The current produced was 0.33 mA cm^{-2} . This peak might be due to oxidation of CO as it is the only feature absent in the CV of AuNRs/C in $0.05 \text{ M H}_2\text{SO}_4$ (figure 4.1.6.2 above).

The inset is a CV of the same electrode in $0.05 \text{ M HCOOH} + 0.05 \text{ M H}_2\text{SO}_4$. Electro-oxidation of HCOOH started at 0.16 V producing a maximum current density peak of 0.35 mA cm^{-2} which is greater than that produced by Au electrode. This shows that the catalytic activity of nanoparticle catalysts (or their loading) can be varied by varying their shapes.

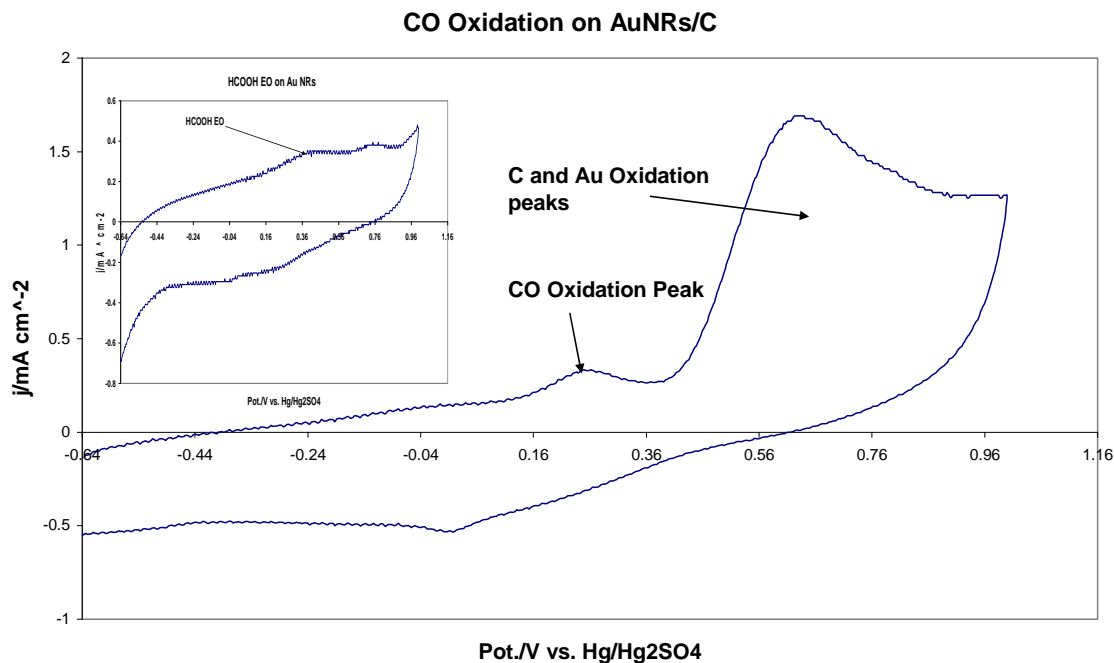


Fig 4.2.5.5: CO stripping and HCOOH EO CV on AuNRs/C on glassy carbon. Scan rate 0.05 V s⁻¹

4.3 Summary

The schematic below represents the step-wise procedure in fabricating Au nanorods in the seed-mediated method.

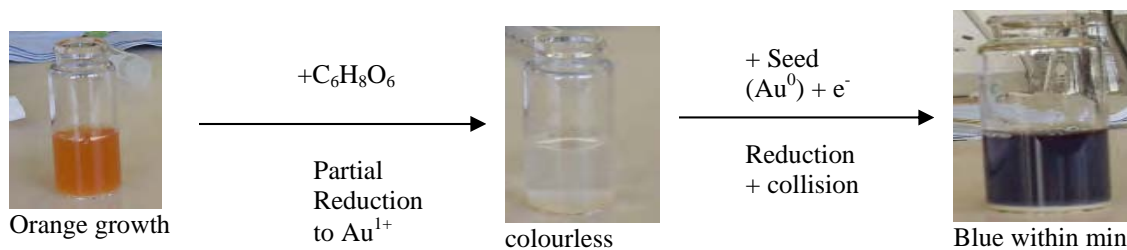


Figure 4.3: Schematic of the 3-step process of gold nanorod synthesis

Table 4.3 below summarises the electro-catalysis experiments performed on different nanoparticles and their results.

Table 4.3: Electro-catalysis

Catalyst Material	Electro-oxidation Test	Applications
Au-Pd NRs	HCOOH and CH ₃ OH successful	DFAFCs and DMFC for power supply in portable electronic devices
Au@Pd NSs	CO, HCOOH successful	DFAFCs for power supply in portable electronic devices
AuNRs	CO and HCOOH successful	DFAFCs for power supply in portable electronic devices
Au@Pt NRs	HCOOH, CH ₃ OH and ORR successful	DFAFCs and DMFC for power supply in portable electronic devices
Au@Rh NRs	HCOOH, CH ₃ OH and ORR successful	DFAFCs and DMFC for power supply in portable electronic devices
Pd particles	The deposition of particles was unsuccessful	

5.0 Conclusions and Future Work

Gold nanorods of a very good yield, high aspect ratios and of good size distributions have been successfully synthesised in this work. By counting the number of rods contained within randomly scanned areas, it is clear that the percentage purity is greater than 20 % as the literature states, conveniently 50 % or slightly above. We have therefore proved that the wet chemical synthesis can produce nanoparticles with over 20% consisting of rods in the as-made solution.

We have shown in this work that Au NRs can be coated with Pd, Rh and Pt in aqueous solutions as well as by UPD of Cu with Pt.

Successful electro-oxidation of HCOOH on Au@Pd, Au@Rh, Au@Pt NRs, and methanol on Au@Pd, and Au@Pt NRs, has proved that the catalytic efficacies of these metals are tremendously enhanced in the bimetallic core-shell structure which surpasses the mono-metallic forms. The results obtained from ORR on Rhodium were quite encouraging implying that Rhodium may be a substitute for Pt in catalyst design for oxygen reduction.

A number of journals state that the applications of gold nanoparticles are on the rise. It will therefore be interesting to adopt other methods by which high yields of AuNRs can be synthesised without the need for purification. It will also be useful to look for a means by which the wet chemical synthetic method can be developed to improve rod yield and minimise the other particles' formation. Ag has been used as an additive to enhance the growth of NRs. If time permitted, it would be worthwhile to test chemical compounds to find one that may retard the growth of the other shapes. It may be useful as well to employ techniques such as EELS (more microscopy), EXAFS and XPS to monitor the surface composition of the bi-metallics before and after electrochemical processes and see if any changes occurred.

Whilst this project has studied the nanomaterials' performance as electrocatalysts, interest also lies in the investigation for improvement and durability of auto-catalytic converters using bimetallic gold alloy nanoparticles. Since gold particles have an enhanced superior

activity in catalysing CO oxidation and others at low temperatures, this could help cut down the amount of CO emissions tremendously during cold engine-start, thereby reducing air pollution.

Bibliography

1. C.R. Martin, *Nanomaterials: A Membrane-Based Synthetic Approach*, Science Vol. 266, **1994**
2. Muhammad Iqbal, Yong-II Chung and Giyoong Tae, *An enhanced synthesis of gold nanorods by the addition of Pluronic (F-127) via a seed mediated growth process* J. Mater. Chem., **2007**, 17, 335–342
3. Babak Nikoobakht, and Mostafa A. El-Sayed, *Preparation and Growth Mechanism of Gold Nanorods (NRs) Using Seed-Mediated Growth Method*, Chem. Mater. **2003**, 15, 1957-1962
4. N.R. Jana, L. Gearheart, C.J. Murphy, *Evidence for Seed-Mediated Nucleation in the Chemical Reduction of Gold Salts to Gold Nanoparticles*, Chem. Mater. **2001**, 13, 2313-2322
5. Jain P.K, El-Sayed I.H, El-Sayed M.A, *Gold Nanoparticles Target Cancer*, Nanotoday **2007**, 2(1), 18-29
6. Thompson D.T., *Using gold nanoparticles for catalysis*, Nanotoday **2007**, 2(4), 40-43
7. Chang S.S., Shih C-W., Chen C-D., Lai W-C., *The Shape Transition of Gold Nanorods*, Wang C.R.C. *Langmuir* **1999**, 15(3), 701-709
8. Roustom B.E., Siné G., Fóti G., Comninellis C., *A novel method for the preparation of bi-metallic (Pt–Au) nanoparticles on boron doped diamond (BDD) substrate: application to the oxygen reduction reaction*, J. Appl Electrochem **2007**, 37, 1227–1236
9. Pérez-Juste J., Correa-Duarte M.A., Liz-Marzán L.M., *Silica gels with tailored, gold*

nanorod-driven optical functionalities, Appl. Surf. Sci. **2004**, 226, 137-143

10. Cepak V. M., Martin C.R., *Preparation and Stability of Template-Synthesised Metal Nanorod Sols in Organic Solvents, J. Phys. Chem. B*, **1998**, 102 (49), 9985-9990
11. Pérez-Juste J., Pastoriza-Santos I., Liz-Marzán L.M., Mulvaney P., *Gold nanorods: Synthesis, characterisation and applications, Coord. Chem. Rev.* **2005**, 249, 1870–1901
12. Sau T.K., Murphy C.J., *Seeded High Yield Synthesis of Short Au Nanorods in Aqueous Solution, Langmuir* **2004**, 20 (15), 6414-6420
13. Aslan K., Zhang J., Lakowicz J.R., Geddes C.D., *Saccharide Sensing Using Gold and Silver Nanoparticles-A Review, Journal of Fluorescence*, **2004**, 14(4), 391-400
14. Haiss W., Thanh N.T.K., Aveyard J., Fernig D.G., *Determination of Size and Concentration of Gold Nanoparticles from UV-Vis Spectra, Anal. Chem.*, **2007**, 79(11), 4215-4221
15. Zhou W., Lee J.Y., *Highly active core-shell Au@Pd catalyst for formic acid electrooxidation, Electrochem. Commun.* **2007**, 9, 1725–1729
16. Ferrando R., Jellinek J., Johnston R.L., *Nanoalloys: From Theory to Applications of Alloy Clusters and Nanoparticles, Chem. Rev.*, **2008**, 108(3), 846-910
17. Toshima N., Yonezawa T., *Bimetallic nanoparticles: novel materials for chemical and physical Applications, New J. Chem.*, **1998**, 1179-1201
18. Binns C., *Nanoclusters deposited on surfaces, Surf. Sci. Reports*, **2001**, 44, 1-49
19. Bönnemann H., Richards R. M., *Nanosopic Metal Particles 2: Synthetic Methods*

and Potential Applications, Eur. J. Inorg. Chem. **2001**, 2455-2480

20. Doudna C. M., Bertino M. F., Blum F. D., Tokuhiko A. T., Lahiri-Dey D., Chattopadhyay S., Terry J., *Radiolytic Synthesis of Bimetallic Ag-Pt*

Nanoparticles with a High Aspect Ratio, J. Phys. Chem. B, **2003**, 107(13), 2966-2970

21. Suslick K.S., Hyeon T., Fang M., *Nanostructured Materials Generated by High-Intensity Ultrasound: Sonochemical Synthesis and Catalytic Studies, Chem. Mater.* **1996**, 8(8), 2172-2179

22. Tagliente M.A., Tapfer L., Antisari M.V., Mattei G., Mazzoldi P., *Synthesis and stability of indium nanoclusters formed in silica by ion implantation, J. Non-Cryst. Solids*, **2004**, 345-6, 663-666

23. Mattei G., Maurizio C., Sada C., Mazzoldi P., Fernandez C. de J., Cattaruzza E., Battaglin G., *Au-Cu and Pd-Cu nanoclusters obtained by ion implantation in silica: stability under thermal annealing, J. Non-Cryst. Solids*, **2004**, 345-6, 667-670

24. Maggioni G., Vomiero A., Carturan S., Scian C., Mattei G., Bazzan M., Fernández C. de J., Mazzoldi P., Quaranta A., Mea G.D., *Structure and optical properties of Au-polyimide nanocomposite films prepared by ion implantation, Appl. Phys. Lett.*, **2004**, 85(23), 5712-5714

25. Liu H.B., Canizal G., Schabes-Retchkiman P.S., Ascencio J.A., *Structural Selection and Amorphization of Small Ni-Ti Bimetallic Clusters, J. Phys. Chem. B* **2006**, 110, 12333-12339

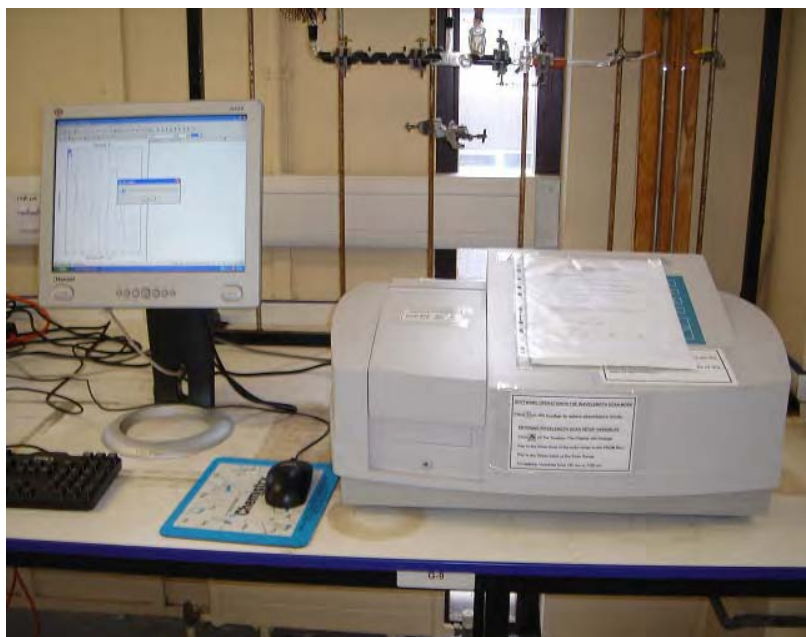
26. Renouprez A., Rousset J.L., Cadrot A.M., Soldo Y., Stievano L., *Structure and catalytic activity of palladium-platinum aggregates obtained by laser vaporisation of bulk alloys, J. Alloy Compd* **2001**, 328, 50-56

27. Rao C.N.R., Kulkarni G.U., Thomas P.J., Edwards P.P., *Metal nanoparticles and their assemblies*, *Chem. Soc. Rev.*, **2000**, 29, 27–35
28. Cortie M.B., van der Lingen E., *Catalytic gold nanoparticles*, *Mater. Forum* **2002**, 26, 1-14
29. Khanal B.P. and Zubarev E.R., *Purification of High Aspect Ratio Gold Nanorods: Complete Removal of Platelets*, *J. Am. Chem. Soc.* **2008**, 130, 12634–12635
30. Pavlov V., Xiao Y., Shlyahovsky B., Itamar Willner I, *Aptamer-Functionalized Au Nanoparticles for the Amplified Optical Detection of Thrombin*, *J. Am. Chem. Soc.* **2004**, 126, 11768-11769
31. Jana N.R., Wang Z.L., Pal T., *Redox Catalytic Properties of Palladium Nanoparticles: Surfactant and Electron Donor-Acceptor Effects*, *Langmuir* **2000**, 16, (6), 2457-2463
32. Kundu S. Lau S., and Liang H., *Shape-controlled catalysis by cetyltrimethylammonium bromide terminated gold nanospheres, nanorods and nanoprisms.*, *J. Phys. Chem. C* **2009**, 113, 5150-5156
33. Guo Y., Zheng D., Liu H., Friedrich A., Garche J., *Investigations of Bifunctional Mechanism in Methanol Oxidation on Carbon-Supported Pt and Pt-Ru Catalysts*, *J. New Mat. Electrochem. Systems* **2006**, 9, 33-39
34. Gasteiger H.A., Markovic N., Ross N.P.Jr, Cairns E.J., *CO Electrooxidation on Well-Characterised Pt-Ru Alloys*, *J. Phys. Chem.* **1994**, 98, 617-625
35. Rose H.H., *Optics of high-performance electron microscopes* *Sci. Technol. Adv. Mater.* **2008**, 9, 014107, 1-30

36. Seiler H., *Secondary electron emission in the scanning electron microscope*, *J. Appl. Phys.* **1983**, 54(11), R1-R18
37. Goodhew P.J. and Humphreys F.J., *Electron Microscopy and Analysis*, **1988**, 2nd Edition
38. Wang J., *Analytical electrochemistry*, **2000**, 2nd Edition
39. Larsen R. and Masel R.I., *Kinetic study of CO tolerance during electro-oxidation of formic acid on spontaneously Pt/Pd and Pt/Ru nanoparticles*, *Electrochem. Solid St. Lett.*, **2004**, 7(6), A148-A150,
40. Macaskie L.E., Baxter-Plant V.S., Creamer N.J., Humphries A.C., Mikheenko I.P., Mikheenko P.M., Penfold D.W., and Yong P., *Applications of bacterial hydrogenases in waste decontamination, manufacture of novel bionanocatalysts and in sustainable energy*, *Biochem. Soc. Trans.*, **2005**, Vol. 33, Part 1
41. Nath N. and Chilkoti A., *A Colorimetric Gold Nanoparticle Sensor To Interrogate Biomolecular Interactions in Real Time on a Surface*, *Anal. Chem.* **2002**, 74, 504-509
42. Denney R.C. and Sinclair R., *Visible and Ultraviolet Spectroscopy.*
43. Choi J-H., Park K-W., Park I-S., Kim K., Lee J-S., and Sung Y-E., *A PtAu Nanoparticle Electrocatalys for Methanol Electro-oxidation in Direct Methanol Fuel Cells*, *J. Electrochem. Soc.*, **2006**, 153 (10), A1812-A1817
44. Jeon M.K., Daimon H., Lee K.R., Nakahara A., Woo S.I., *CO Tolerant Pt/WC methanol electro-oxidation catalyst*, *Electrochem. Commun.*, **2007**, 9, 2692-2695

45. Maciá M.D., Campiña J.M., Herrero E., Feliu J.M., *On the kinetics of oxygen reduction on platinum stepped surfaces in acidic media, J. Electroanal. Chem.*, **2004**, 564, 141-150
46. Kunitatsu K., Senzaki T., Samjeské G., Tsushima M., Osawa M., *Hydrogen adsorption and hydrogen evolution reaction on a polycrystalline Pt electrode studied by surface-enhanced infrared absorption spectroscopy Electrochim. Acta* **2007**, 52, 5715-5724
47. Brussel M.V., Kokkinidis G., Vandendael I. And Buess-Herman C., *High performance gold-supported platinum electrocatalyst for oxygen reduction, Electrochem. Commun.* **2002**, 4, 808-813
48. Beltramo G.L., Shubina T.E. and Marc T. M. Koper M.T.M., *Oxidation of Formic Acid and Carbon Monoxide on Gold Electrodes Studied by Surface-Enhanced Raman Spectroscopy and DFT, ChemPhysChem* **2005**, 6, 2597-2606
49. Mrozek M.F., Xie Y. and Weaver M., *Surface-Enhanced Raman Scattering On Uniform Platinum-Group Overlayers: Preparation by Redox Replacement of Underpotential-Deposited Metals on Gold, Anal. Chem.*, **2001**, 73(24), 5953-5960

Appendix
Instrumentation
CAMSPEC M550 Spectrophotometer



Spectrometer Specifications

Light sources: Tungsten-Halogen and Deuterium

Monochromator: Littrow type with 1200 lines/mm grating

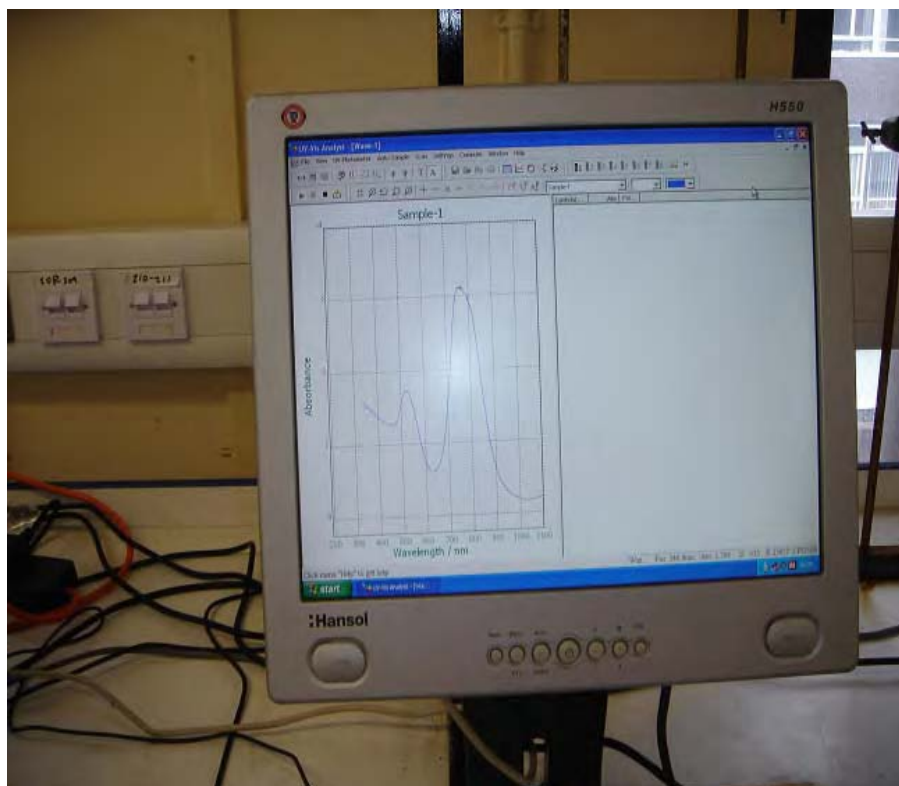
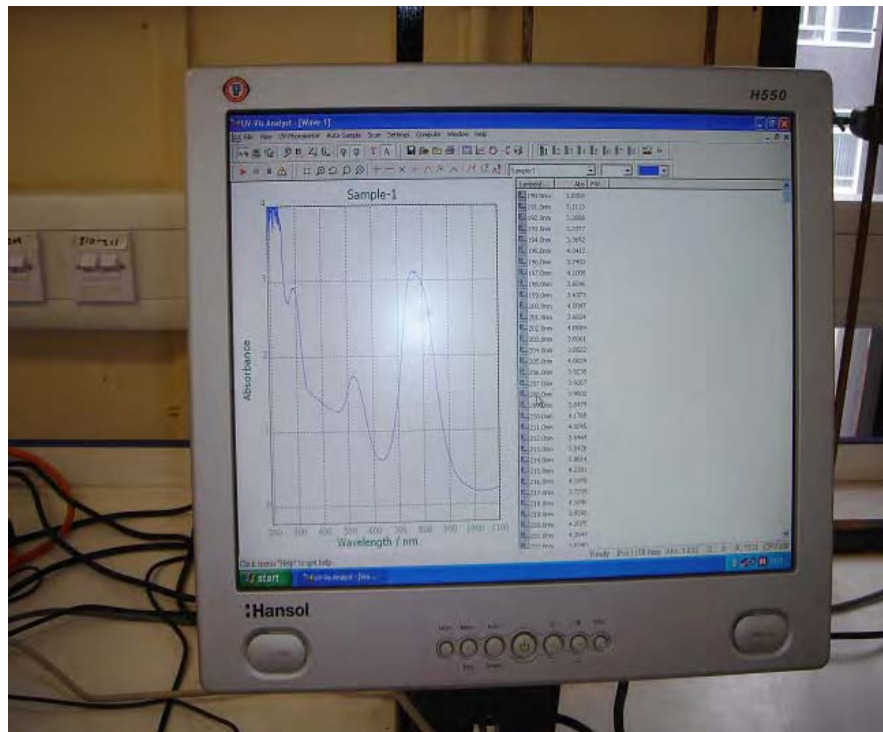
Detectors: Silicon Photodiodes

Scan Speed: Up to 2500nm/min (Return 3000nm/min)

Wavelength Range: 190 – 1100nm

Noise: < 0.0001A @ 500nm 0A

For more specifications, please visit the CAMSPEC homepage www.camspec.co.uk



Autolab Potentiosta/Galvanostat



